Black Holes & Gravitational Waves



Astroparticle, Paris, 29th October 2026

Juan García-Bellido
IFT-UAM/CSIC

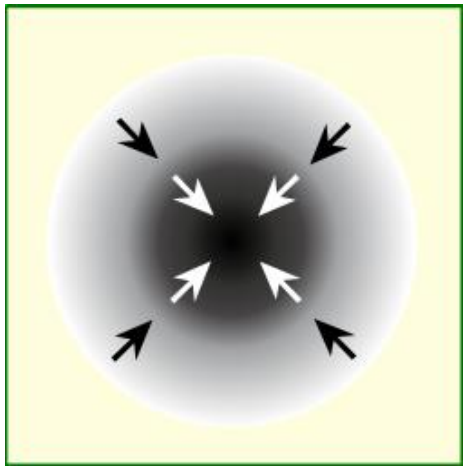
EXCELENCIA SEVERO OCHOA

Campus Internacional excelencia UAM CSIC+

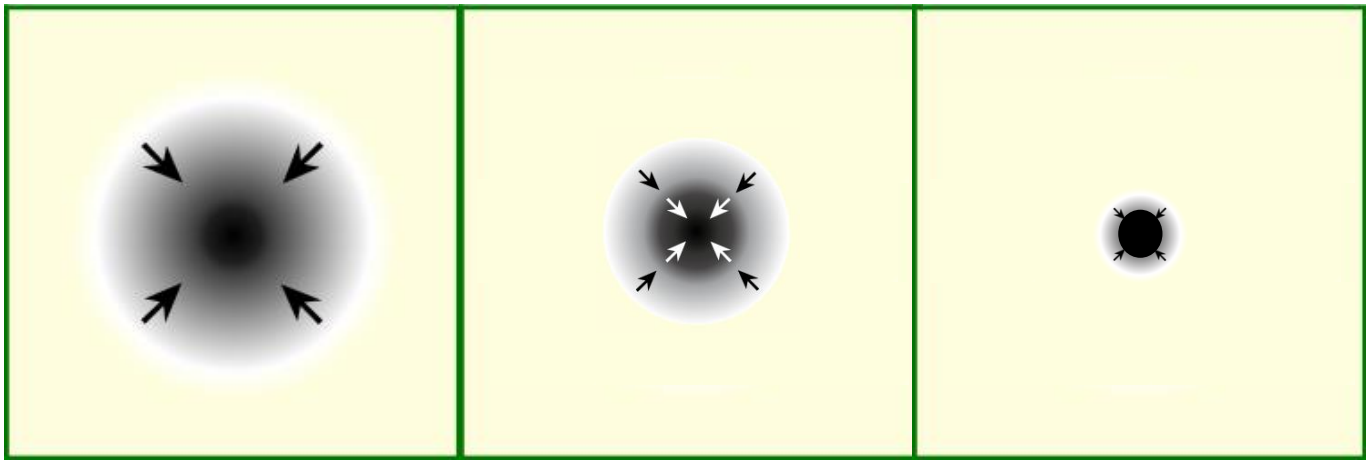
Outline

- Fundamental Physics and PBH:
  - Critical Higgs Inflation (SM-3loop)
  - Quantum Diffusion and PNG tails
- PBH cluster dynamics:
  - Binary parameter distributions
  - Spin induction in dense clusters
- Observational Evidences:
  - Gravitational Waves (GWTC-5)
  - Gravitational Lensing (HypSupCam)

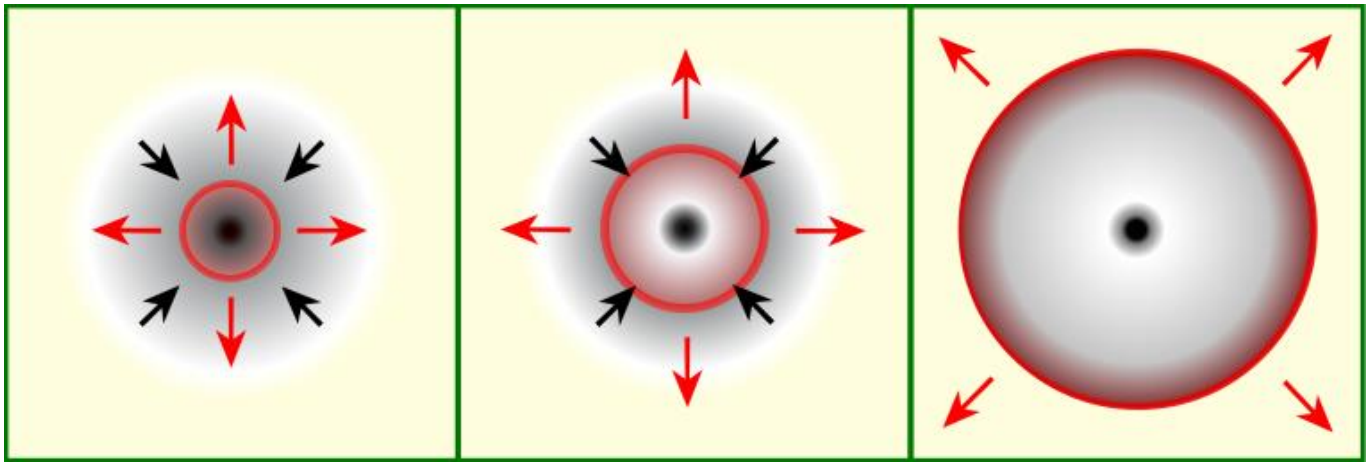
Gravitational Collapse

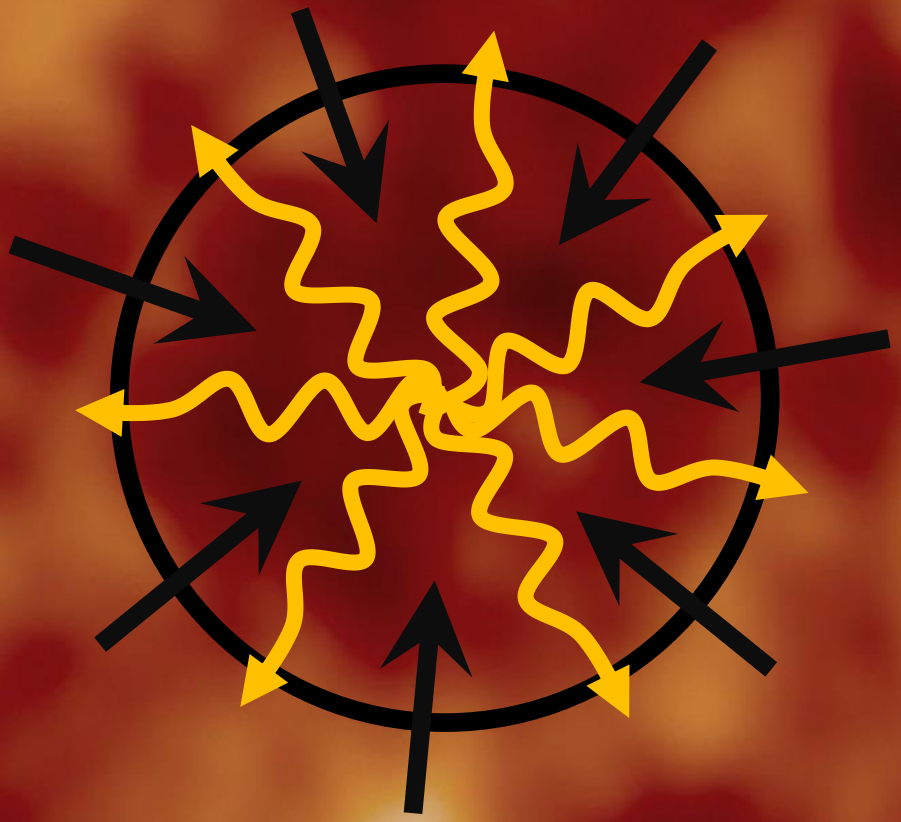


Direct Collapse: Black Hole formation



Radiation pressure : Supernova



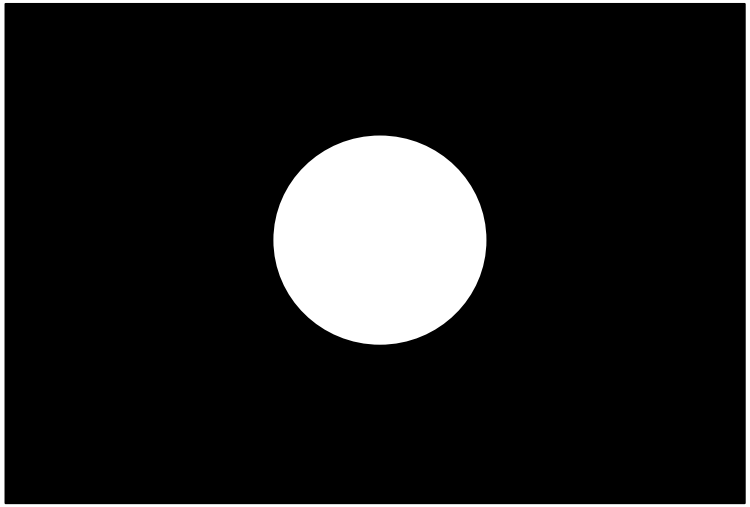


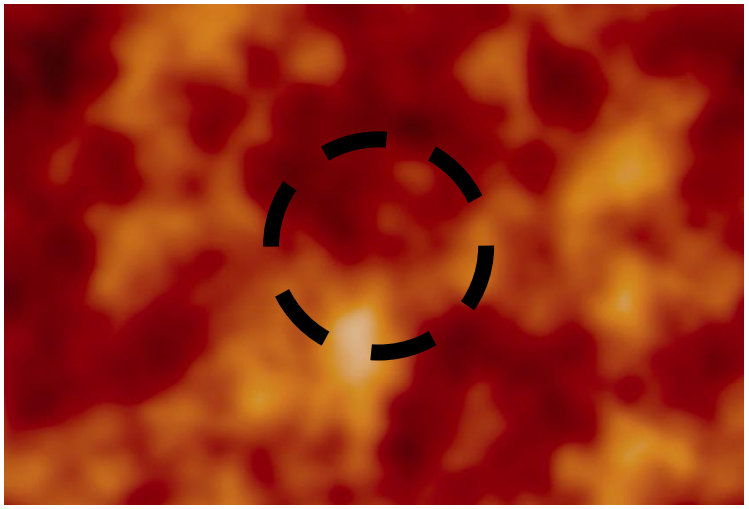
Primordial plasma

Mass origin of ABH & PBH

Chandrasekhar mass
(Pauli Excl.)

Horizon mass
QCD-era (Causality)



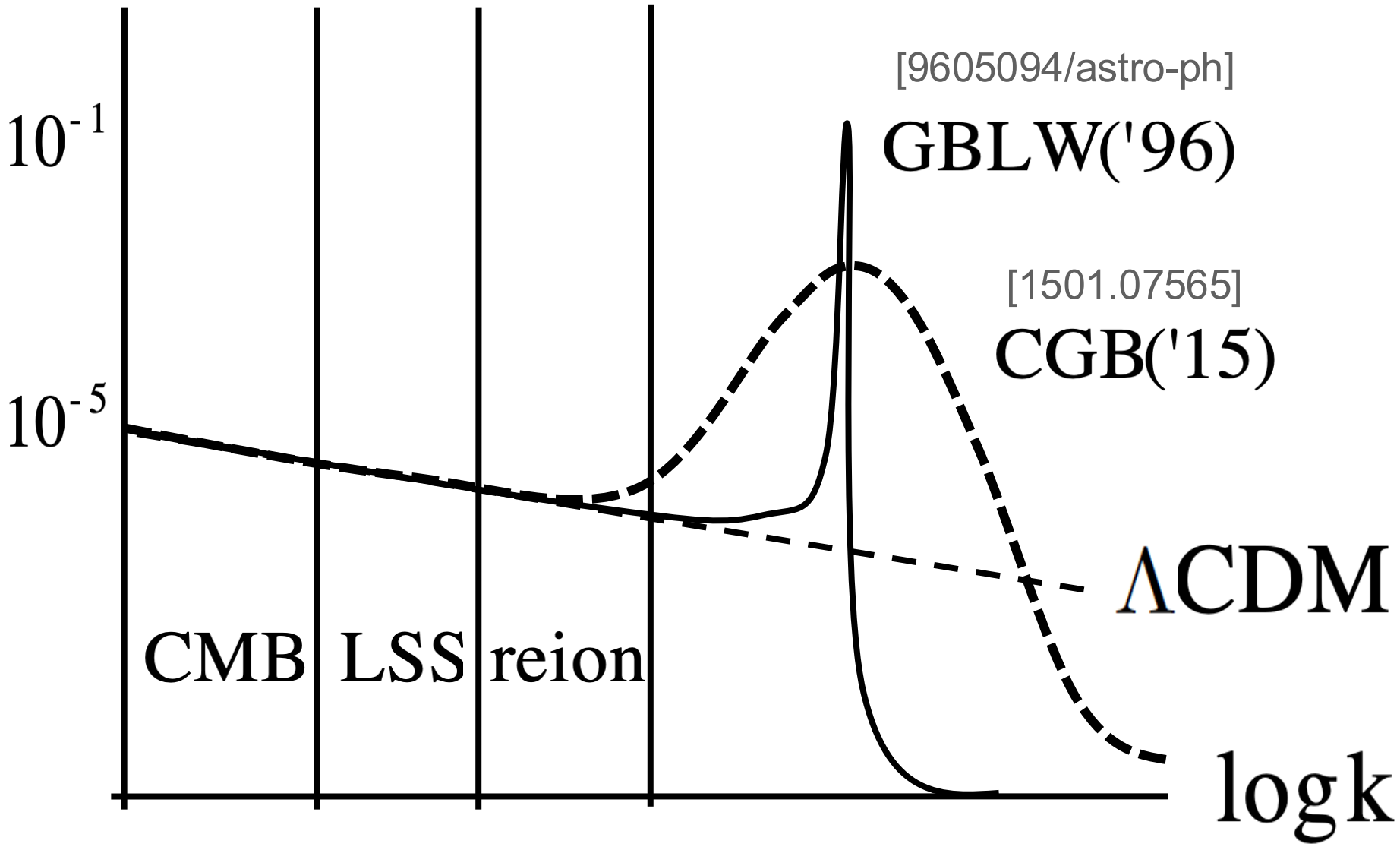


Fermionic ABH

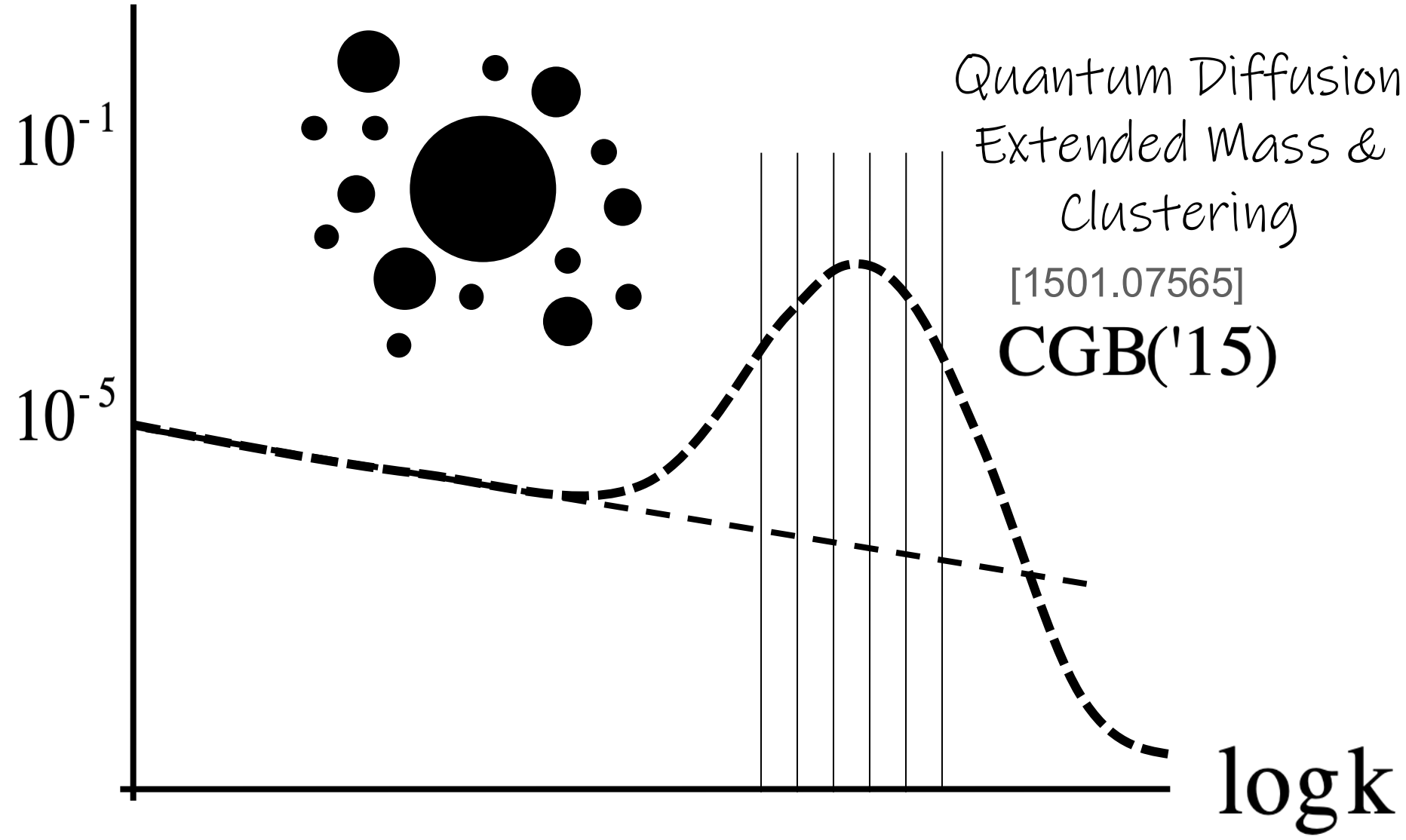
Bosonic PBH

$$M_{\rm BH} \sim \frac{M^3_{\rm Planck}}{m^2_{\rm proton}} \sim M_\odot$$

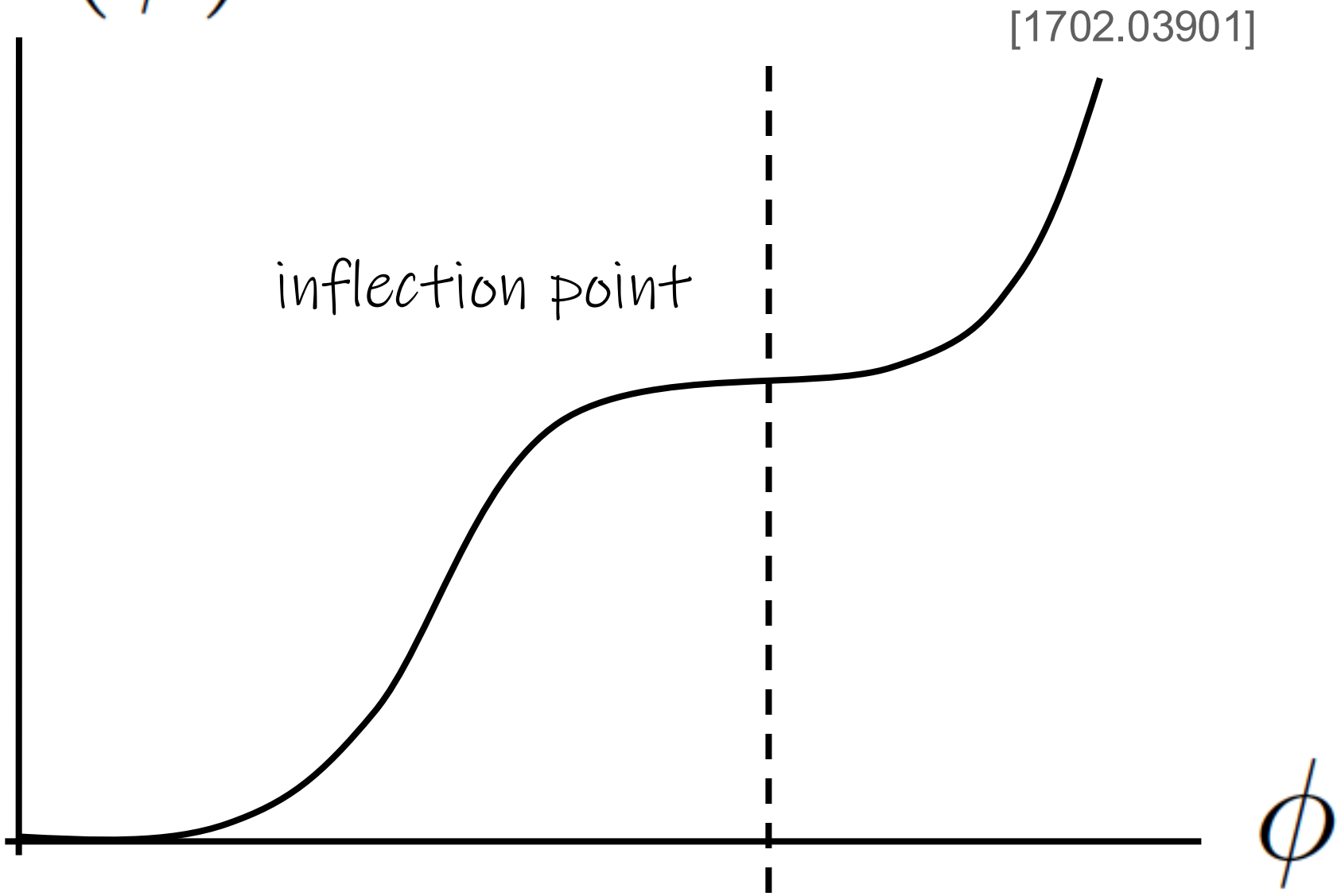
Power spectrum



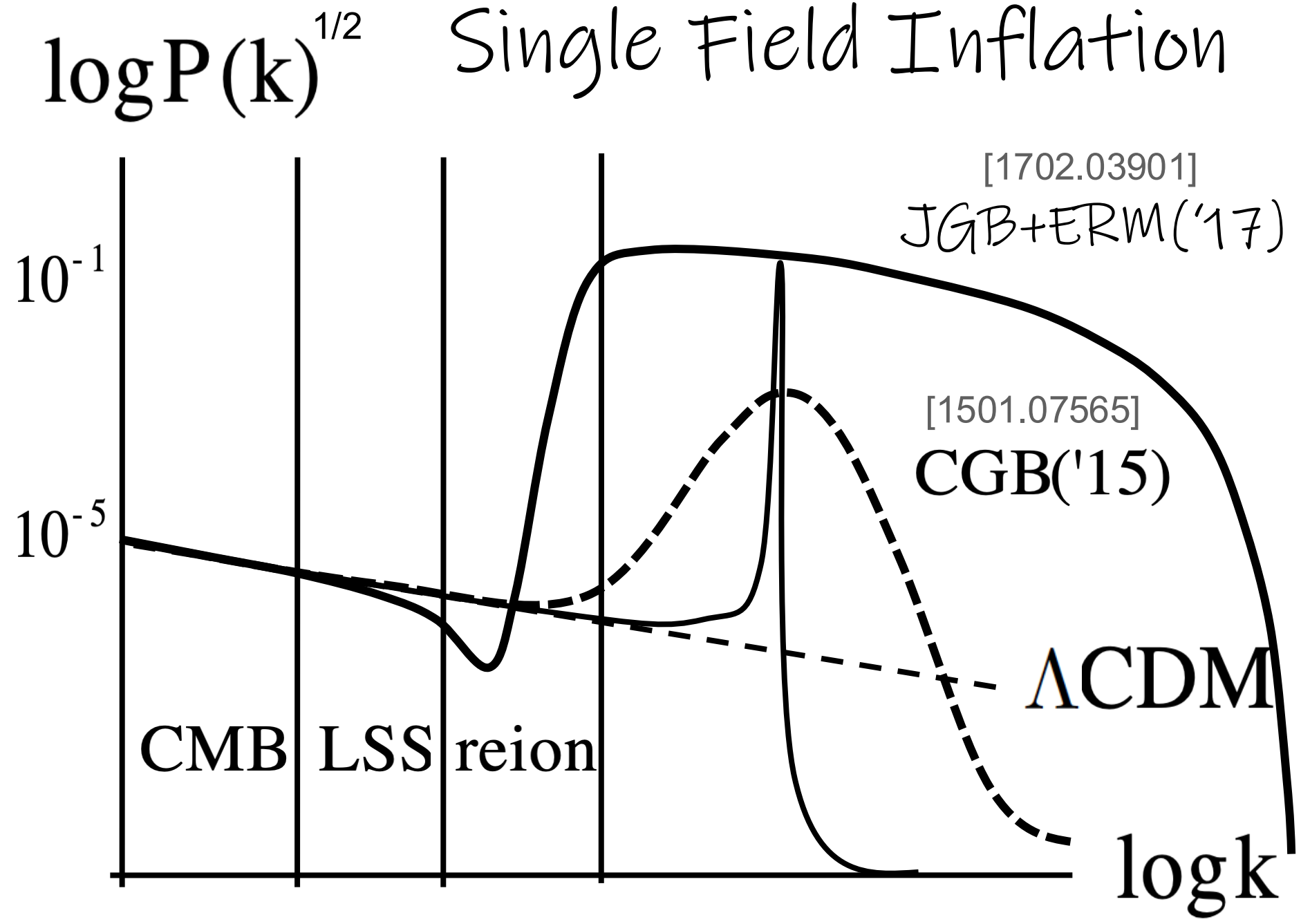
Power spectrum



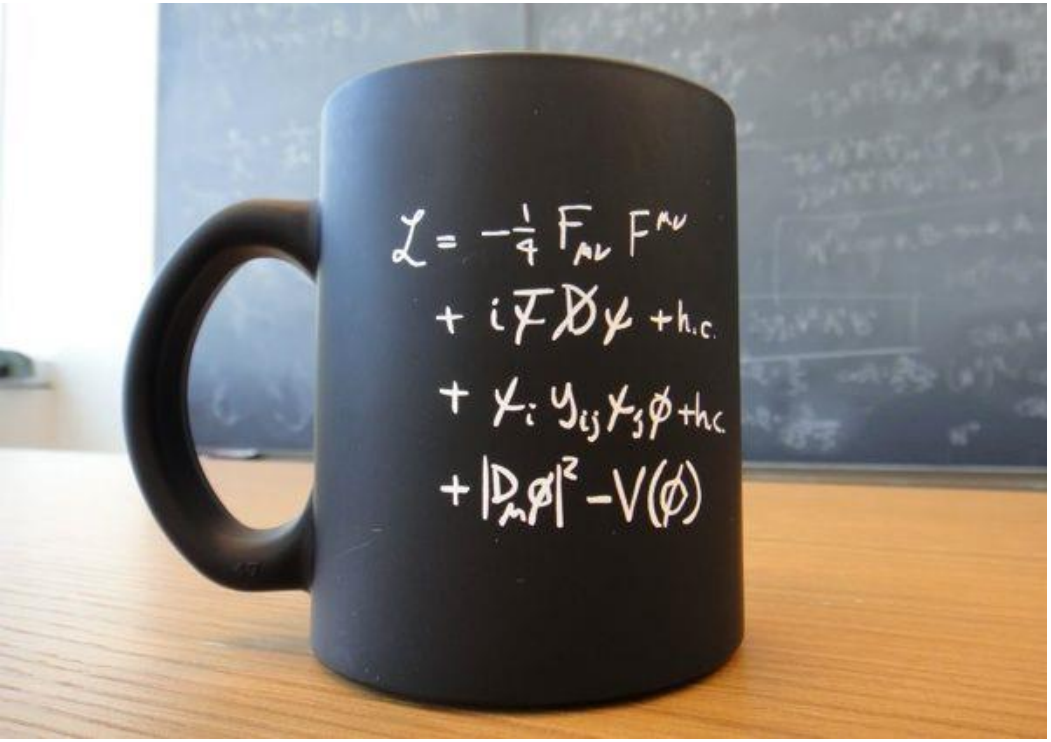
Single Field Inflation



Single Field Inflation



Standard Model Lagrangian



$$\mathcal{L} = -\frac{1}{4} F_{\mu\nu} F^{\mu\nu}$$

$$+ i\bar{\psi} \not{D} \psi + h.c.$$

$$+ \bar{\psi}_i y_{ij} \psi_j \phi + h.c.$$

$$+ |D_\mu \phi|^2 - V(\phi)$$

$$+ \xi |\phi|^2 R$$

$$R = 12H^2 + 6\dot{H} \rightarrow R_0 = 9.2\, H_0^2 \rightarrow m_H = \sqrt{\xi R_0} = 2\times10^{-32}\ \text{eV}$$

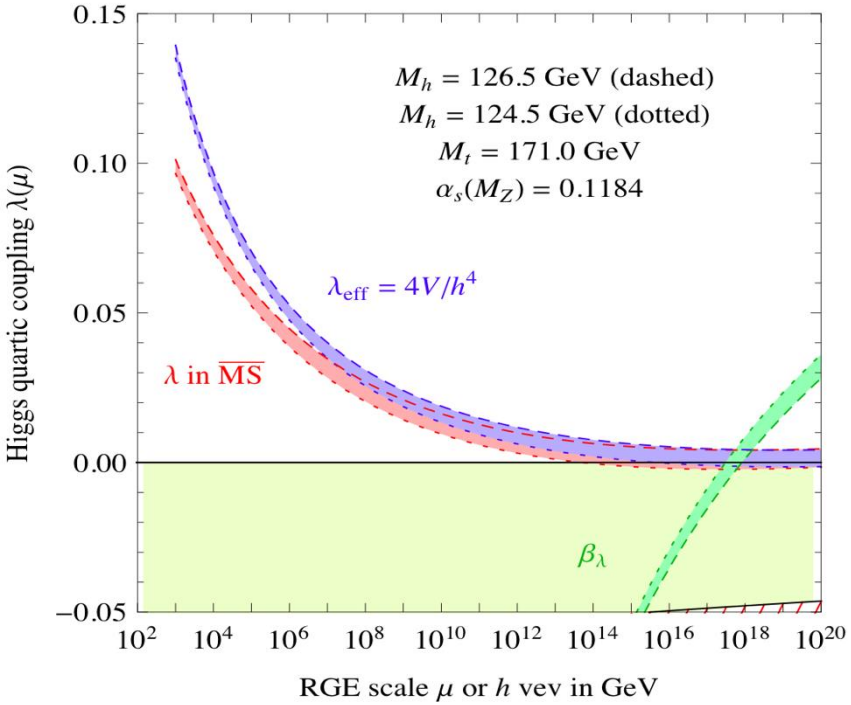
Renormalization of Higgs couplings

Ezquiaga, JGB, Ruiz [1705.04861]

$$\lambda(\phi) = \lambda_0 + b_\lambda \ln^2(\phi/\mu) ,$$

$$\xi(\phi) = \xi_0 + b_\xi \ln(\phi/\mu) ,$$

Buttazzo et al (2014)



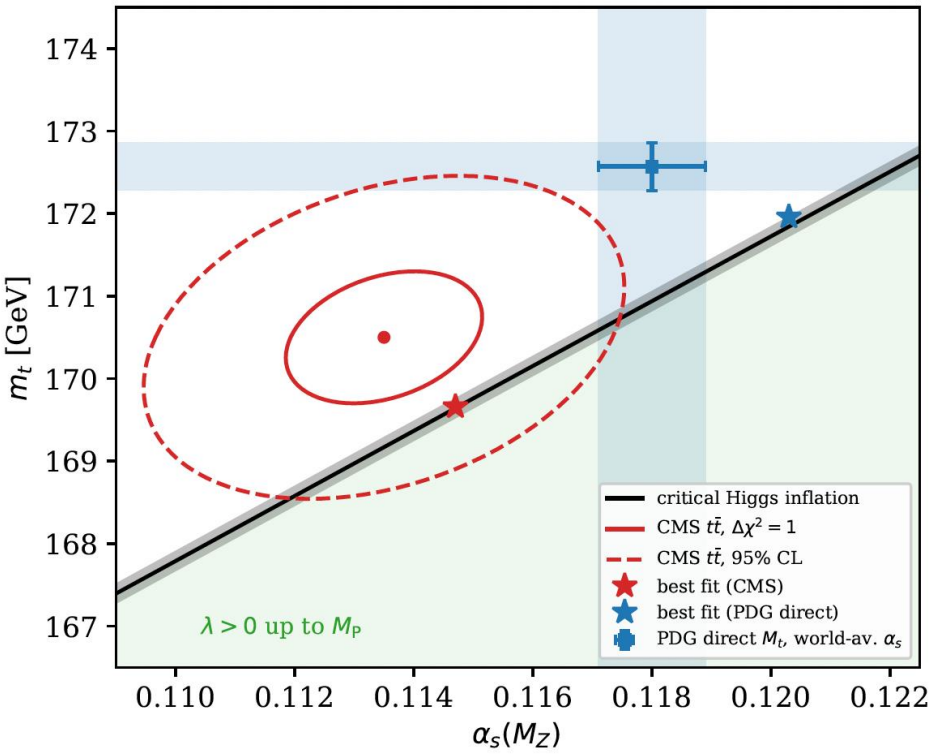


FIG. 5. The critical Higgs-inflation line $M_t^{\rm crit}(\alpha_s)$ (black, with the band from M_h and the matching uncertainties) in the (α_s, m_t) plane. Below the line λ remains positive up to $M_{\rm P}$. Red: CMS simultaneous determination of $m_t^{\rm pole}$ and α_s from $t\bar{t}$ cross sections [22], $\Delta\chi^2 = 1$ and 95% CL contours. Blue: direct top-mass average and world average of α_s [45]. Stars mark the points of the critical line closest to each likelihood maximum.

Critical Higgs Inflation

Ezquiaga, JGB, Ruiz Morales [1705.04861]

$$S=\int d^4x\sqrt{g}\left[\left(\frac{1}{2\kappa^2}+\frac{\xi(\phi)}{2}\phi^2\right)R-\frac{1}{2}(\partial\phi)^2-\frac{1}{4}\lambda(\phi)\phi^4\right]$$

$$g_{\mu\nu}\to h_{\mu\nu}=(1+\xi\phi^2)g_{\mu\nu}$$

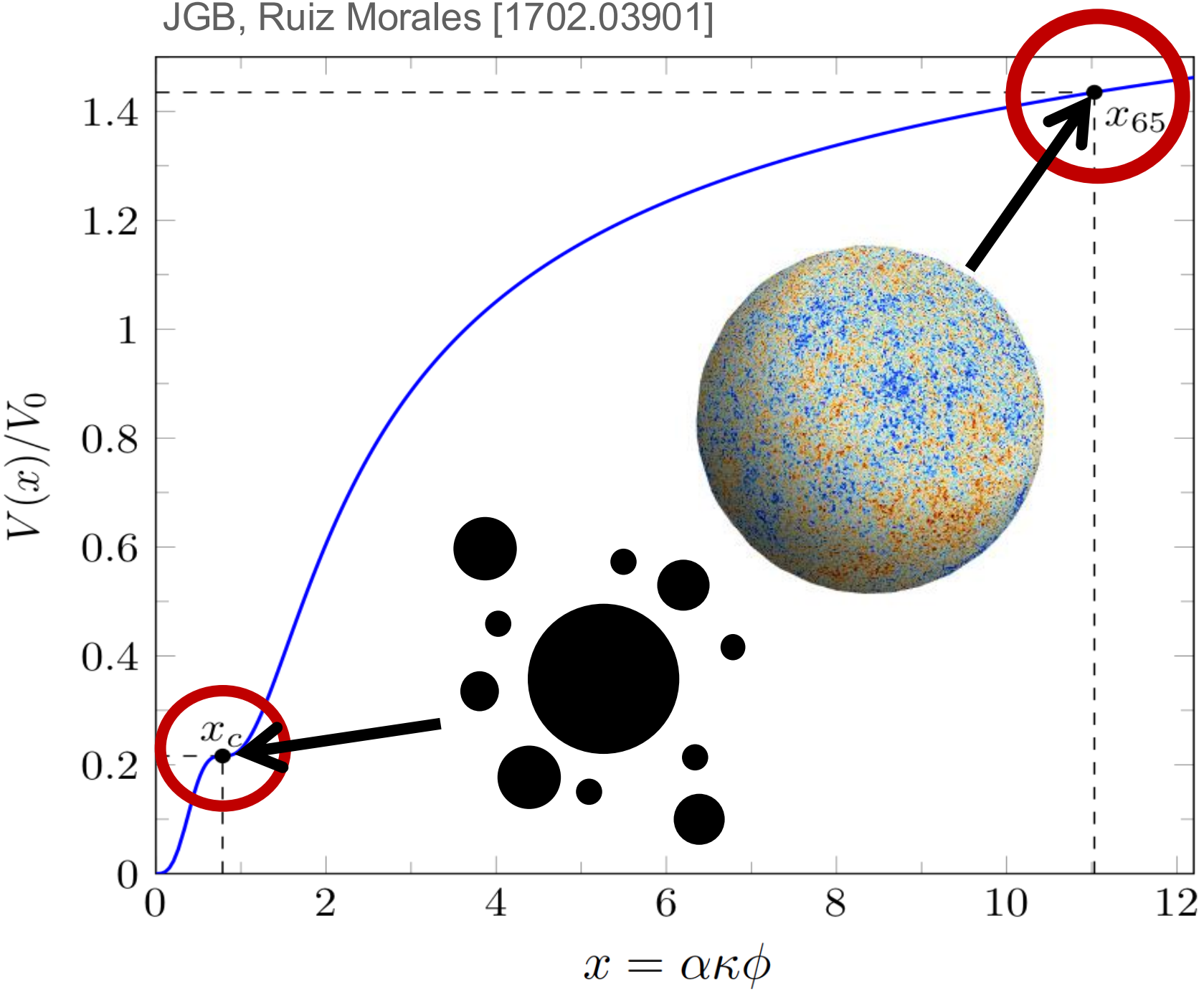
$$\begin{aligned}\lambda(\phi) &= \lambda_0+b_\lambda\ln^2(\phi/\mu)\ ,\\ \xi(\phi) &= \xi_0+b_\xi\ln(\phi/\mu)\ ,\end{aligned}$$

$$\frac{d\varphi}{d\phi}=\frac{\sqrt{1+\xi(\phi)\,\phi^2+6\,\phi^2\,(\xi(\phi)+\phi\,\xi'(\phi)/2)^2}}{1+\xi(\phi)\,\phi^2}$$

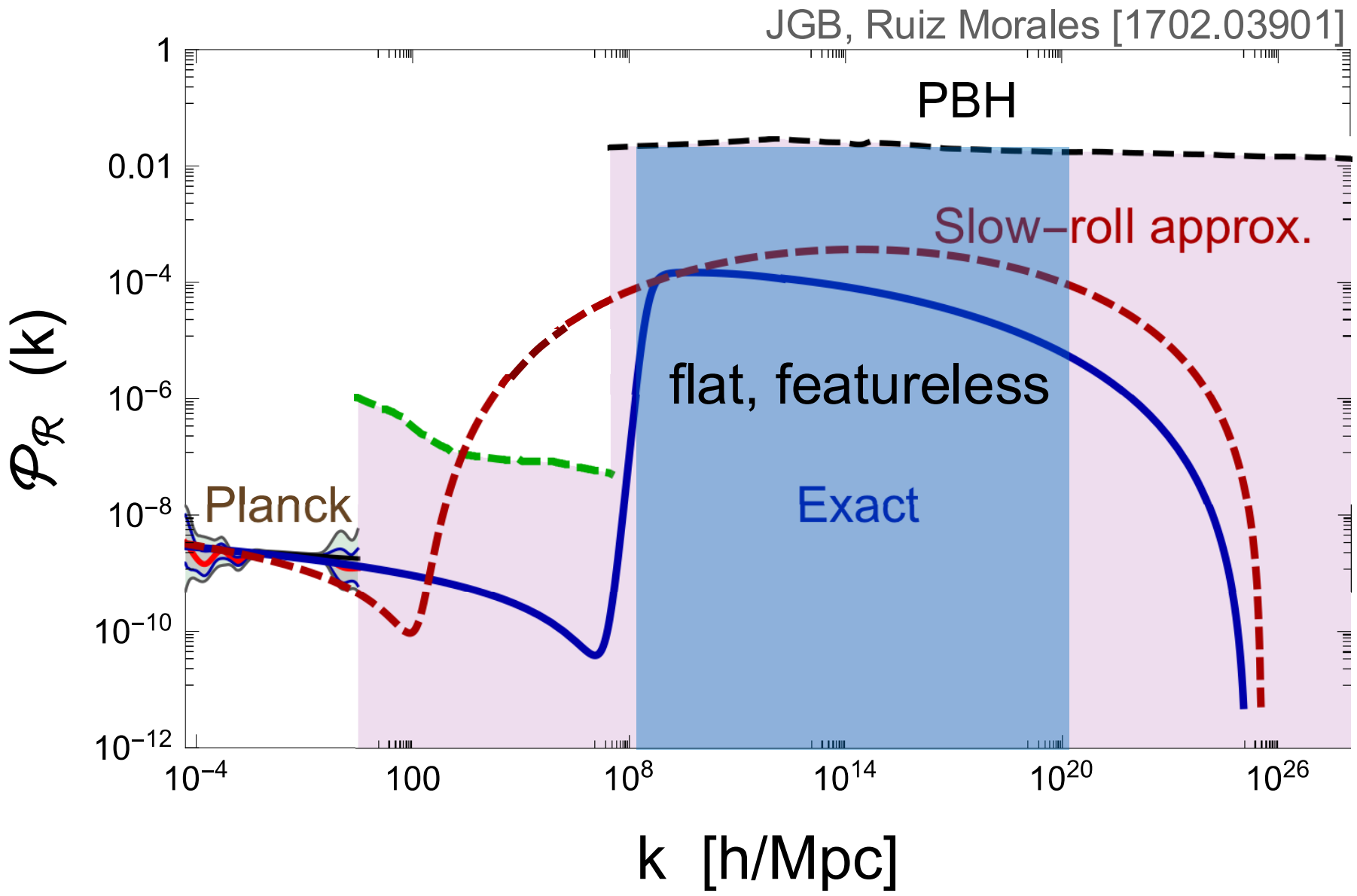
$$V(x)=\frac{V_0\,(1+a\,\ln^2 x)\,x^4}{(1+c\,(1+b\,\ln x)\,x^2)^2}\qquad x=\phi/\mu$$

$$V_0=\lambda_0\mu^4/4,\ a=b_\lambda/\lambda_0,\ b=b_\xi/\xi_0 \text{ and } c=\xi_0\,\kappa^2\mu^2$$

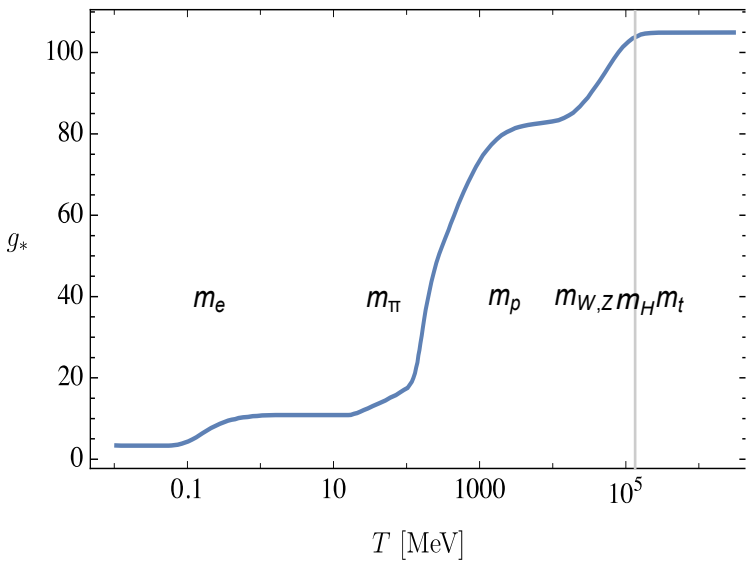
JGB, Ruiz Morales [1702.03901]

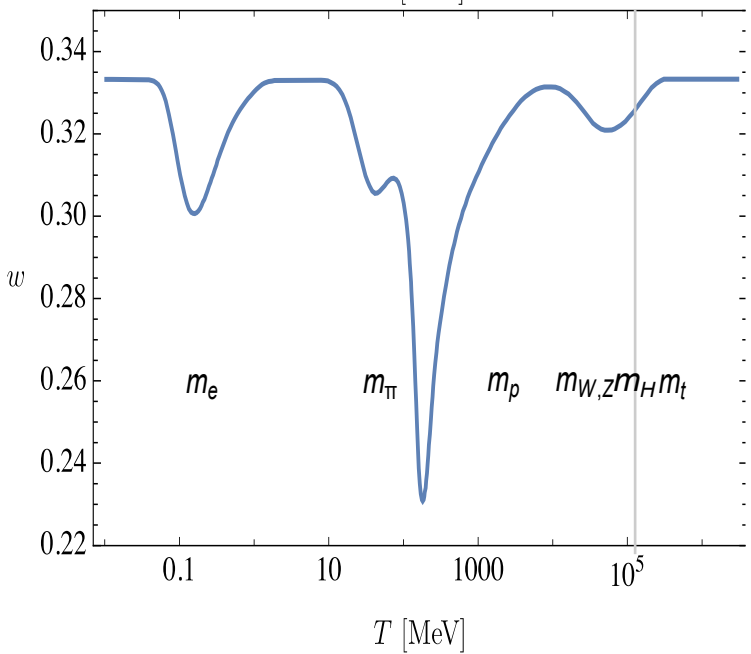


Primordial Power Spectrum



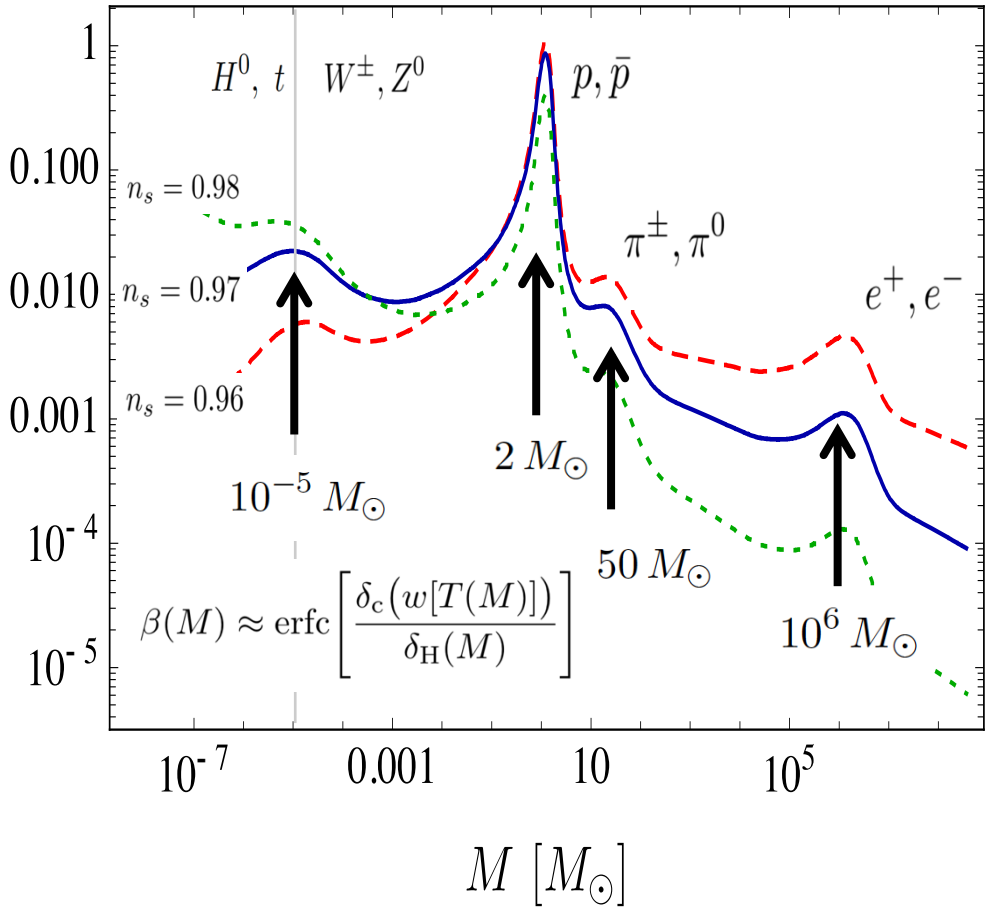
Thermal history of the universe





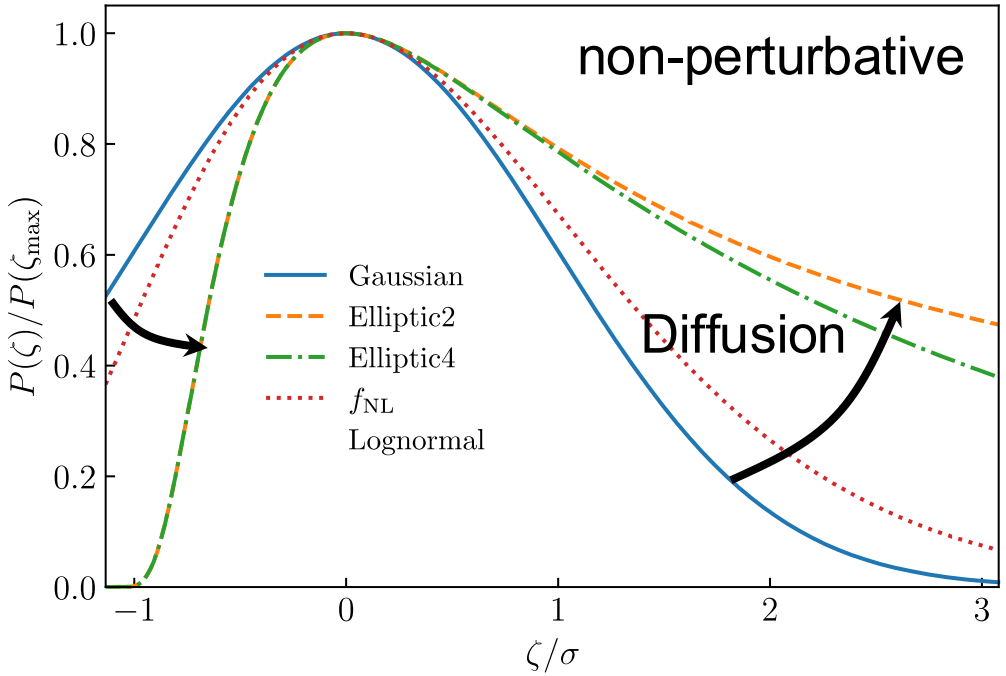
Carr, Clesse, JGB, Kühnel [1906.08217]

PBH mass spectrum



Quantum Diffusion @ CMB & LSS

Ezquiaga, JGB, Vennin [2207.06317]



Elliptic Functions

$$P_2(\zeta_k) = -\frac{\pi}{2\mu^2}\vartheta_2'\left(\frac{\pi\alpha_k}{2}, e^{-\frac{\pi^2}{\mu^2}\mathcal{N}_k}\right)$$

$$P_4(\zeta_k) = \frac{\pi}{2\mu^2\alpha_k}\vartheta_4'\left(\frac{\pi\alpha_k}{2}, e^{-\frac{\pi^2}{\mu^2}\mathcal{N}_k}\right)$$

$f_{\rm NL}$ – expansion (not enough)

$$\zeta(x) = \zeta_{\rm G}(x) + \frac{3}{5}f_{\rm NL}\left[\zeta_{\rm G}^2(x) - \sigma_{\rm G}^2(x)\right]$$

Lognormal distributions

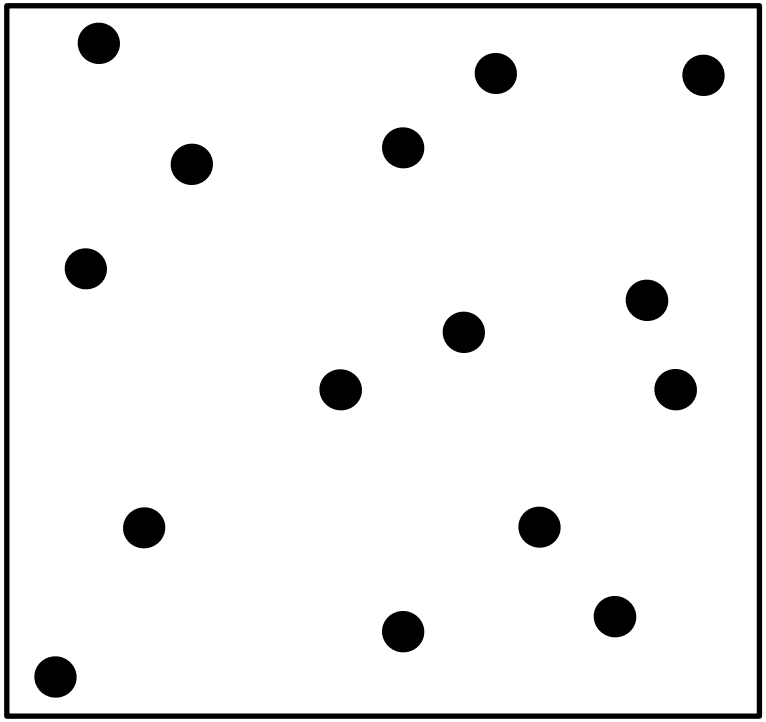
$$\mathrm{LN}(x,\,\rho,\,\sigma) = \frac{1}{\rho\,\sigma\sqrt{2\pi}}\,\exp\left[-\frac{\ln(x/\rho)^2}{2\sigma^2} - \frac{\sigma^2}{2}\right]$$

$$\mathrm{G}(x,\,\rho,\,\sigma_{\rm G}) = \frac{1}{\sigma_{\rm G}\sqrt{2\pi}}\,\exp\left[-\frac{(x-\rho)^2}{2\sigma_{\rm G}^2}\right]$$

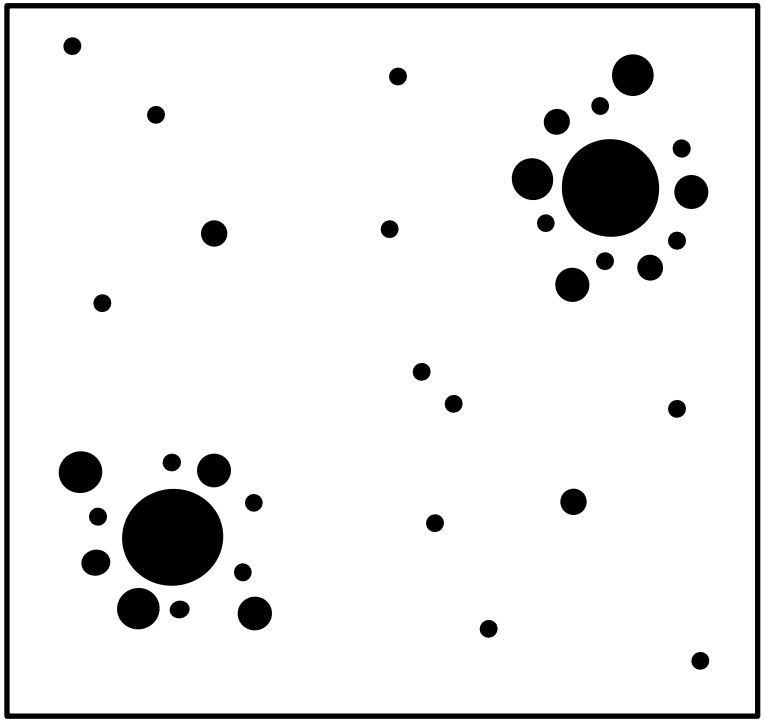
$$P_{\rm NL}(\zeta) = \frac{1}{\sqrt{2\pi\sigma_{\rm G}^2\Delta}}\left[e^{-\frac{25(\sqrt{\Delta}-1)^2}{72f_{\rm NL}^2\sigma_{\rm G}^2}} + e^{-\frac{25(\sqrt{\Delta}+1)^2}{72f_{\rm NL}^2\sigma_{\rm G}^2}}\right]$$

$$\text{where}\quad \Delta(\zeta) = 1 + \frac{12}{5}f_{\rm NL}\zeta + \frac{36}{25}f_{\rm NL}^2\sigma_{\rm G}^2.$$

What about clusters of PBH?



- Monochromatic (m)
- Uniformly distributed
- Gaussian statistics



- Broad range of masses
- PBH in dense clusters
- Non-Gaussian tails

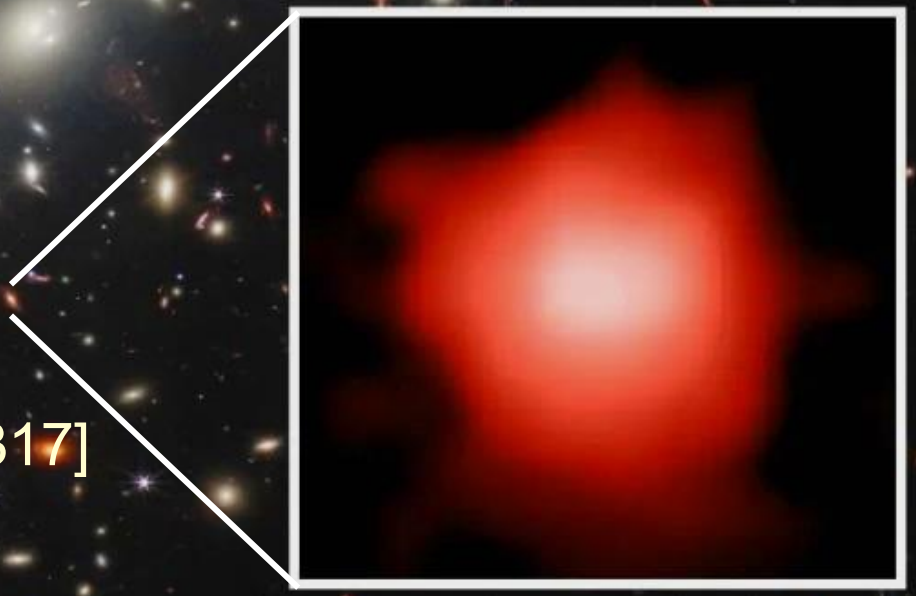


JGB [1702.08275]



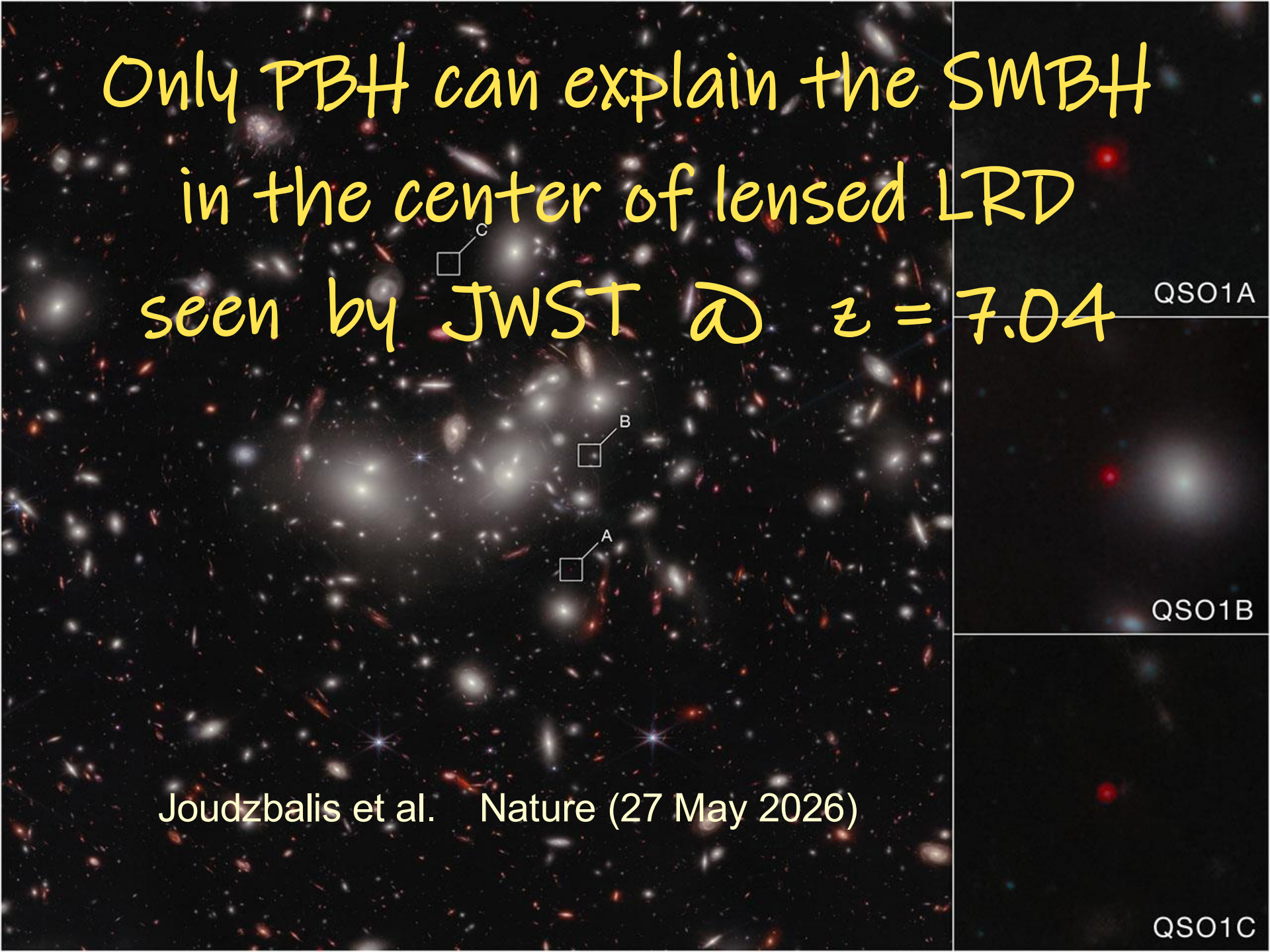
PBH could explain the SMBH in the center of galaxies seen by JWST at $z \sim 13\text{-}16$

"Little Red Dots"



JGB, Clesse [1501.07565]
Ezquiaga, JGB, Vennin [2207.06317]

Only PBH can explain the SMBH in the center of lensed LRD seen by JWST @ z = 7.04



Joudzbalis et al. Nature (27 May 2026)

PBH clusters explain the cumply Nature of Little Red Dots

Tanaka et al. [2410.00104]

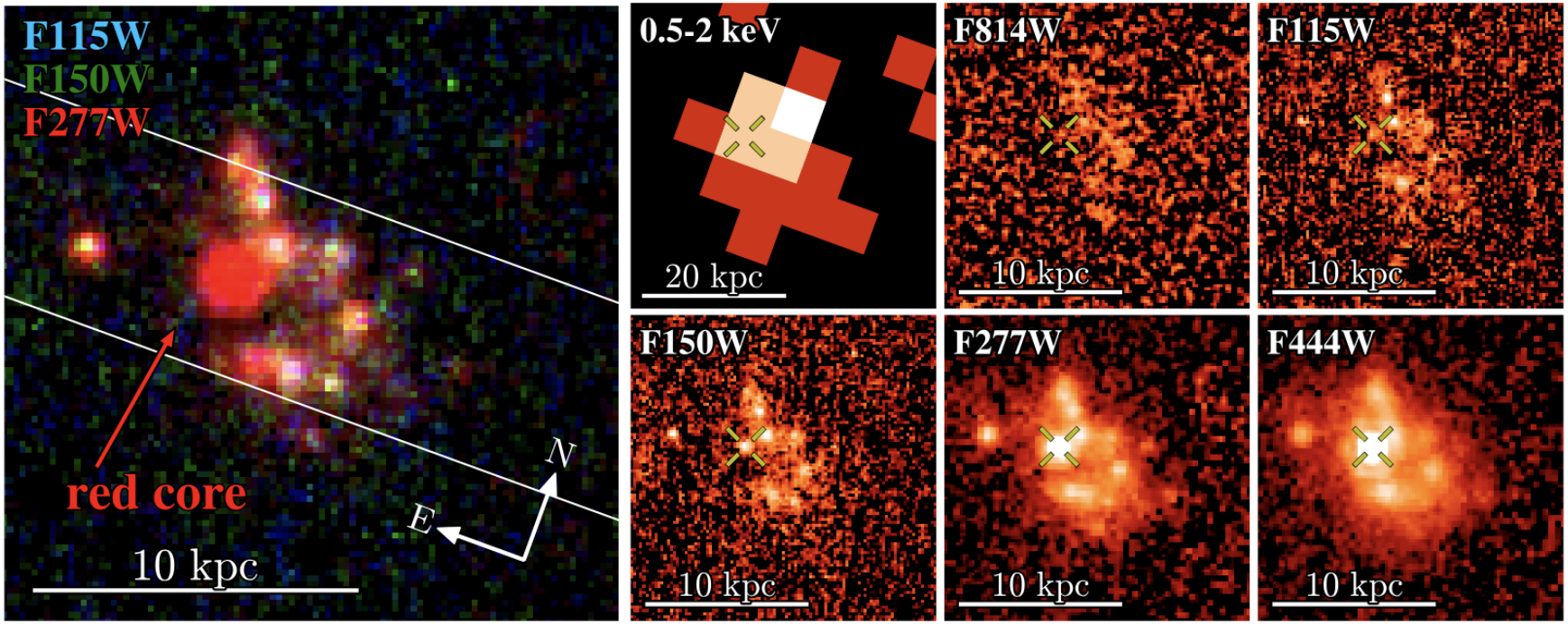
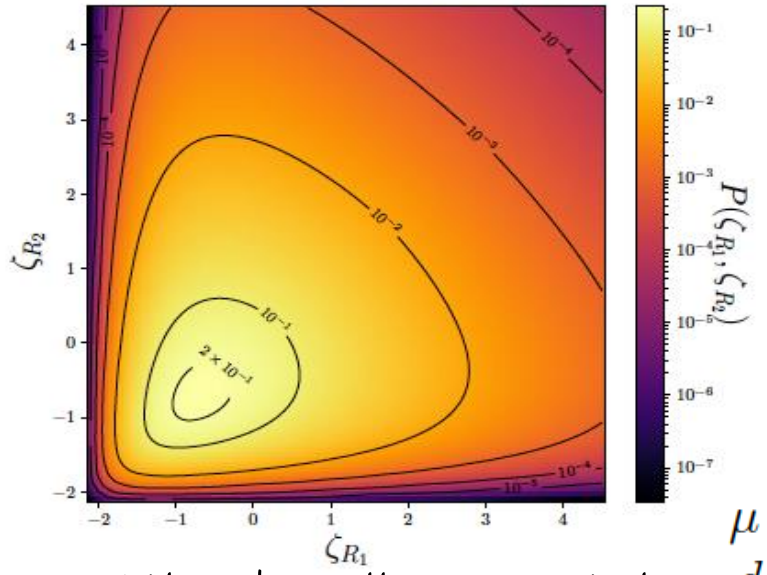


Fig. 1. Three-color (JWST/NIRCam F277W, F150W, and F115W for RGB) image and separate filter images of CID-931. The slit position of Keck-II/DEIMOS observation is shown by the white lines. Note that the Chandra 0.5-2 keV image has a different cutout size ($6'' \times 6''$) due to a much lower pixel scale ($0.''984/\mathrm{pixel}$) than the HST and JWST images ($3'' \times 3''$ cutout with the pixel scale of $0.''03/\mathrm{pixel}$). Yellow bars in right panels indicate the position of the red core.

Clusters from Quantum Diffusion

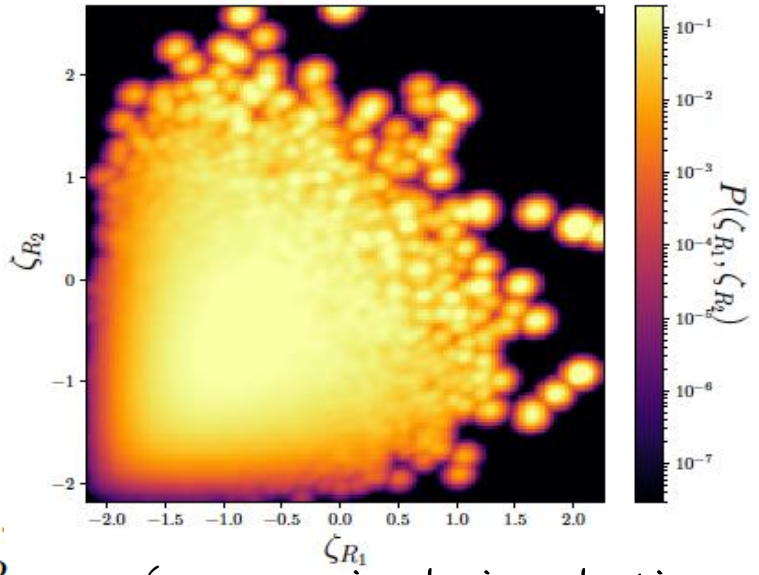
2-pt distribution function

Animali, Vennin [2402.08642]

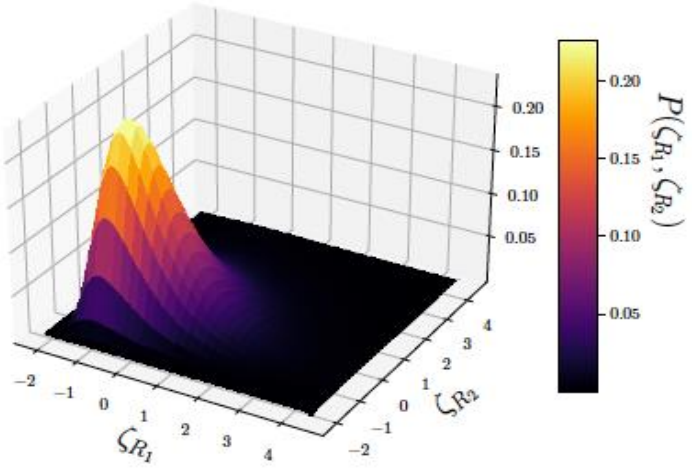


$\mu = 13$

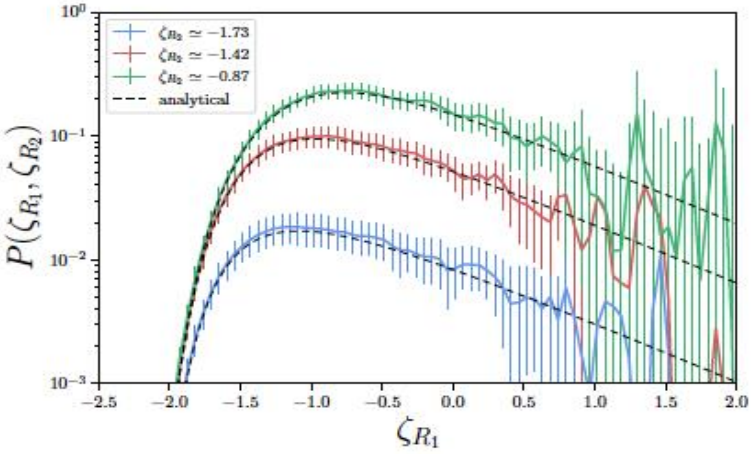
$d = 0.3$



Tilted-well potential

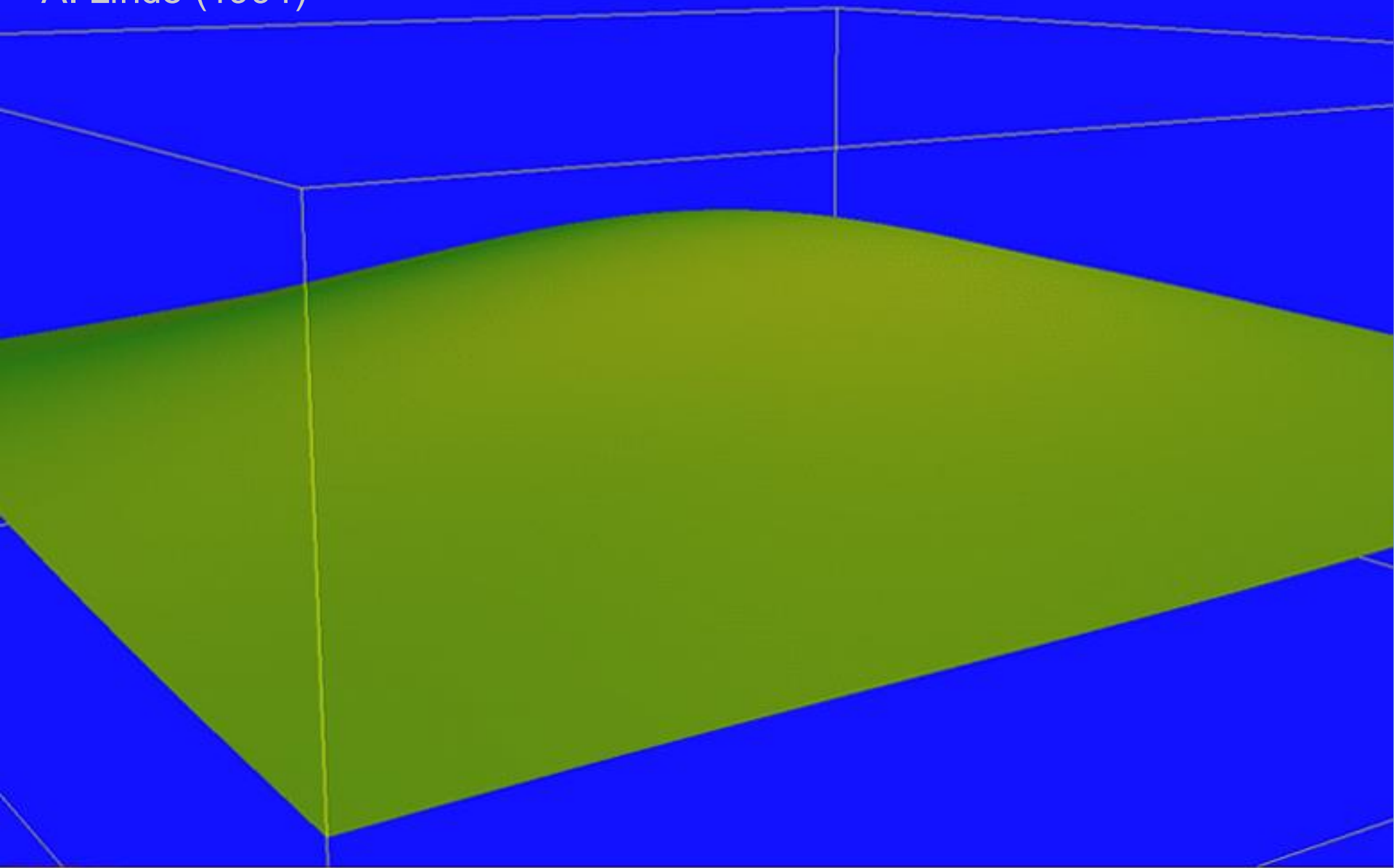


10^6 numerical simulations



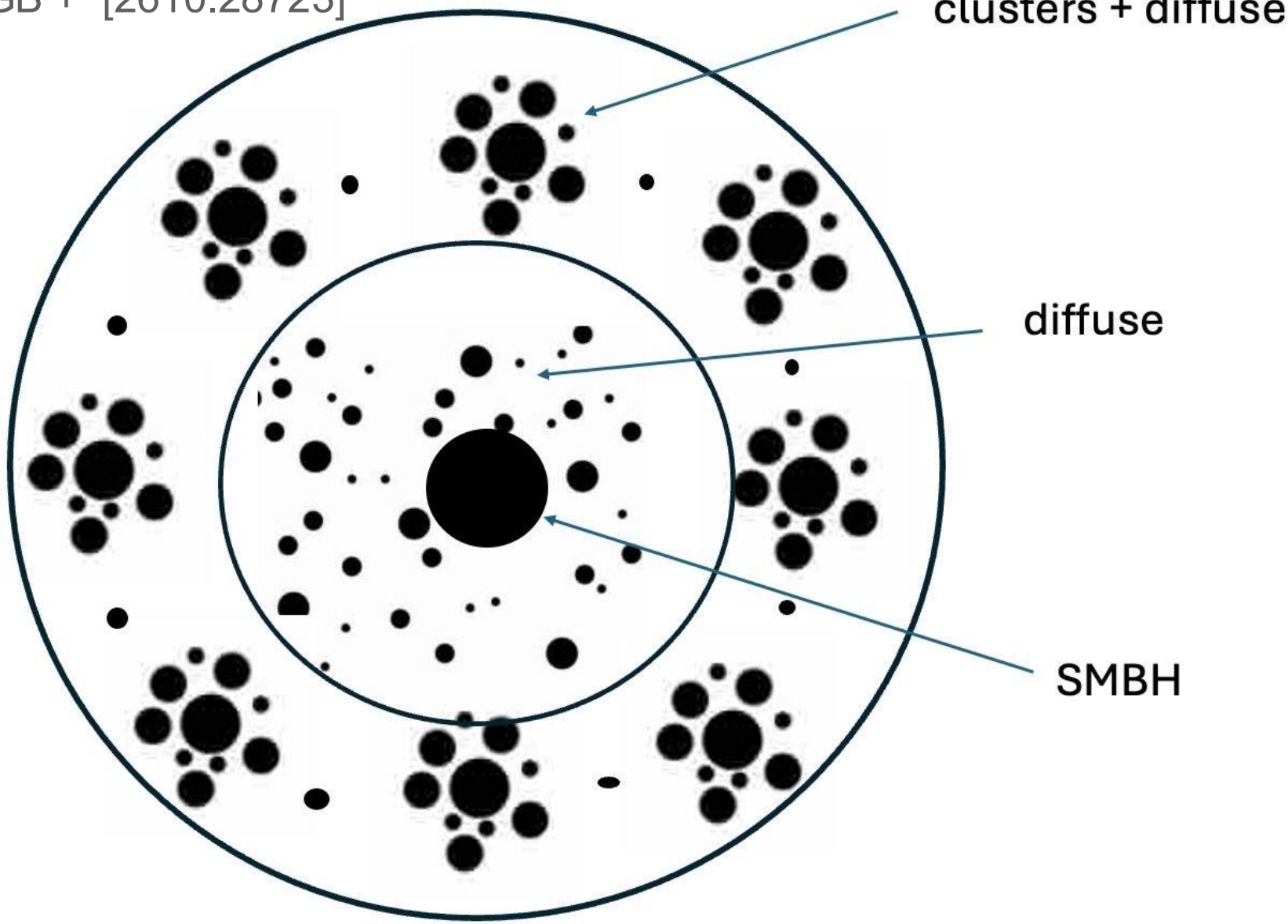
PBH and Stochastic Inflation

A. Linde (1994)



Milky Way - like galaxy

Carr, JGB + [2610.28723]



Cluster Dynamics

J.F. Nuño Siles, JGB [2405.06391]

$\{M\&A, \sigma_{0.5}, \sigma_1, \sigma_{1.5}\}$

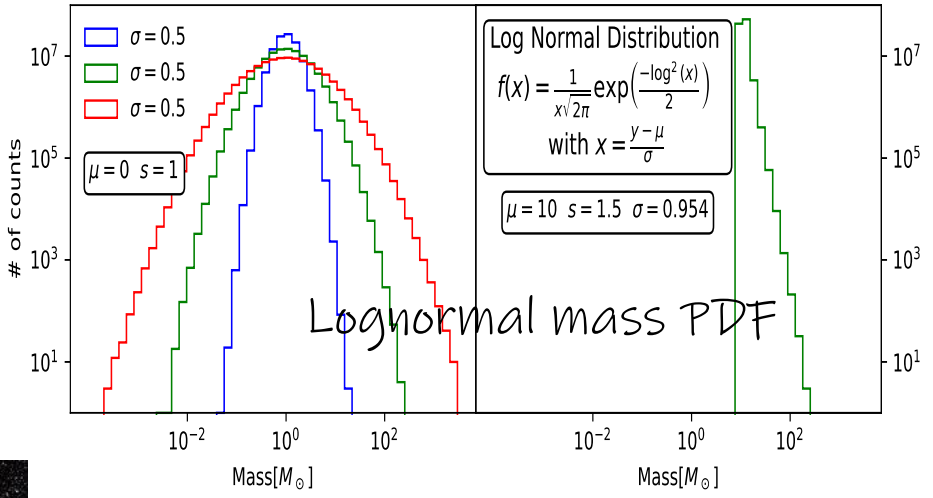
Lognormal mass distribution

$$N \sim \mathcal{O}(10^3 - 20 \cdot 10^3)$$

$$M_{\rm tot} \sim \mathcal{O}(10^3 - 10^5) M_\odot$$

Maxwellian velocity distribution

Plummer density profile



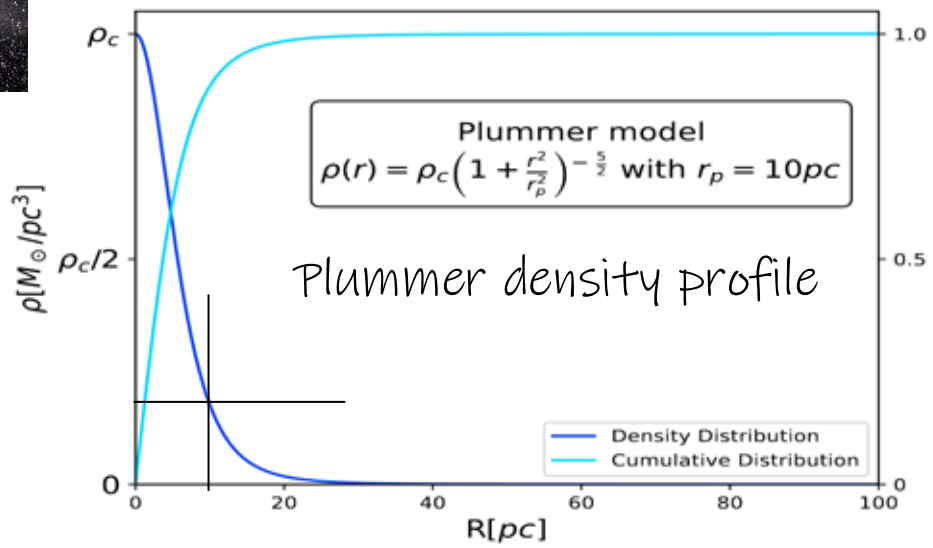
Lognormal mass PDF

Galactic potential MW (point-mass galaxy)

M=4.36953E+10 $M_\odot$

with circular orbit at R=34 kpc





Plummer density profile

No primordial binaries

Zero natal spin

Code used: [Nbody6++GPU]

Multiple simulations

J.F. Nuño Siles, JGB [2405.06391]

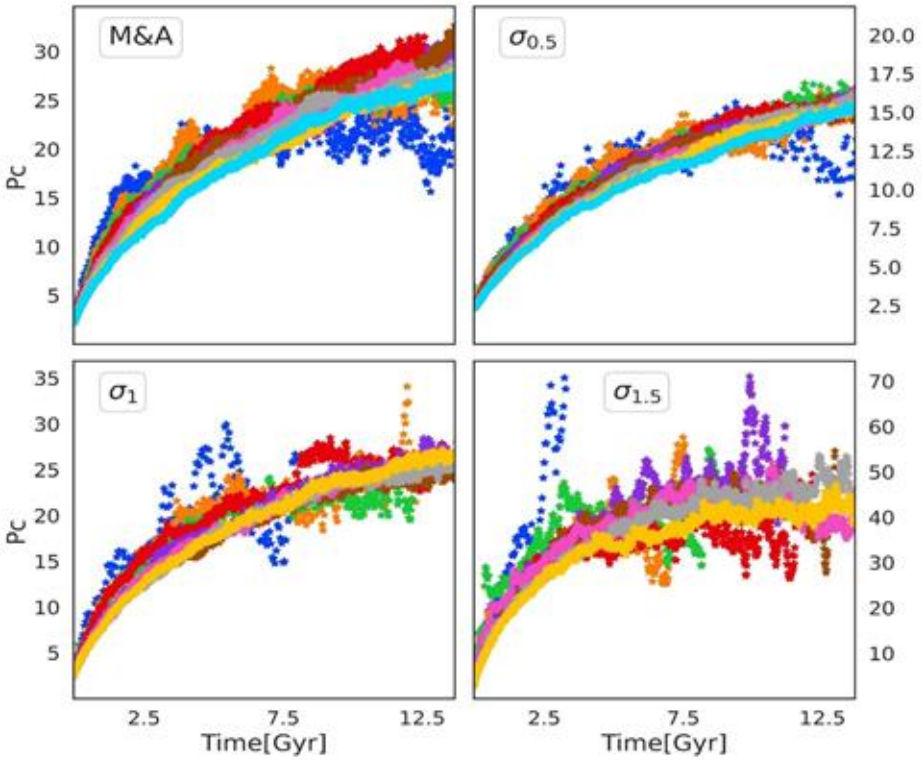
ID M&A	$M_{\rm total}[M_\odot]$ $t=0$	$M_{\rm max}[M_\odot]$ $t=0$	$M_{\rm max}[M_\odot]$ $t=T_U$	$R_{\rm HM}[pc]$ $t=0$	$R_{\rm HM}[pc]$ $t=T_U$	ID $\sigma_{0.5}$	$M_{\rm total}[M_\odot]$ $t=0$	$M_{\rm max}[M_\odot]$ $t=0$	$M_{\rm max}[M_\odot]$ $t=T_U$	$R_{\rm HM}[pc]$ $t=0$	$R_{\rm HM}[pc]$ $t=T_U$
1295	16140	46.54	46.54	2.20	27.04	1520	1389	5.03	5.03	9.72	12.25
2570	32166	66.10	97.80	2.38	27.17	3345	3007	4.50	5.08	3.23	15.55
4046	50088	63.64	91.98	4.27	26.74	5480	5009	6.67	6.67	0.77	16.21
5199	64280	69.98	74.80	2.20	28.39	7678	7008	5.69	7.52	1.92	15.15
8077	100116	78.27	78.27	12.53	29.50	9937	9001	5.48	5.48	1.25	15.85
8922	110196	76.15	81.52	13.31	32.01	12201	11001	5.00	7.77	2.90	15.29
10372	128337	104.26	104.26	6.20	27.54	14366	13005	5.42	8.22	2.65	16.04
10535	130198	68.50	74.35	9.72	28.20	16428	14912	7.72	7.72	0.48	16.04
16159	200392	57.75	113.59	4.44	27.24	18776	17007	5.40	6.51	2.29	15.00
20738	256346	134.10	145.70	1.37	26.65	20866	18918	5.31	7.36	3.91	15.35
ID σ_1	$M_{\rm total}[M_\odot]$ $t=0$	$M_{\rm max}[M_\odot]$ $t=0$	$M_{\rm max}[M_\odot]$ $t=T_U$	$R_{\rm HM}[pc]$ $t=0$	$R_{\rm HM}[pc]$ $t=T_U$	ID $\sigma_{1.5}$	$M_{\rm total}[M_\odot]$ $t=0$	$M_{\rm max}[M_\odot]$ $t=0$	$M_{\rm max}[M_\odot]$ $t=T_U$	$R_{\rm HM}[pc]$ $t=0$	$R_{\rm HM}[pc]$ $t=T_U$
1505	2003	32.07	32.07	1.93	27.07	1220	3020	63.67	63.67	3.37	58.92
3090	4004	18.56	18.56	7.52	22.21	3423	8010	105.74	105.74	7.15	41.00
5288	7007	34.14	34.14	7.60	21.97	5258	13014	541.18	541.18	1.95	40.15
7507	10001	25.82	34.29	3.95	24.77	8025	20021	157.23	157.23	0.41	41.62
10663	14000	46.77	46.77	6.64	26.96	10011	24187	179.83	280.36	1.45	60.33
12834	17004	32.81	58.06	4.41	23.91	12409	30007	114.51	114.51	0.07	55.98
15136	20000	58.31	58.31	0.47	25.47	14691	38027	731.69	1004.13	1.40	37.81
17554	23008	45.68	64.90	0.82	25.62	17182	43013	554.27	554.27	5.59	46.36
20590	27008	51.60	76.41	4.70	26.64	20261	49021	657.47	784.02	3.52	41.41

Cluster Dynamics

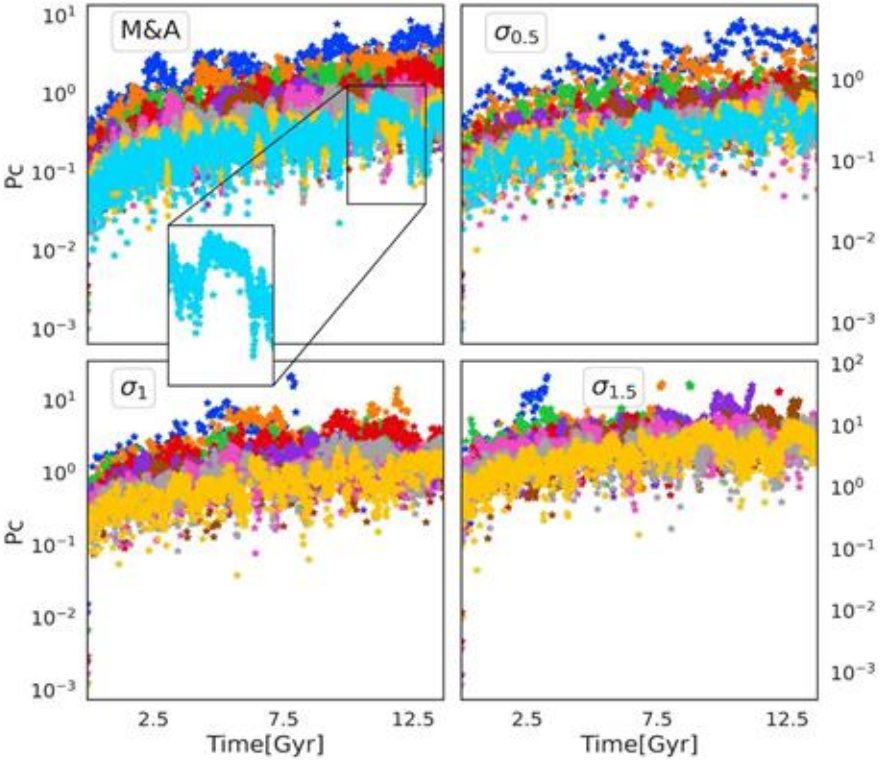
Clusters expand with time while core radius stays almost constant

JFN+JGB [2405.06391]

$R_{HM}(t)$

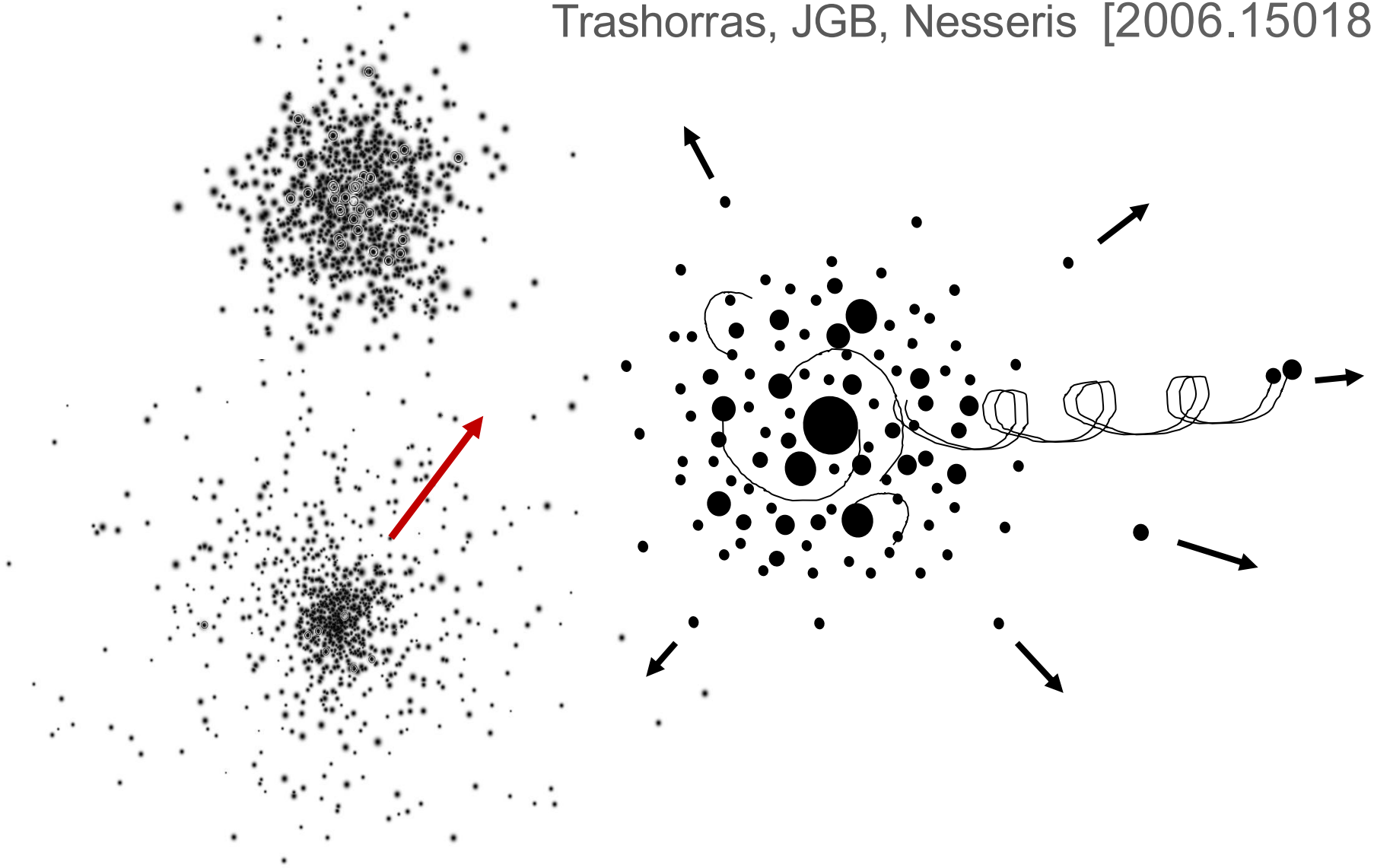


$R_c(t)$



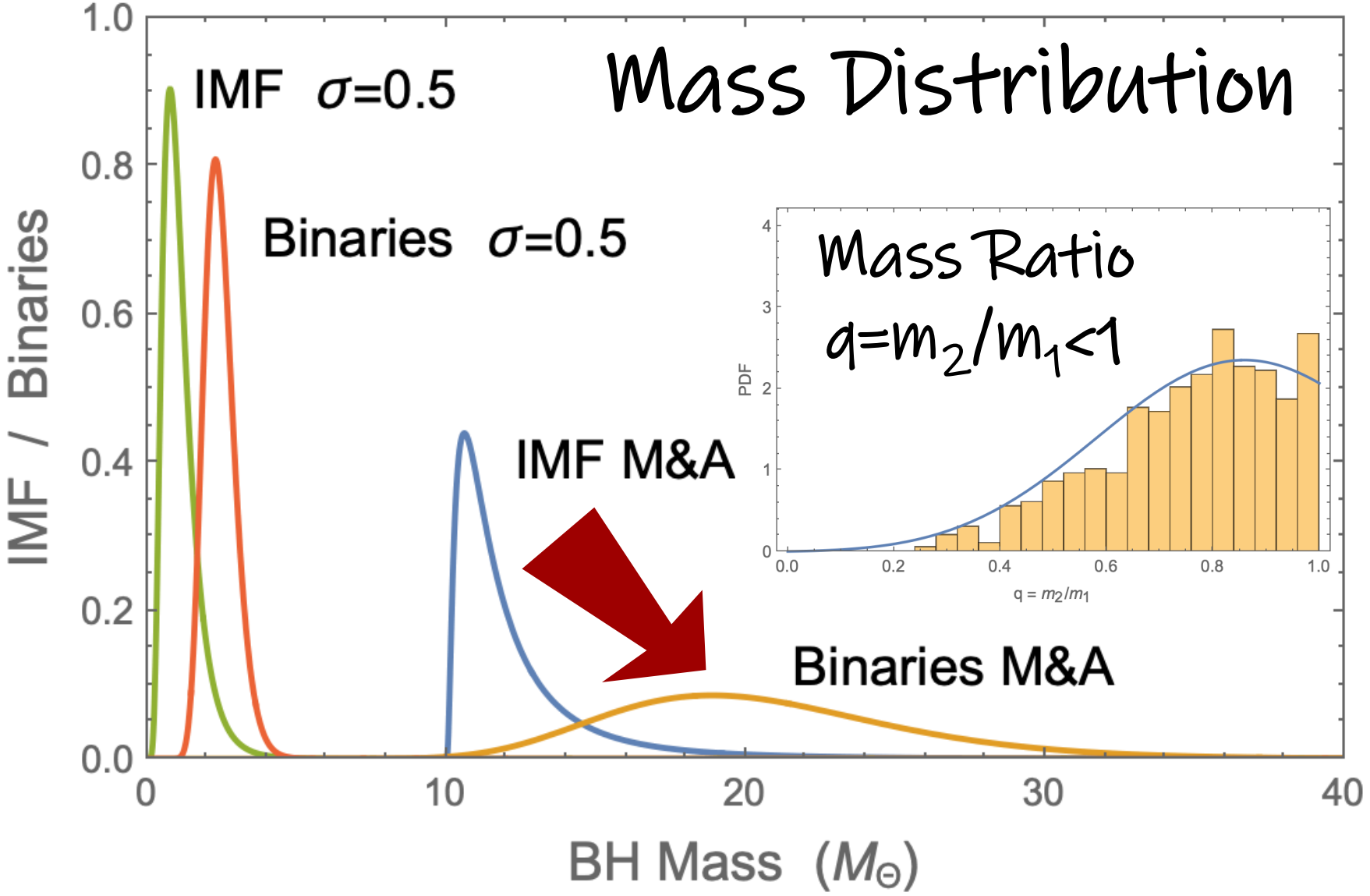
Cluster Dynamics

Trashorras, JGB, Nesseris [2006.15018]

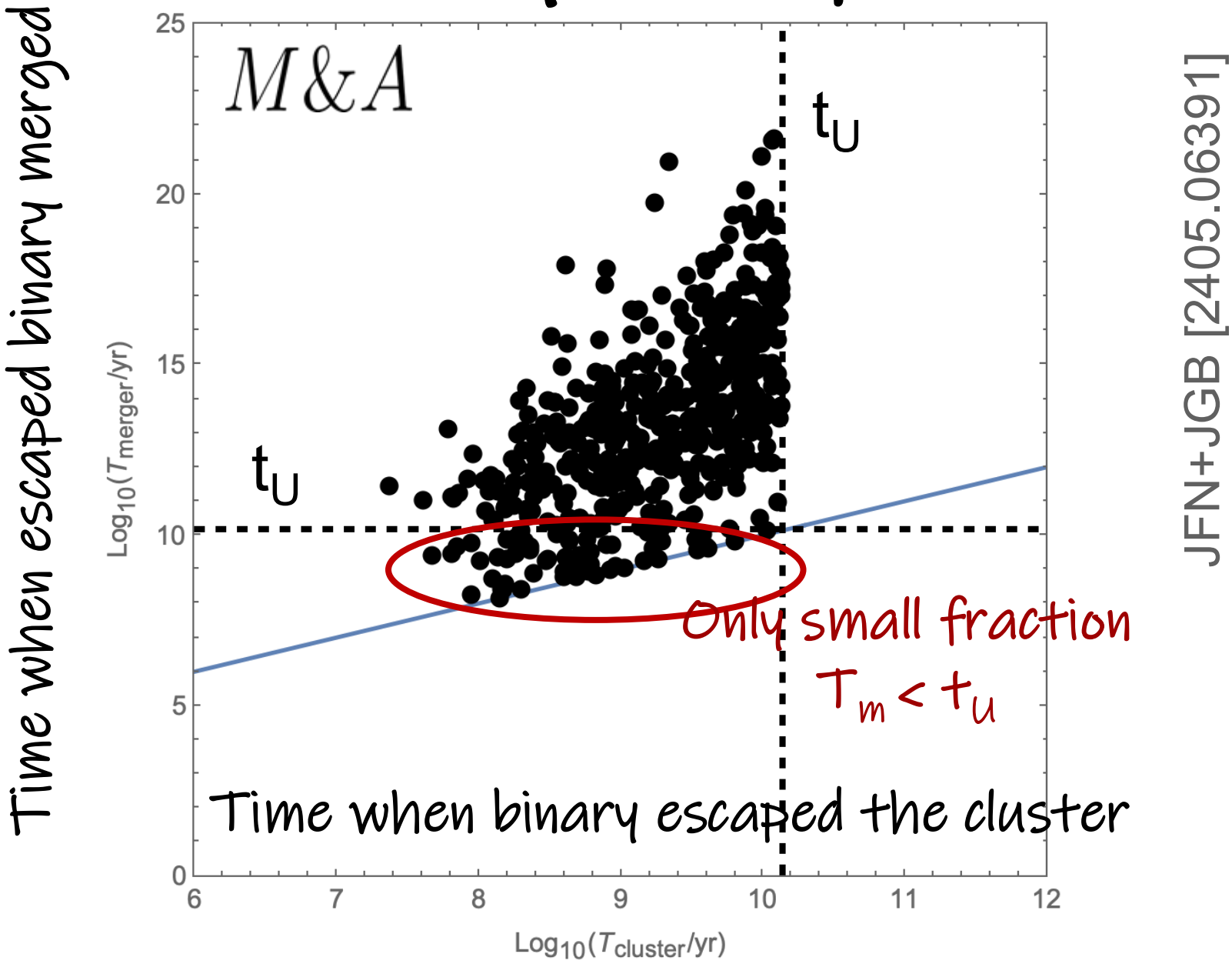


Binary escapers

JFN+JGB [2405.06391]



Binary escapers

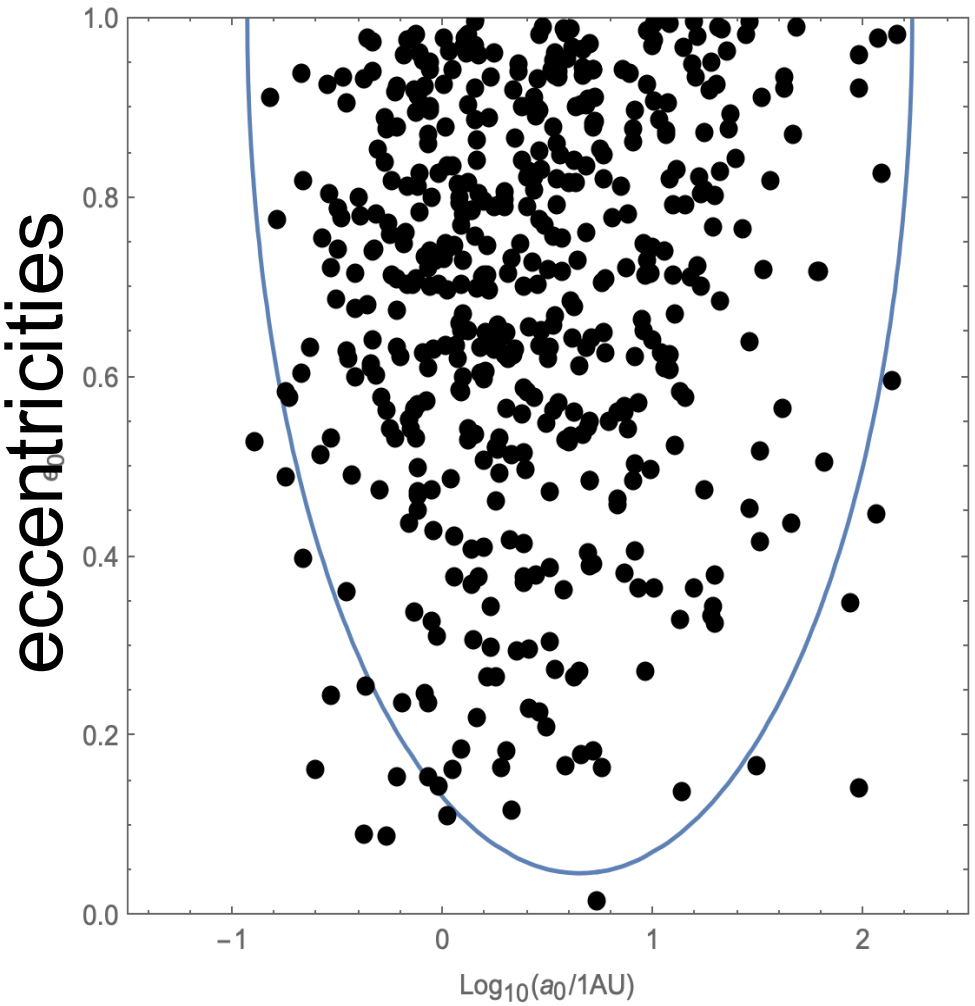


JFN+JGB [2405.06391]

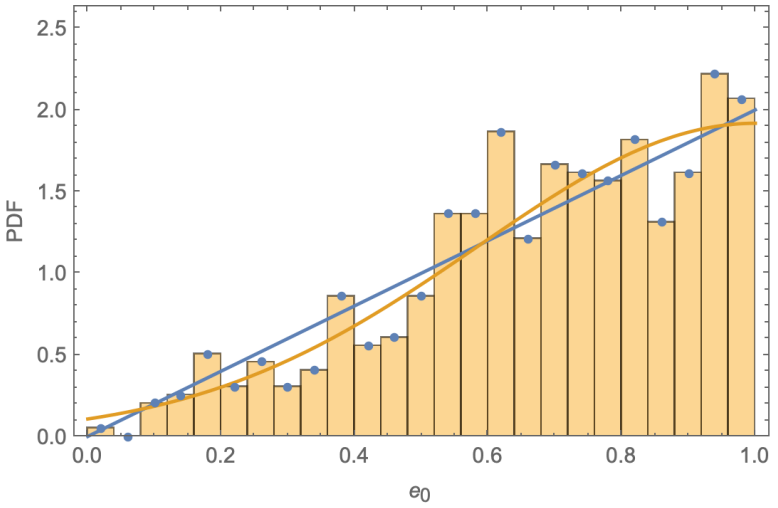
Binary escapers

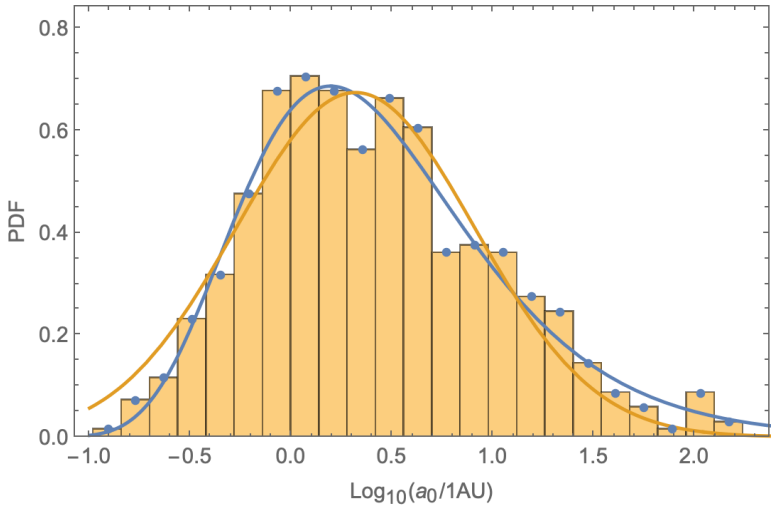
M&A

JFN+JGB [2405.06391]



semimajor axis [AU]

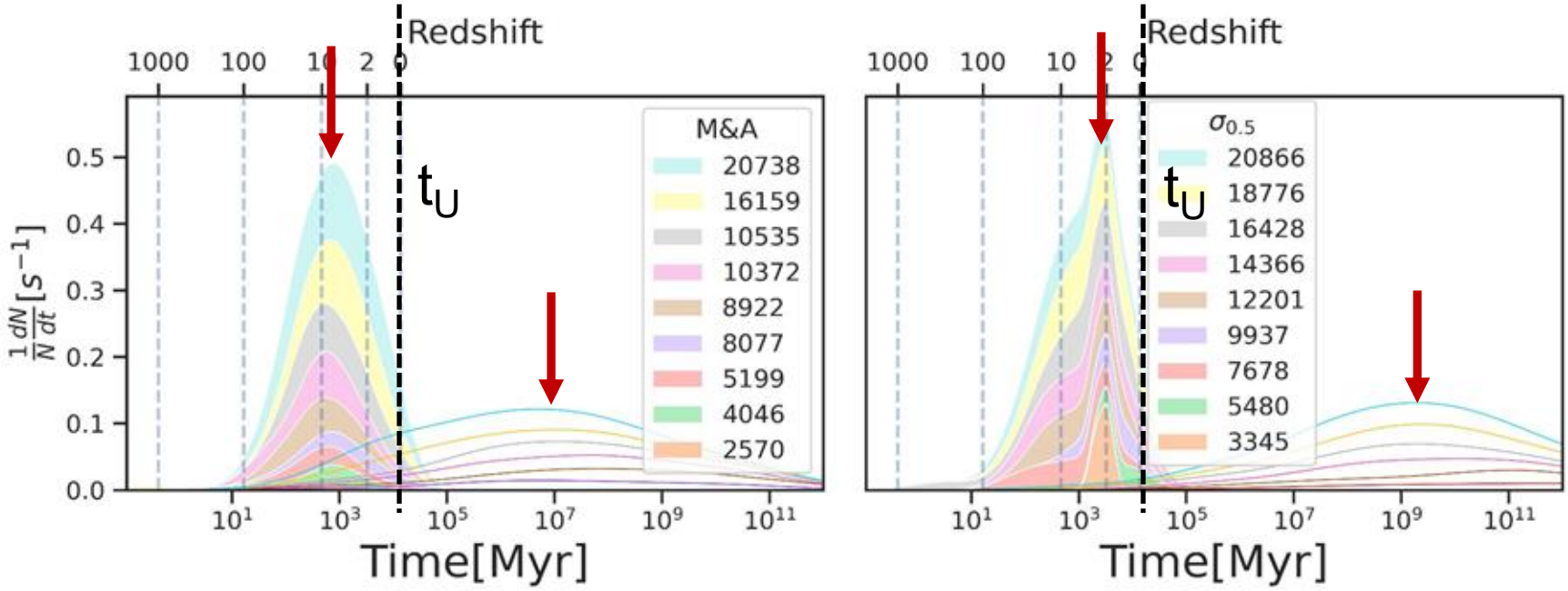




BBH merger rates

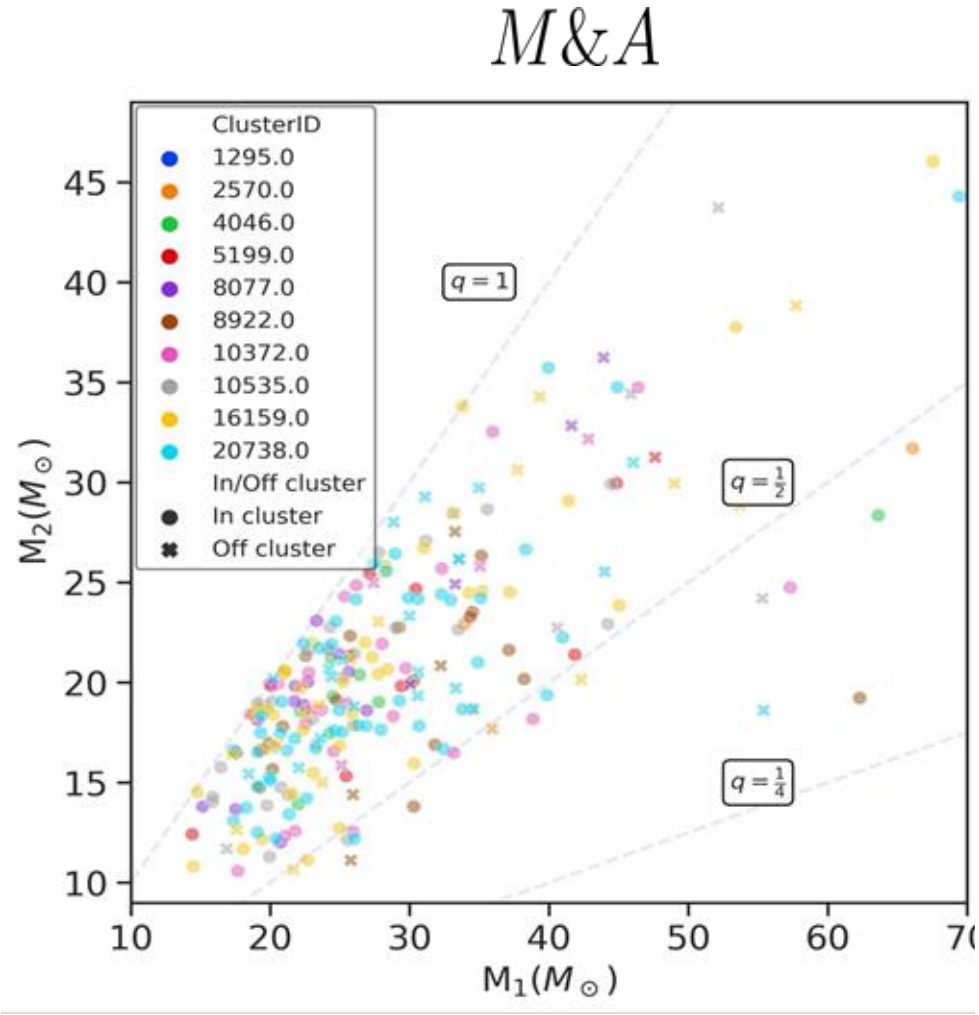
In-cluster merger rate
for $\sigma_{0.5}$ peaks at z~8
for $M\&A$ peaks at z~2

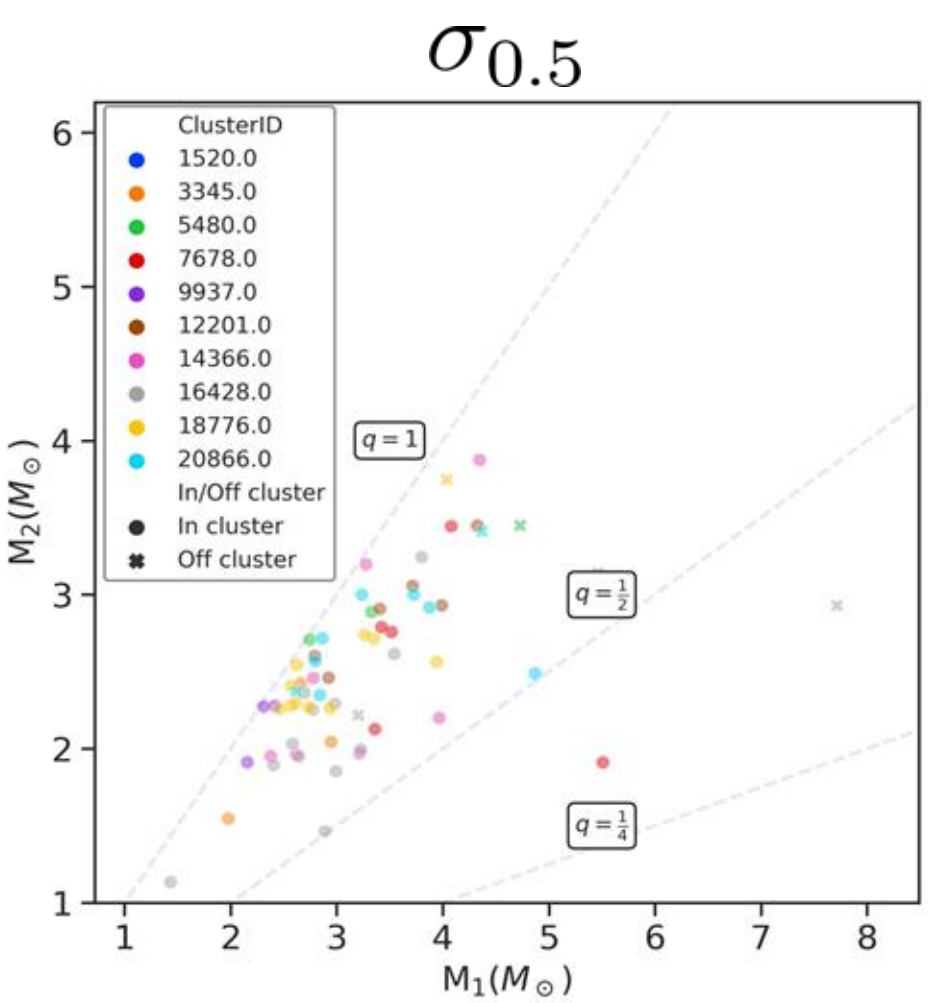
Escapers merger rate
$\sigma_{0.5}$ peaks at 10^3 t_U
$M\&A$ peaks at 10^5 t_U



In-cluster and binary escapers merger rate

BBH merger masses

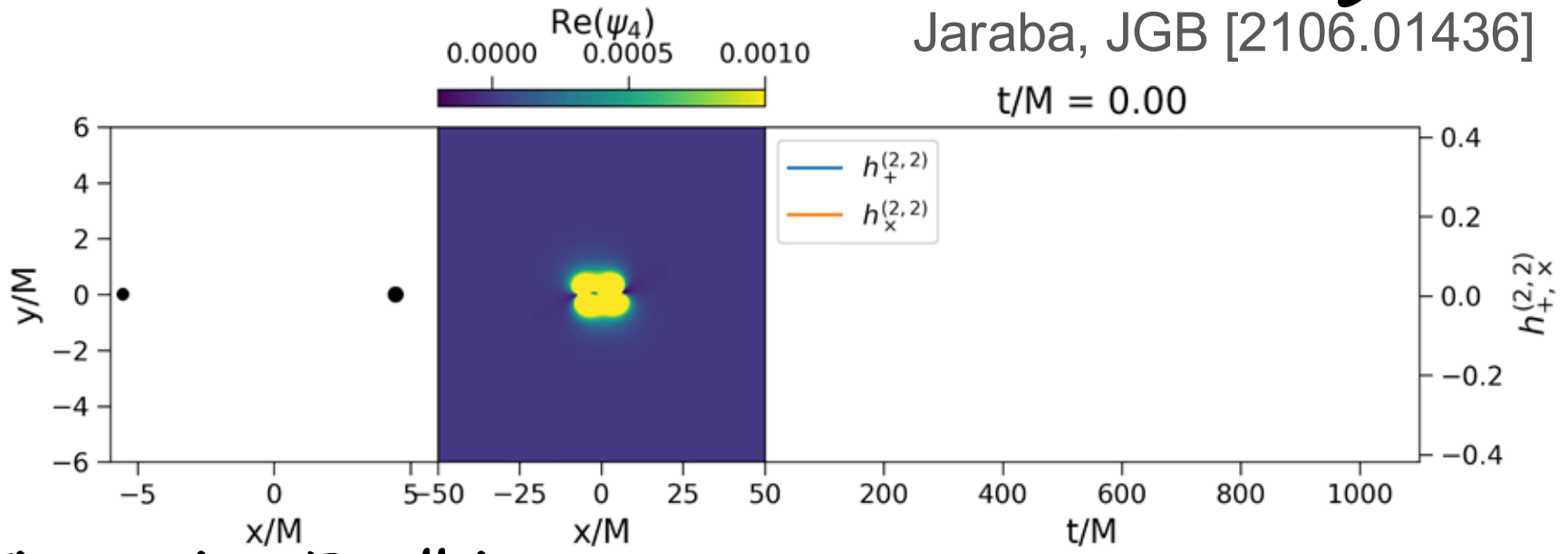




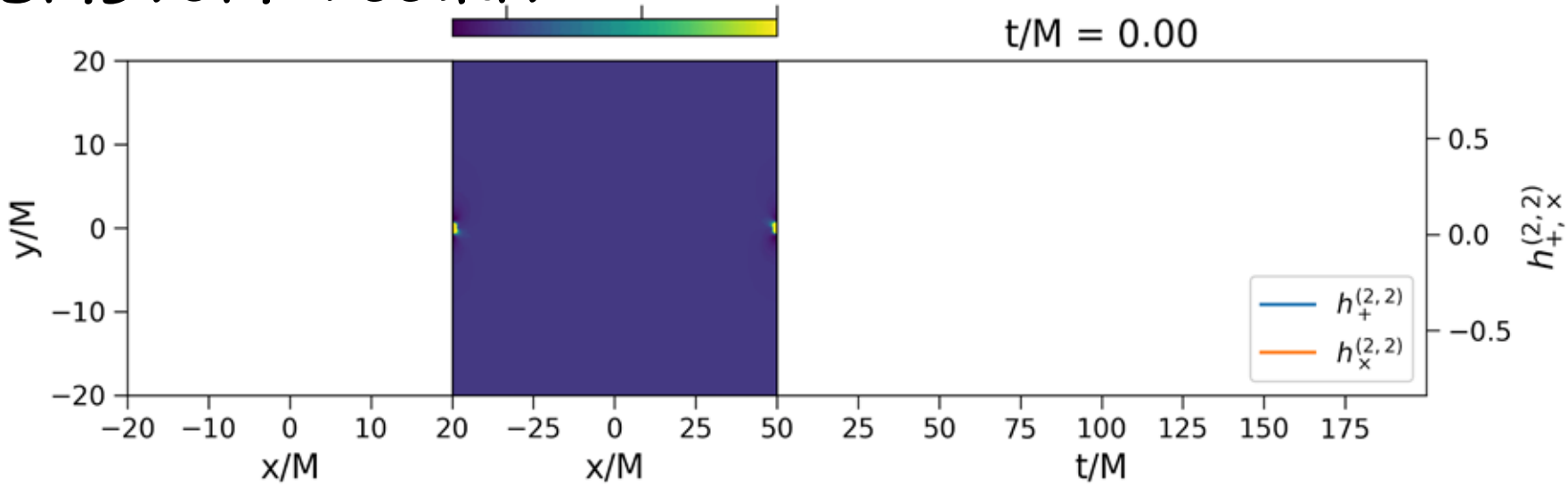
Distribution of the masses (m_1, m_2) of the BBHs mergers

Inspirals vs scatterings

Jaraba, JGB [2106.01436]

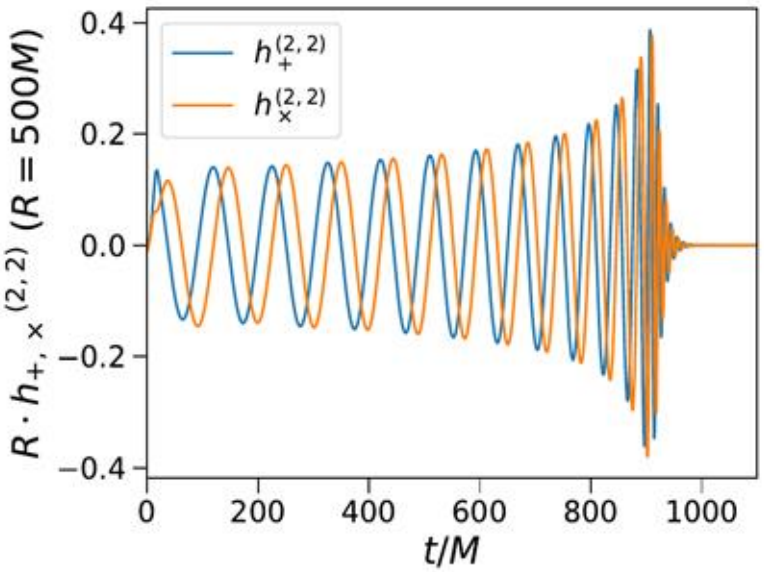


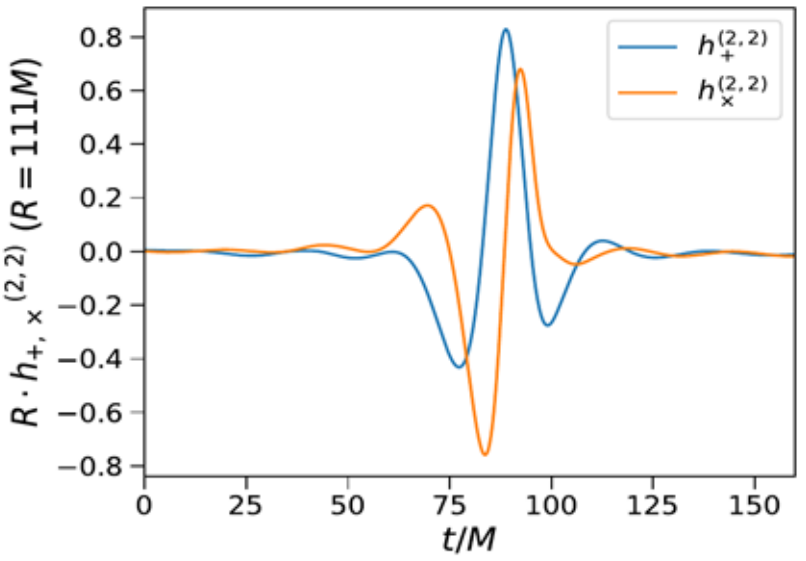
Einstein Toolkit



Inspirals vs scatterings

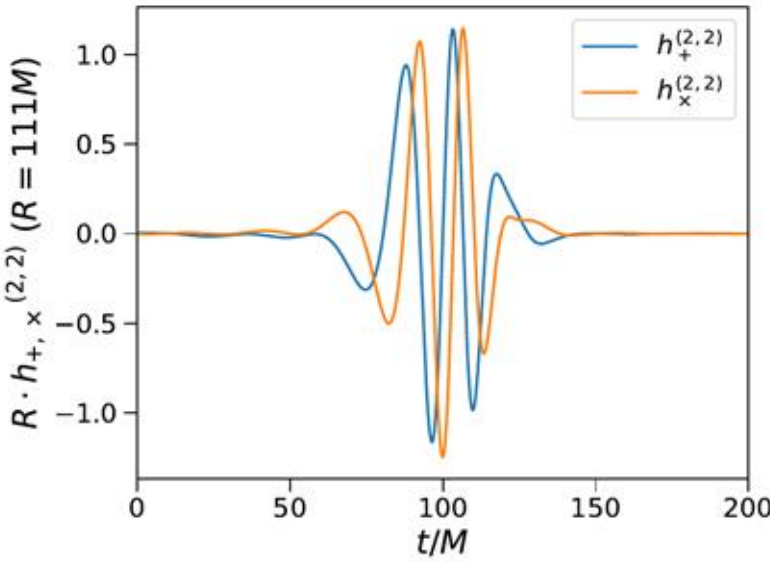
CBC (GW150914)

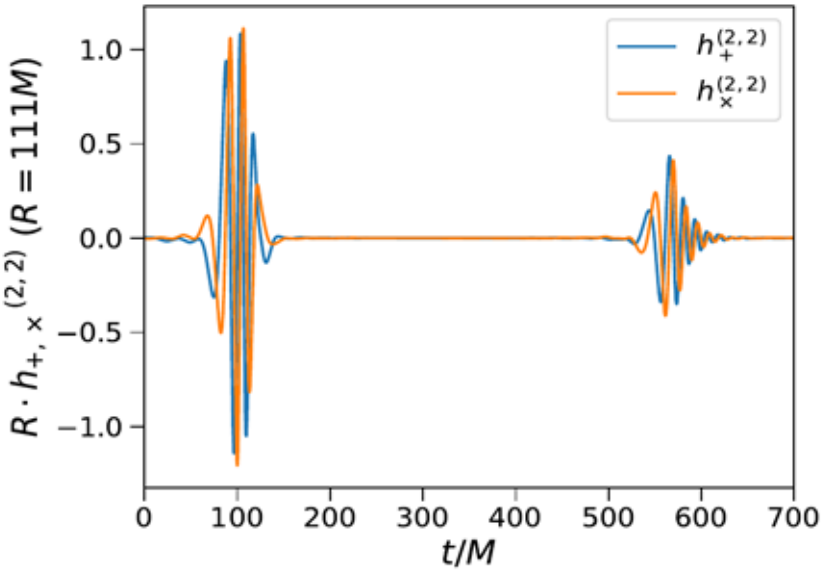




CHE (d/M=100, q=1, p/M=0.49, θ=4.01°)

CHE (d/M=100, q=1, p/M=0.49, θ=3.12°)



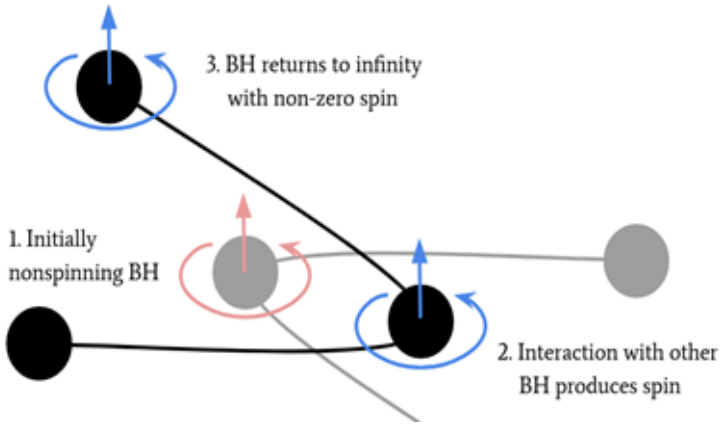


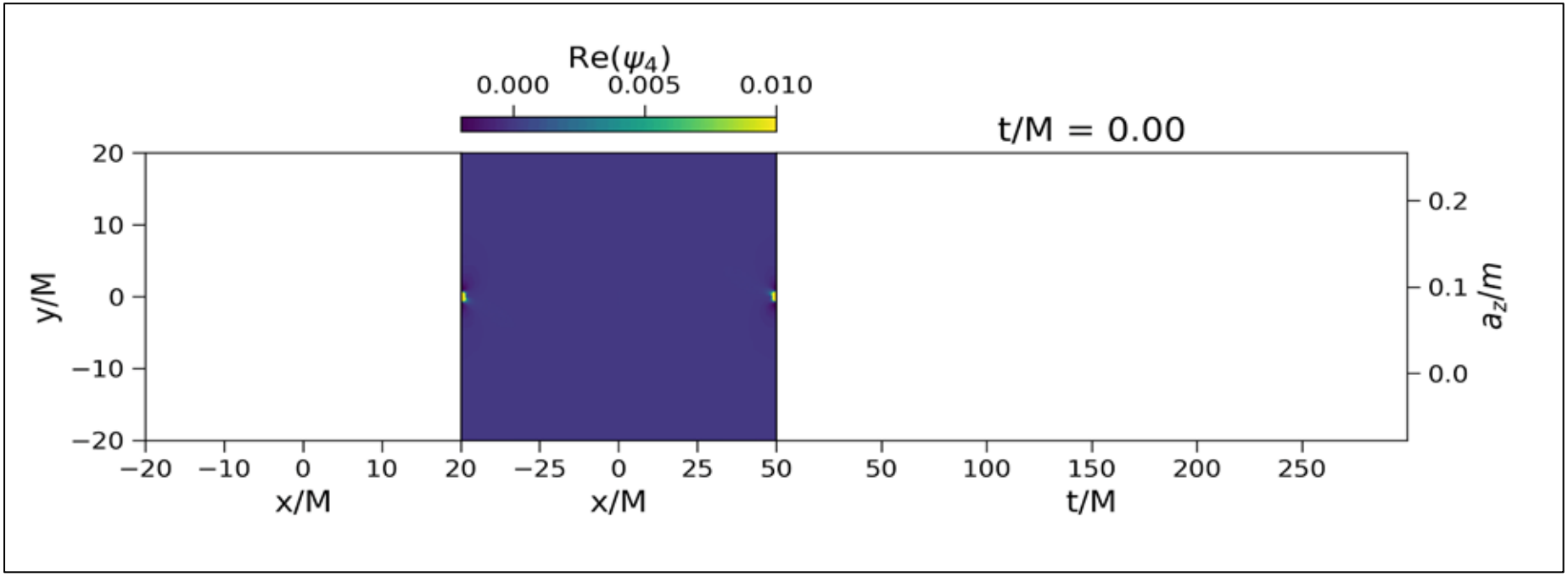
Dynamical capture (d/M=100, q=1, p/M=0.49, θ=3.11°)

Spin induction in dense clusters

Spin acquired at periastron, during GW emission.

Characterized by Kerr parameter **a**.

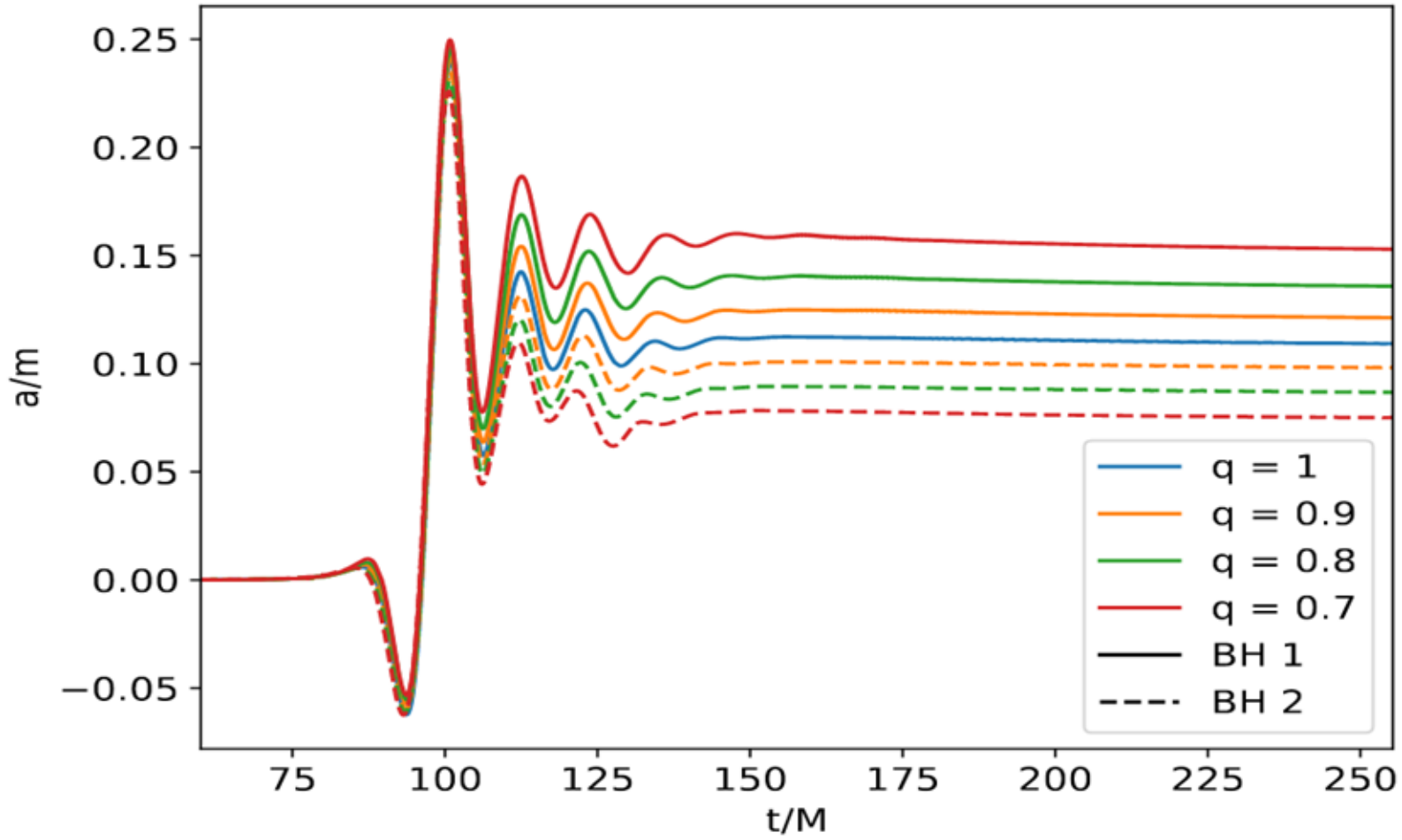




Spin induction in dense clusters

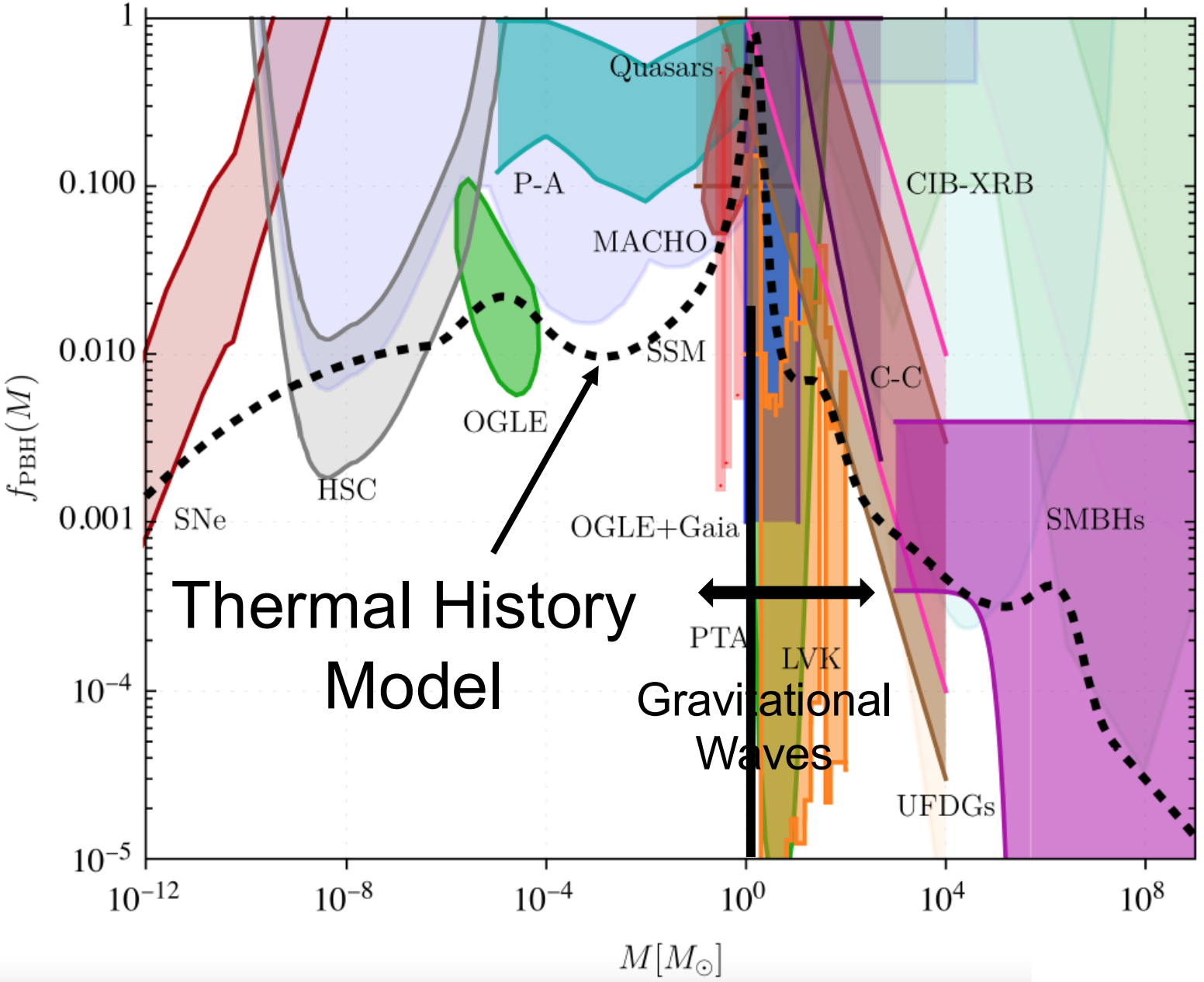
Highest spin is induced in most massive black hole. $q = m_2/m_1 \leq 1$.

Spin induction is enhanced for the massive black hole when $q << 1$.



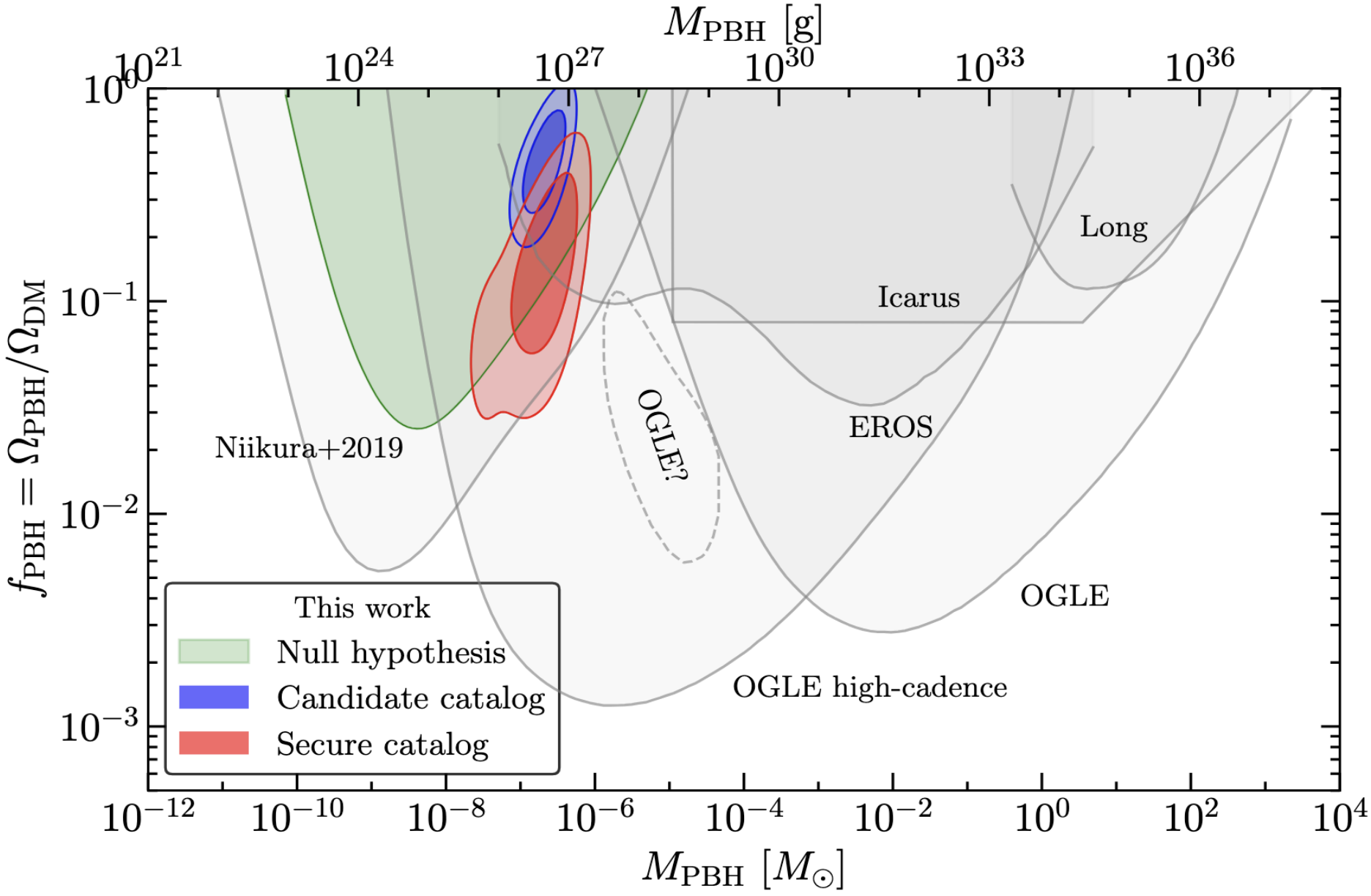
Observational evidence for primordial black holes

Carr, Clesse, JGB, Hawkins, Kühnel [2306.03903]

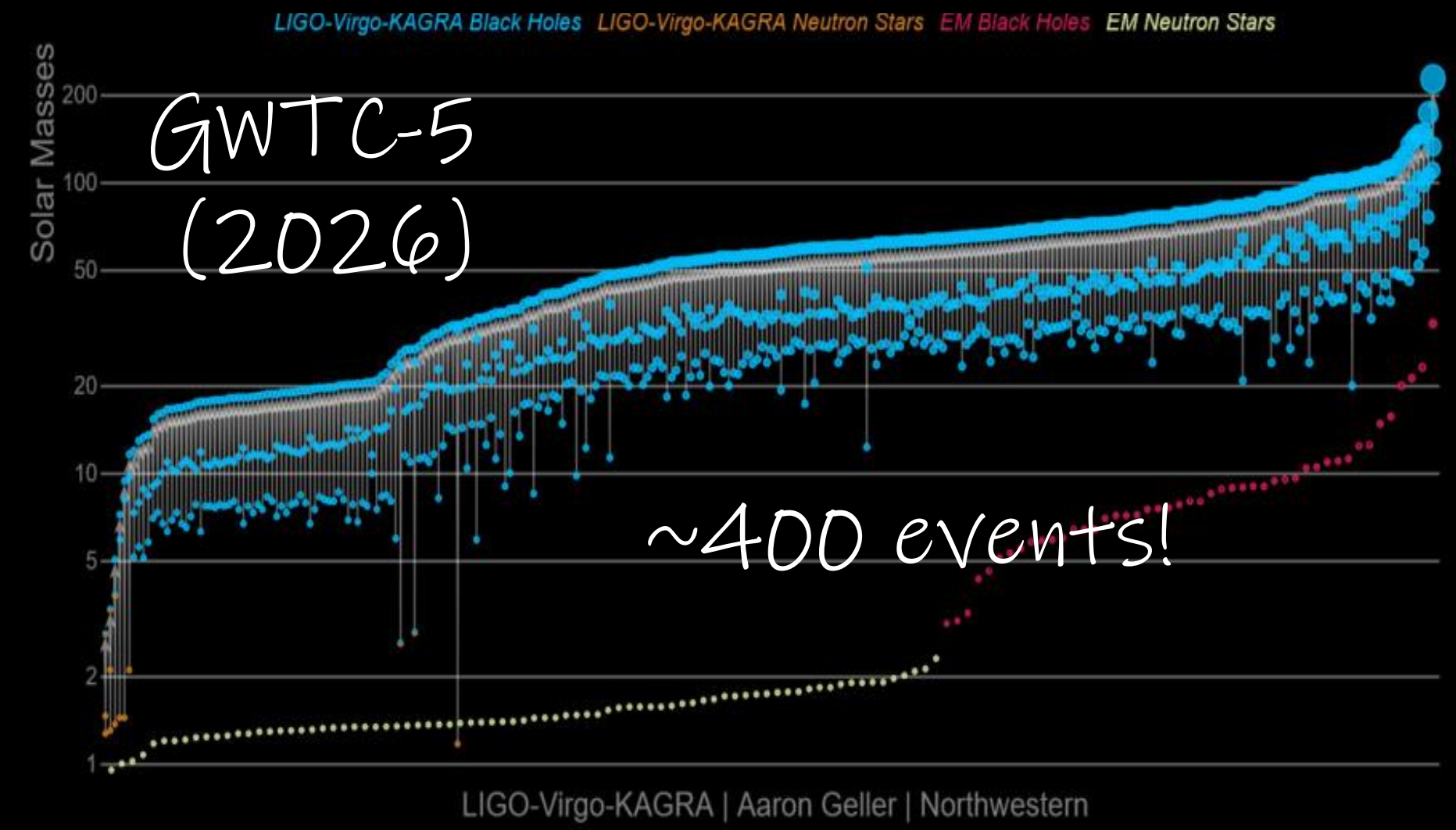


μlensing to Andromeda

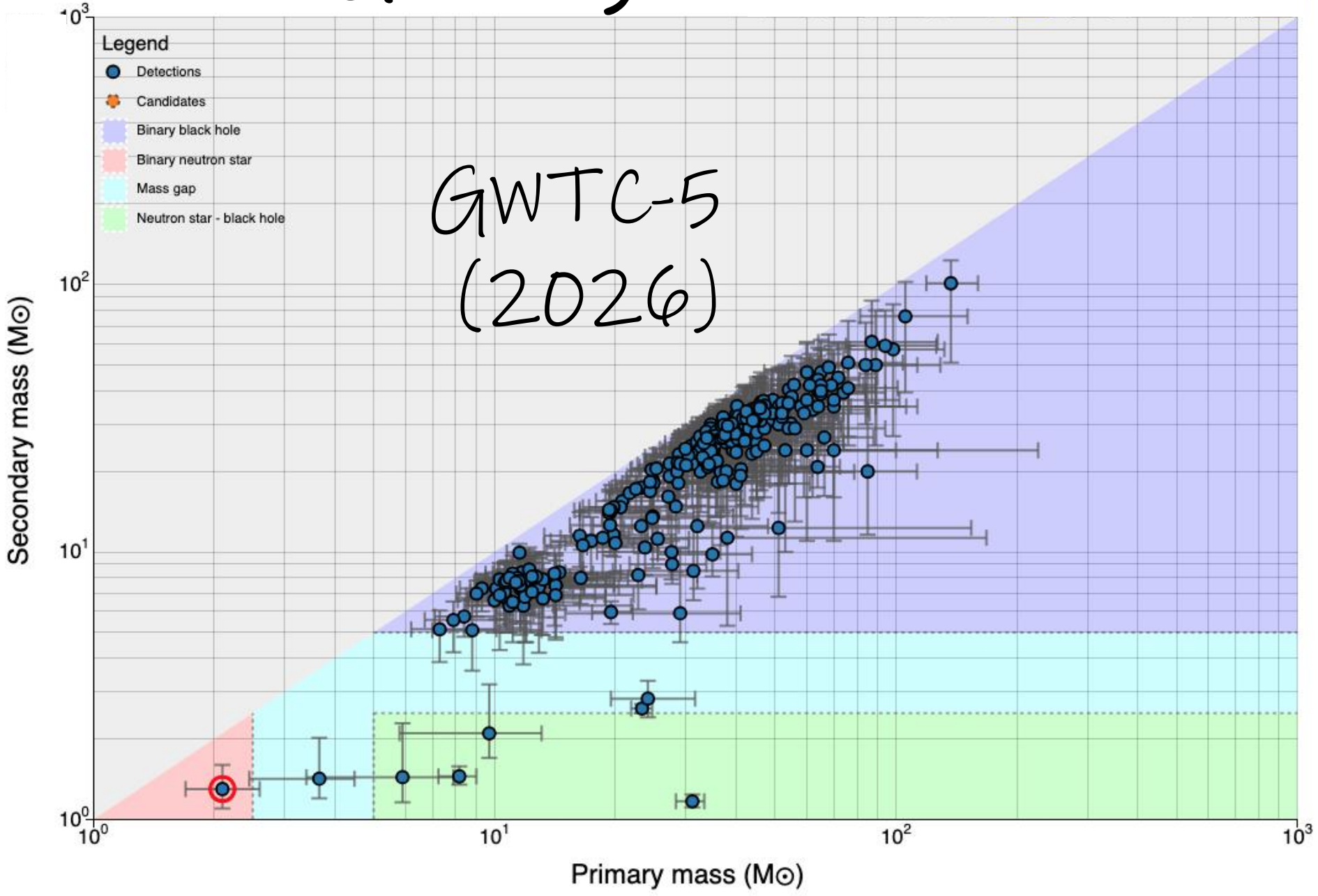
Sugiyama et al. [2602.05840]



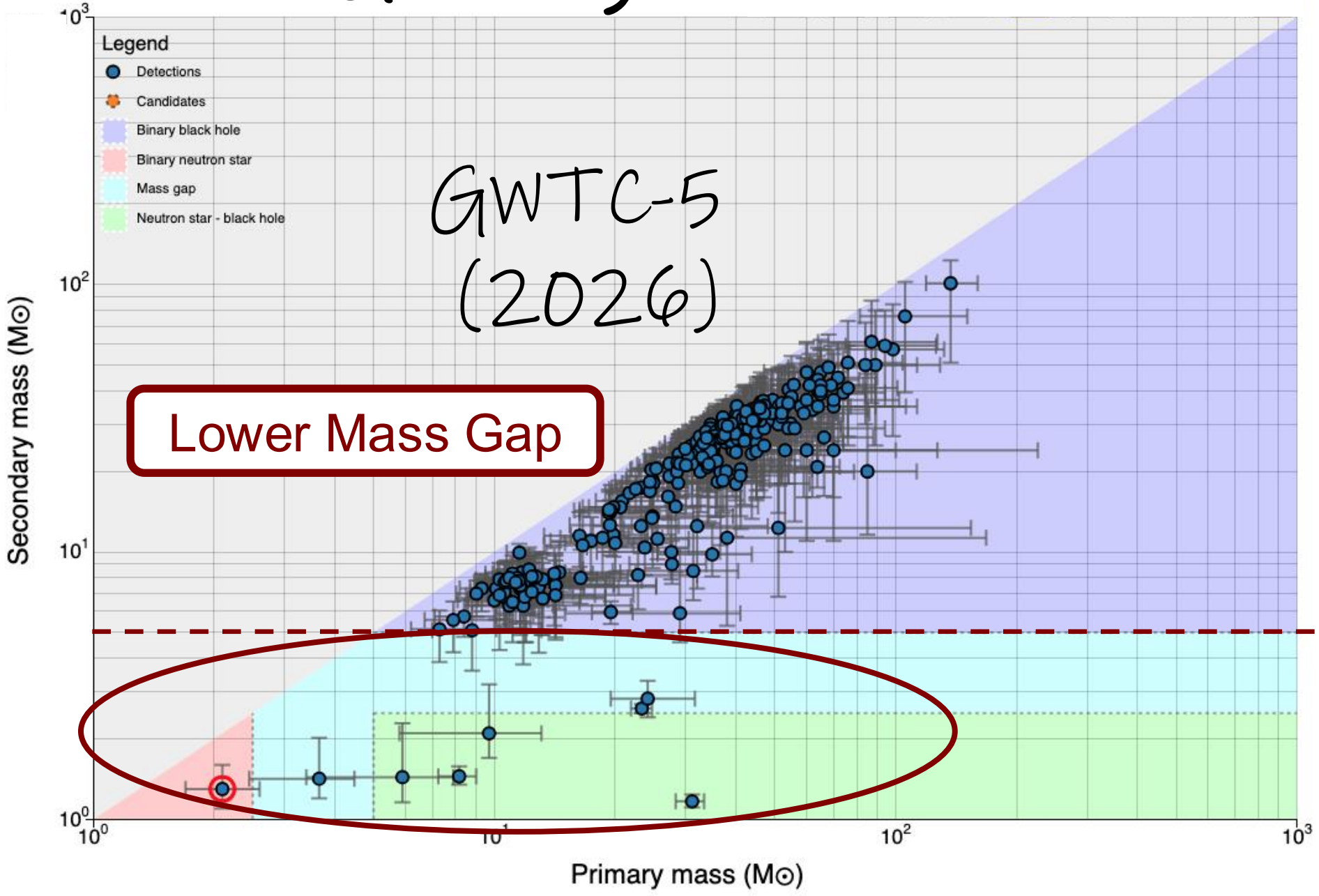
Masses of Black Holes and Neutron Stars



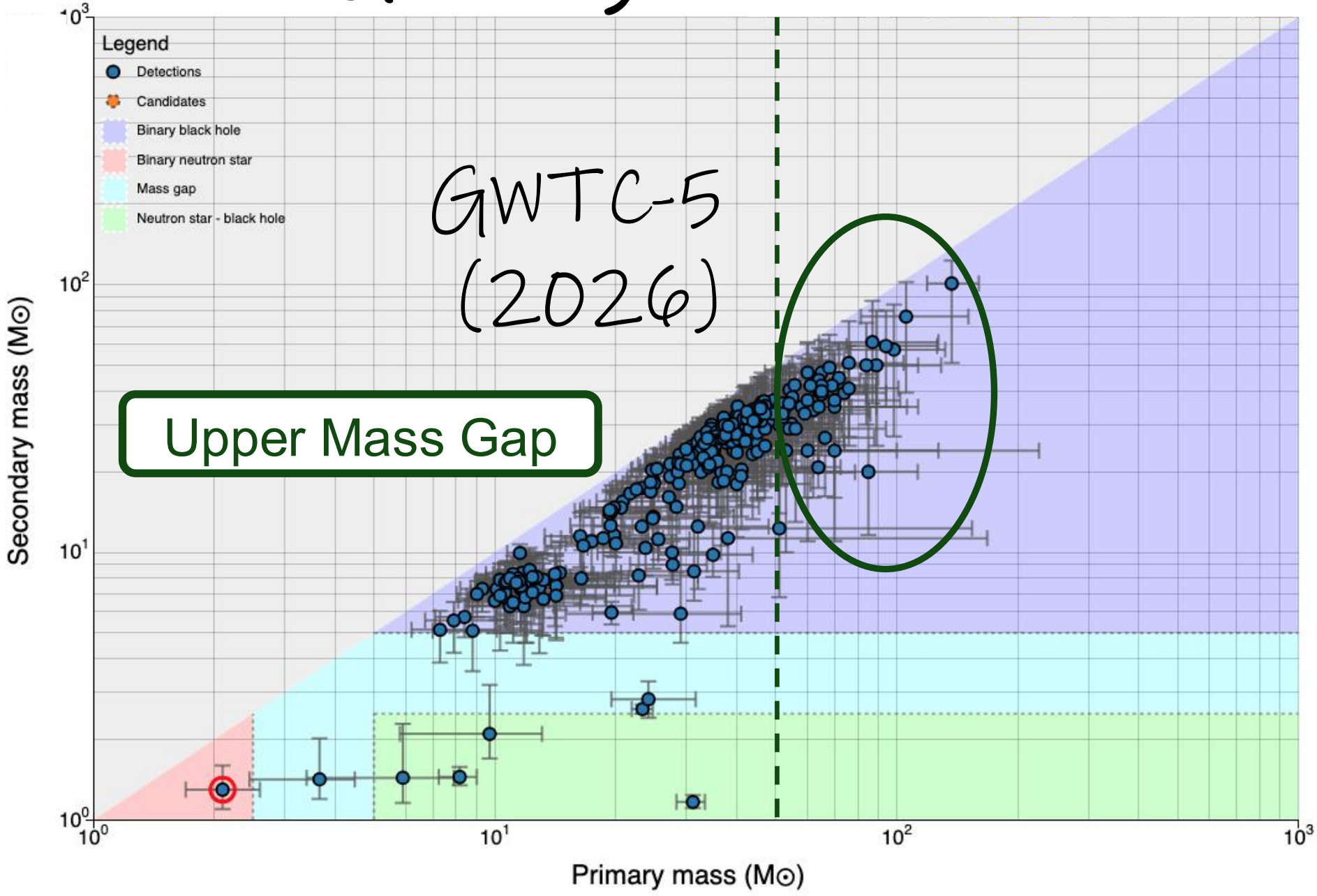
Are LIGO/Virgo BH Primordial?



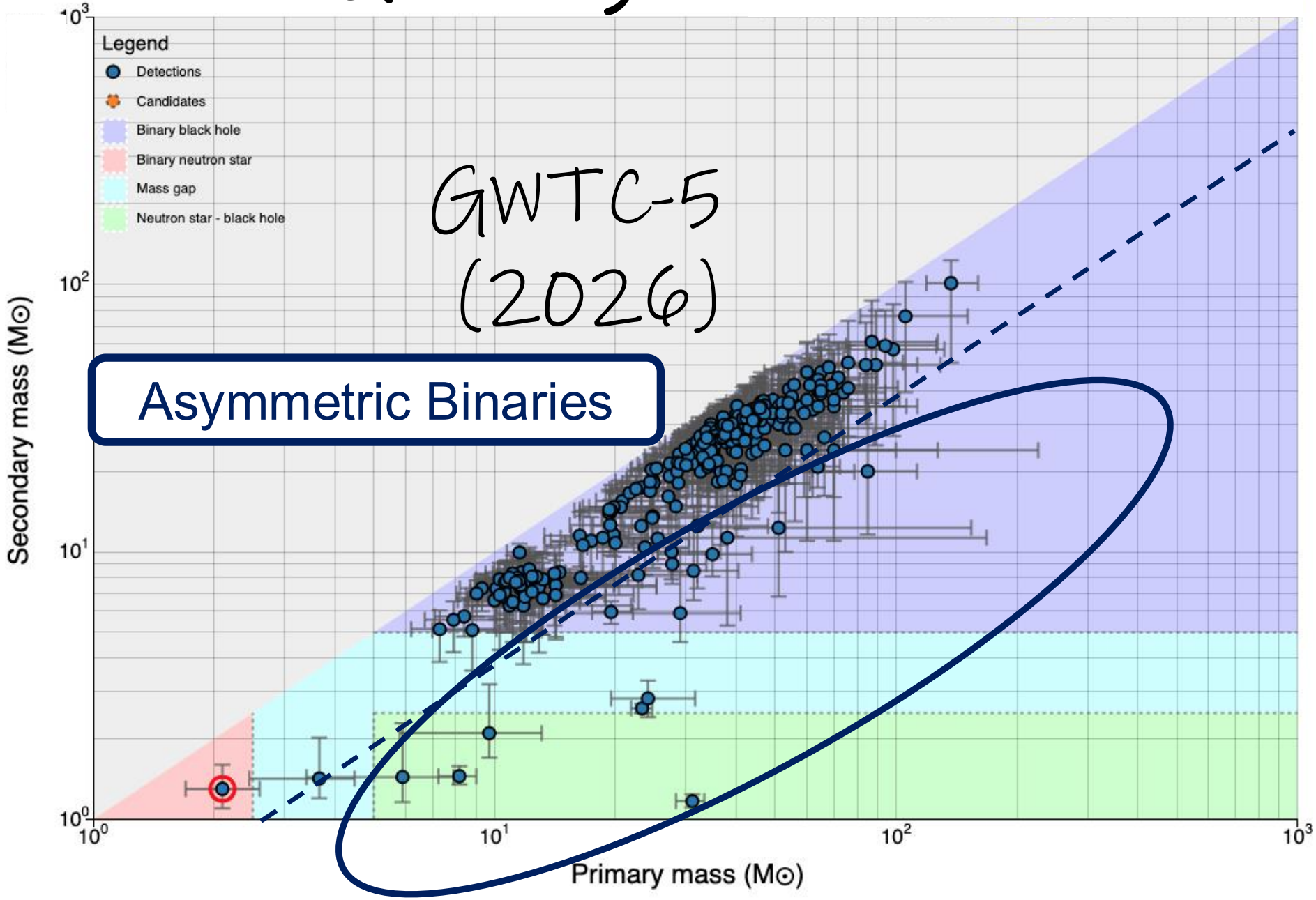
Are LIGO/Virgo BH Primordial?



Are LIGO/Virgo BH Primordial?

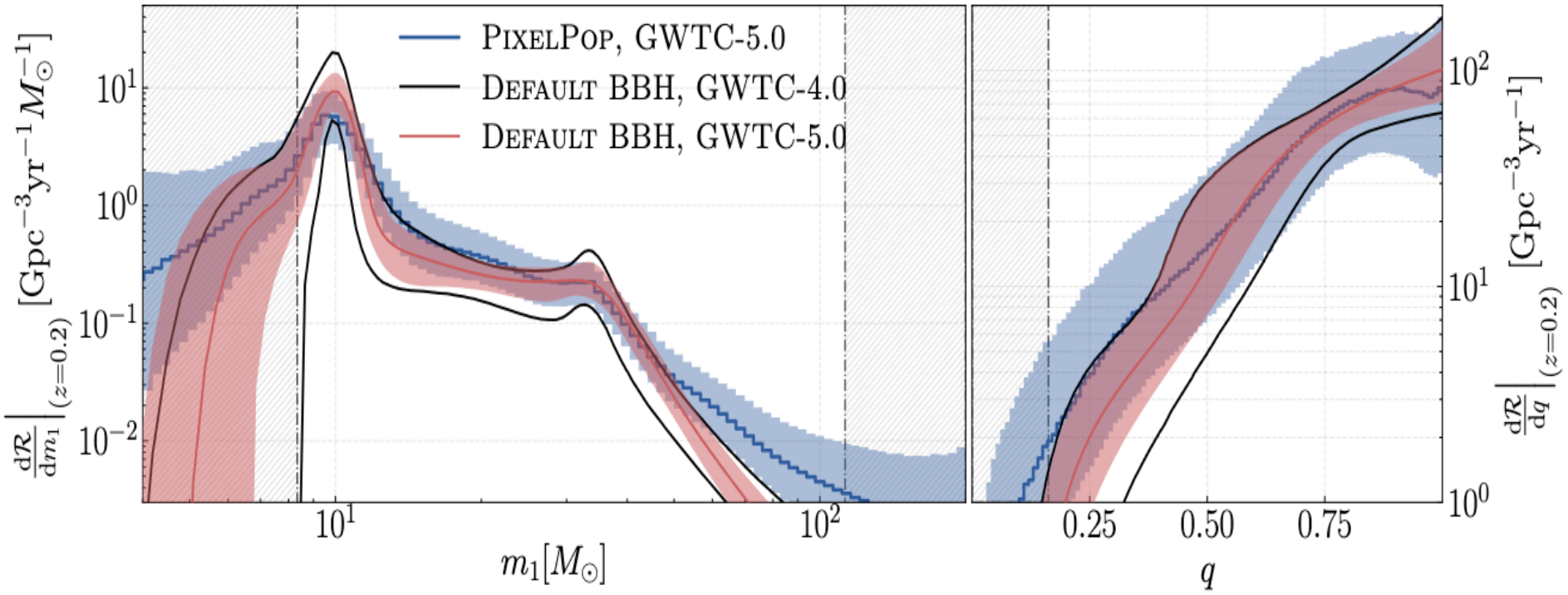


Are LIGO/Virgo BH Primordial?



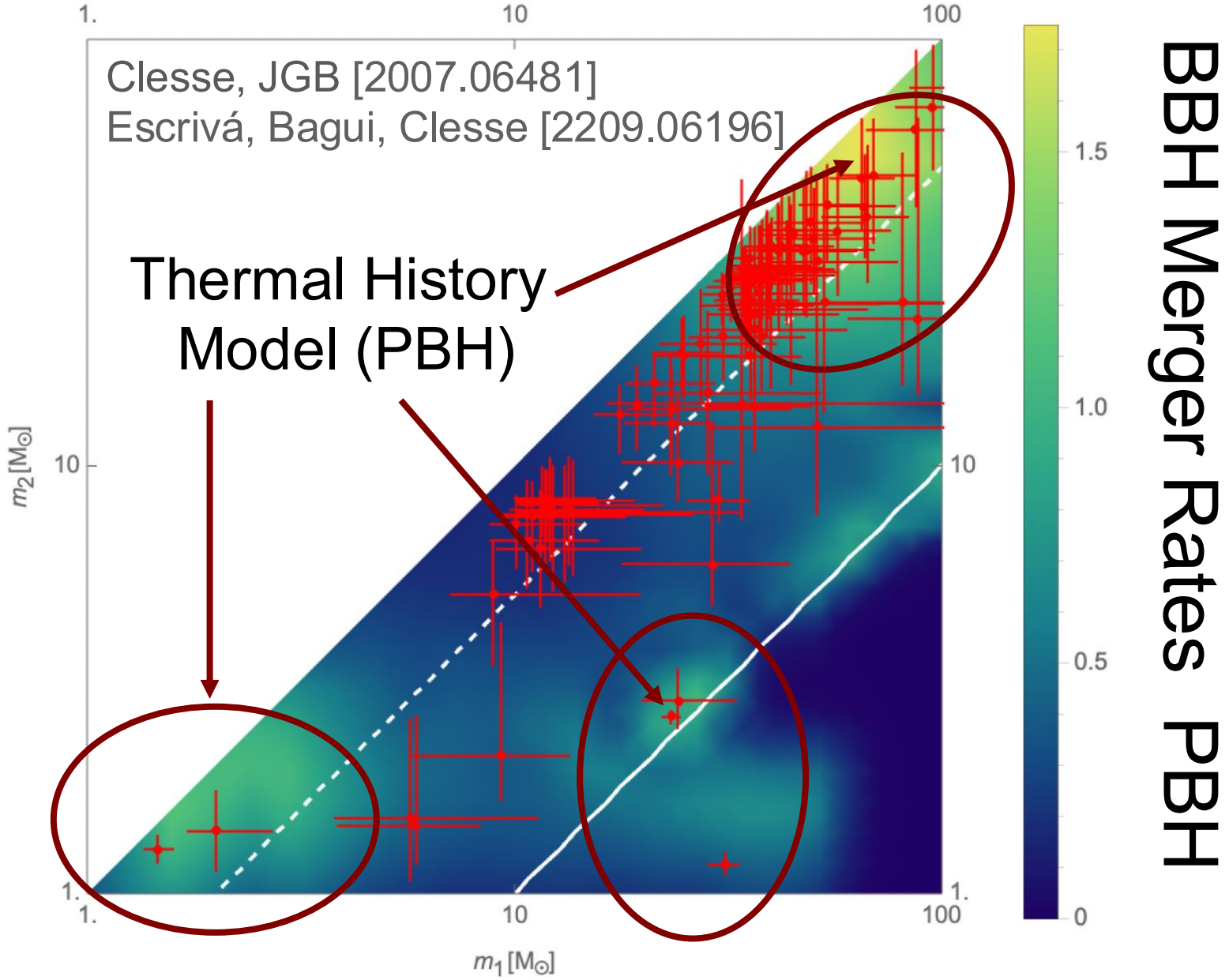
Mass distributions GWTC-5

LVK [2605.27226]



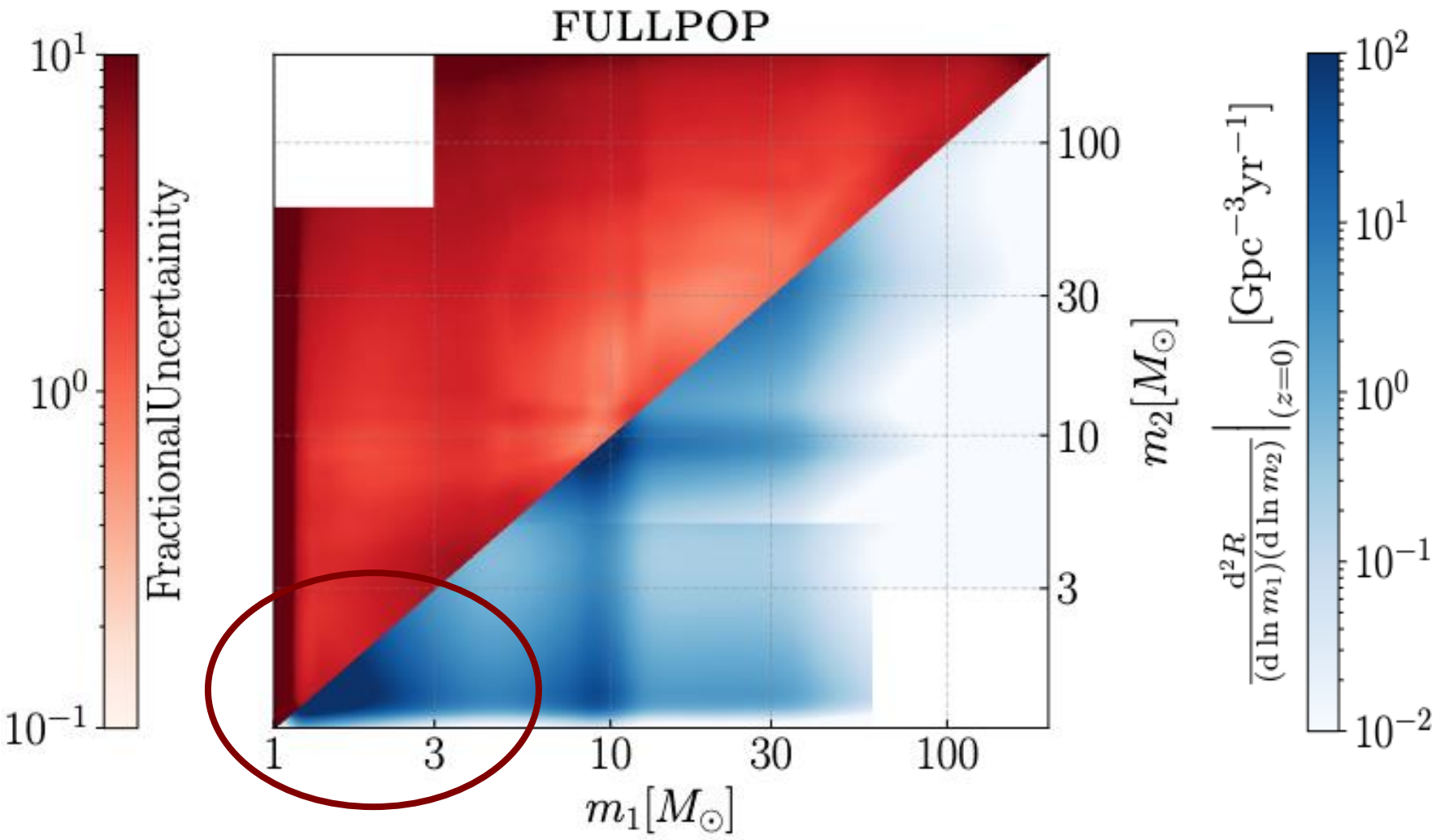
PBH Transfer function: From IMF to Binary Escapers

Are LIGO/Virgo BH Primordial?



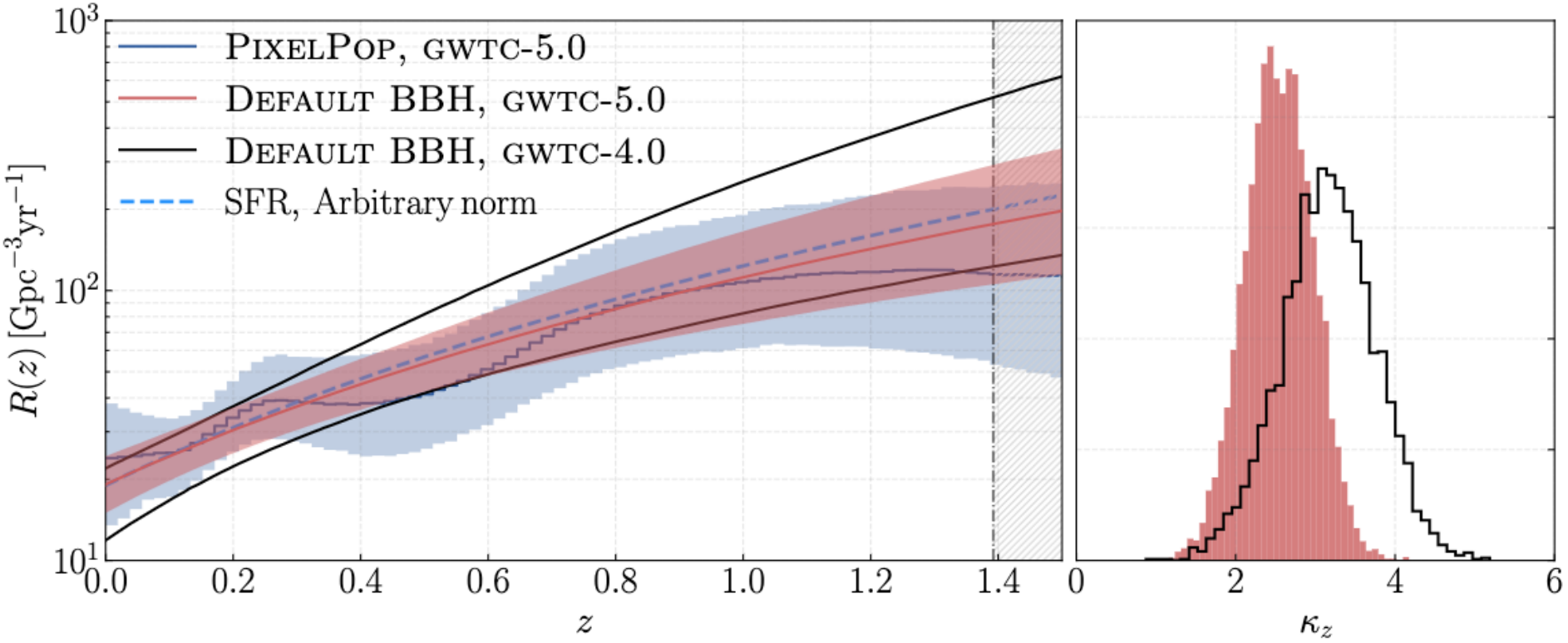
BBH Merger Rates GWTC-5

LVK [2605.27226]



Merger Rates (z) GWTC-5

LVK [2605.27226]



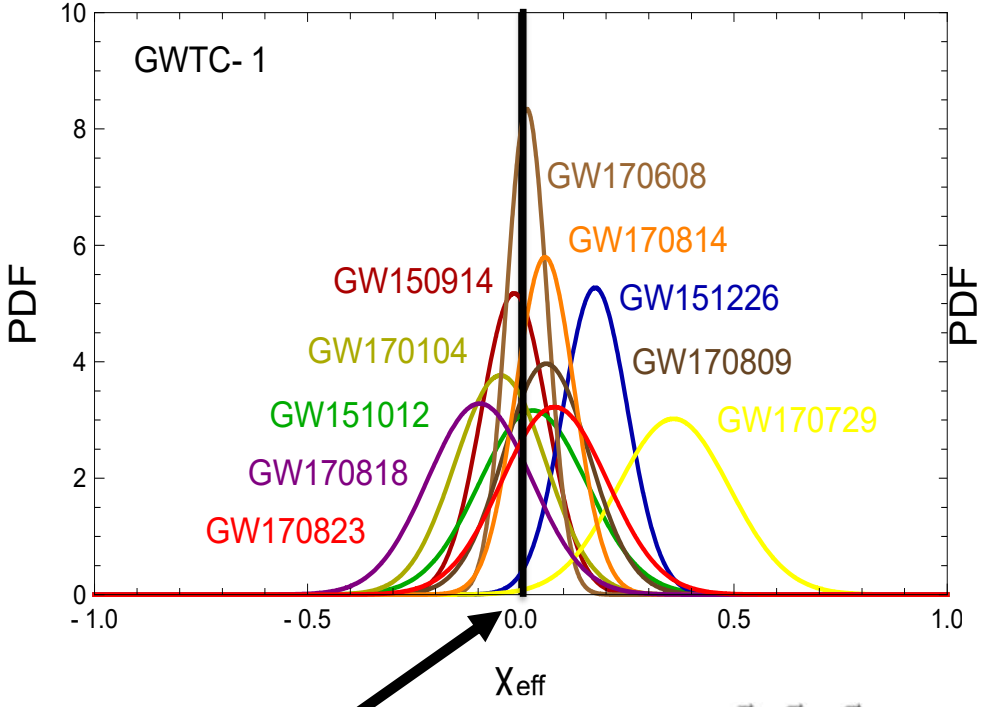
PBH : R(z) ~ $(1+z)^3$ up to z~20-50

$p(z) \propto (1+z)^{\kappa_z}$

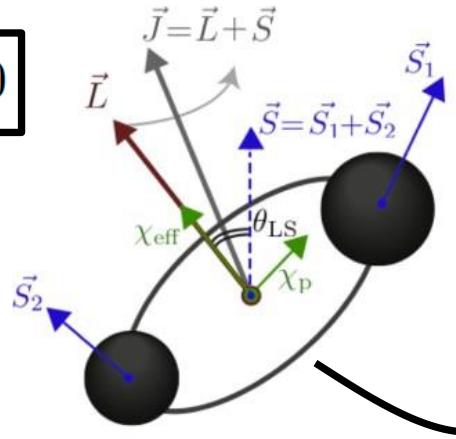
ABH : SFR peak at z~1.9 (Madau-Dickinson 2014)

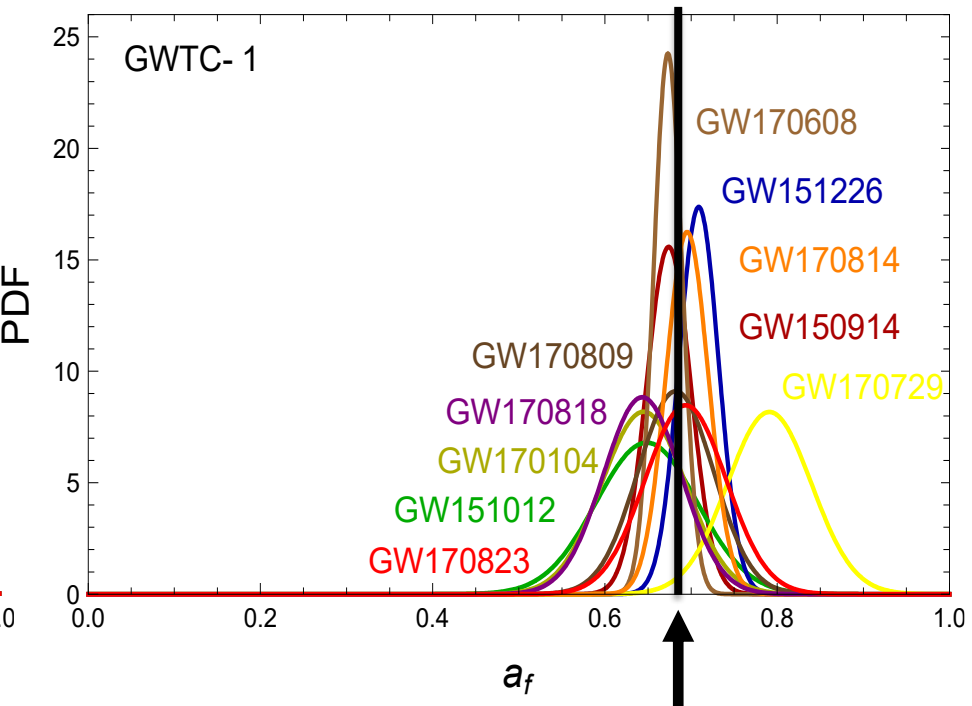
Effective and Final Spin

JGB – Phil.Trans.Roy.Soc.A 0091 (2019)



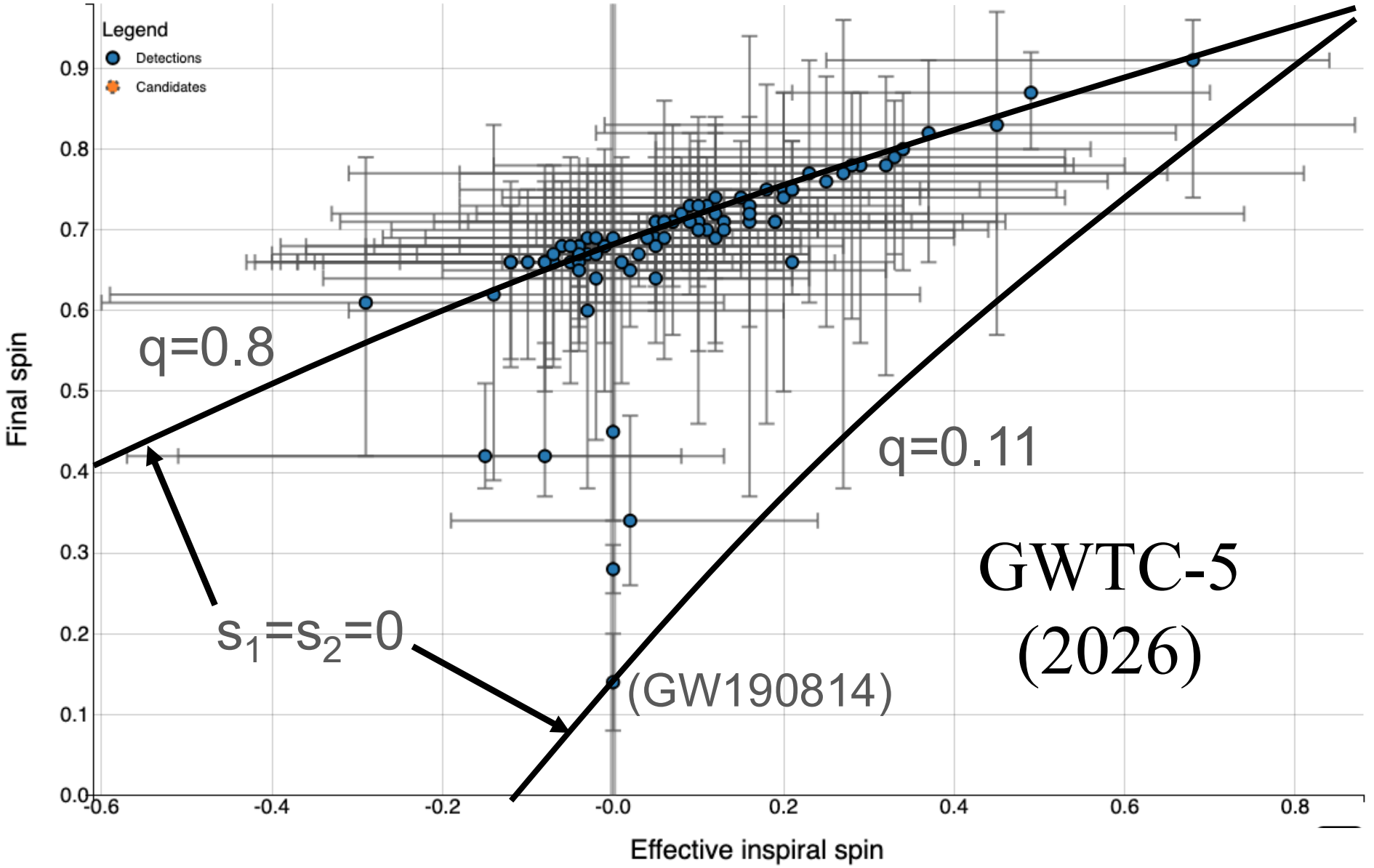
$$\chi_{\rm eff}(S_1 = S_2 = 0) = 0$$





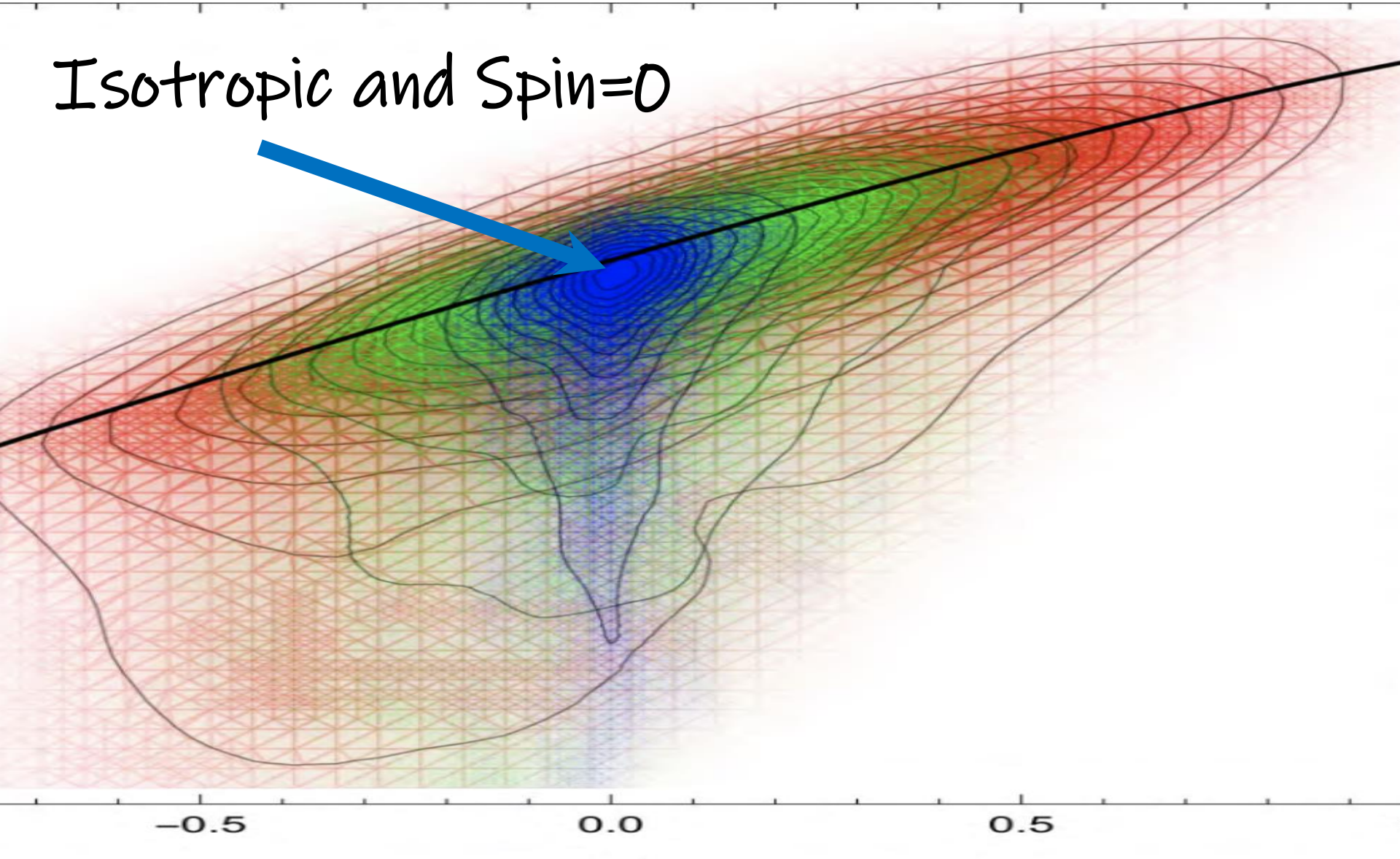
$$a_f(S_1 = S_2 = 0) = 0.686$$

Effective and Final Spin



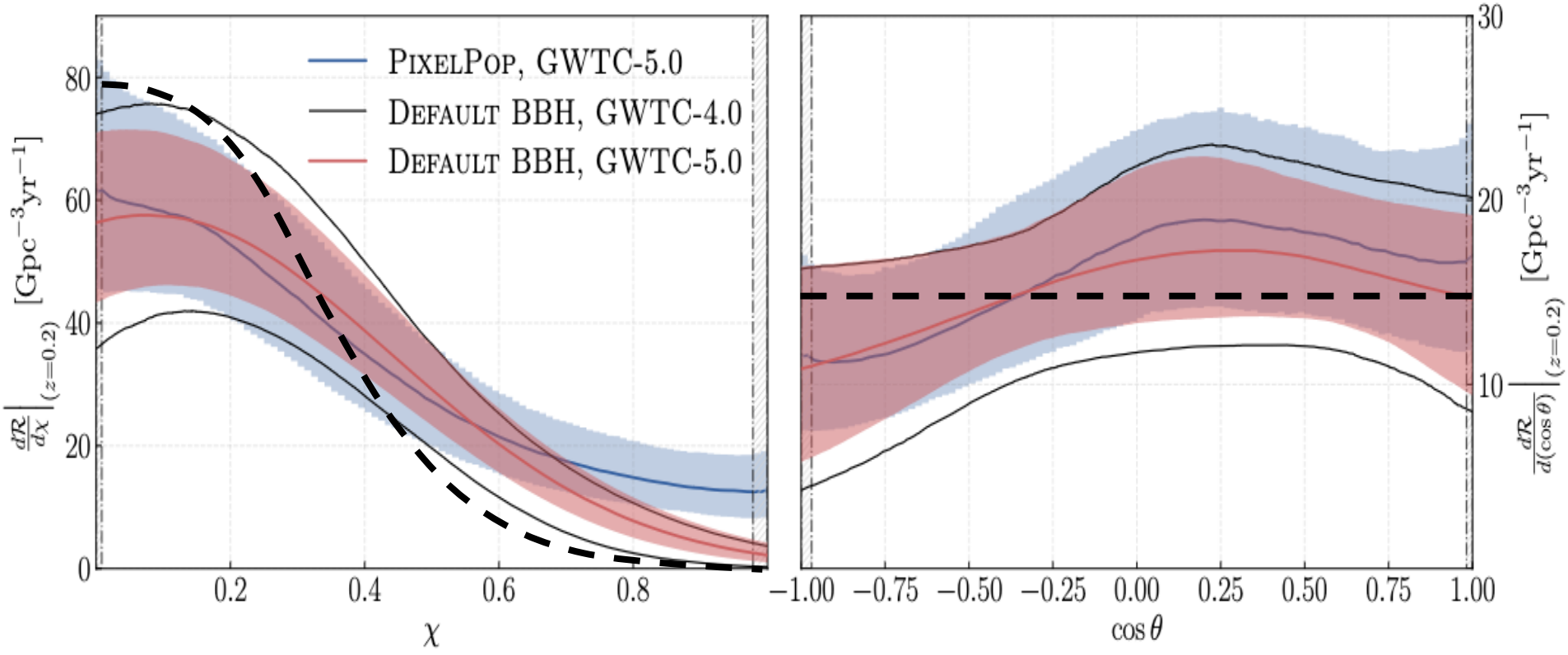
Effective and Final Spin

JGB, Nuño-Siles, Ruiz Morales [2010.13811]



Spin distributions GWTC-5

LVK [2605.27226]

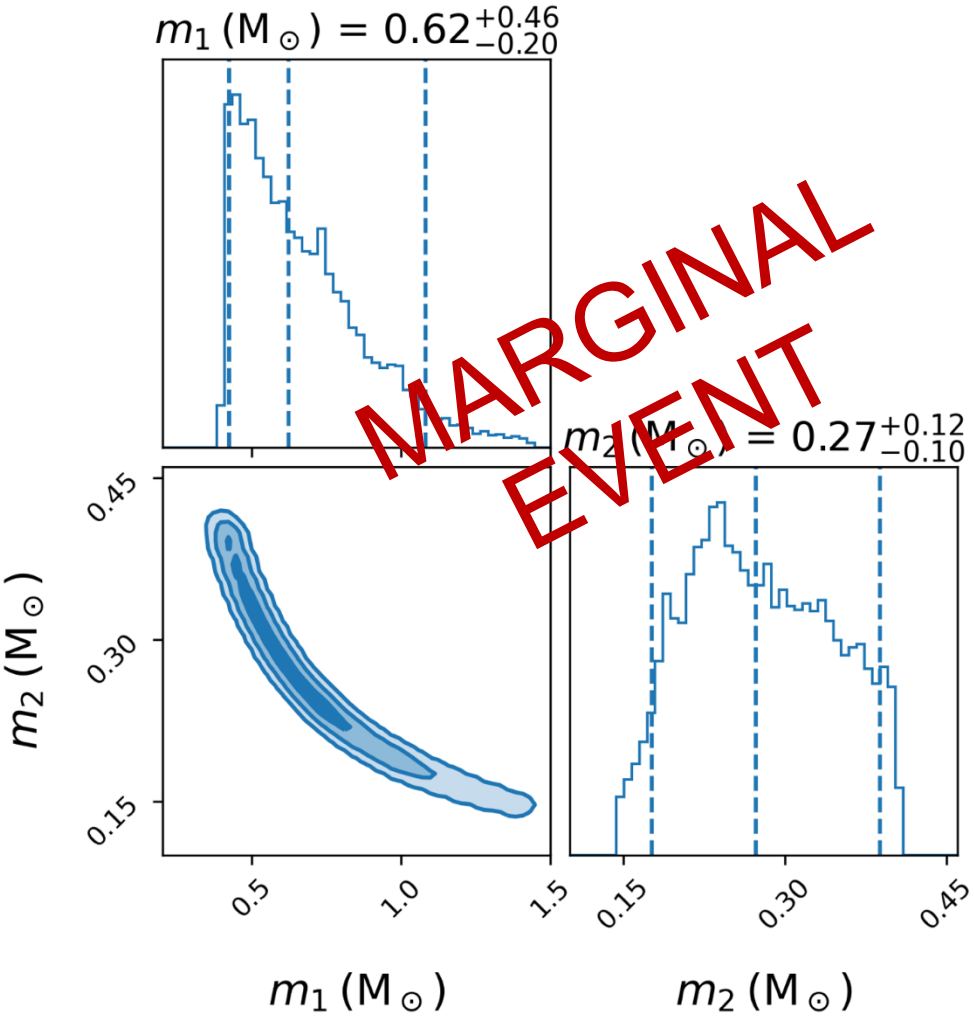


Gaussian (mean = 0, rms = 0.3)

Isotropic

Are there PBH in LIGO/Virgo?

SSM200308



Prunier et al. [2311.16085]

Parameter	
Matched Filter SNR	$8.02^{+0.49}_{-0.85}$
Primary mass ($M_\odot$)	$0.62^{+0.46}_{-0.20}$
Secondary mass ($M_\odot$)	$0.27^{+0.12}_{-0.10}$
Primary spin magnitude	$0.66^{+0.13}_{-0.25}$
Secondary spin magnitude	$0.44^{+0.33}_{-0.39}$
Total mass ($M_\odot$)	$0.88^{+0.35}_{-0.08}$
Detector-frame chirp mass ($M_\odot$)	$0.3527^{+0.0003}_{-0.0001}$
Mass ratio ($m_2/m_1 \leq 1$)	$0.44^{+0.48}_{-0.28}$
$\chi_{\rm eff}$ [27, 28]	$0.41^{+0.08}_{-0.04}$
$\chi_{\rm p}$ [29]	$0.37^{+0.24}_{-0.24}$
Luminosity Distance (Mpc)	90^{+43}_{-39}
Redshift	$0.02^{+0.01}_{-0.01}$
$P(m_1 < 1\ M_\odot)$	92%
$P(m_2 < 1\ M_\odot)$	100%

Primordial Black Hole 3G GW

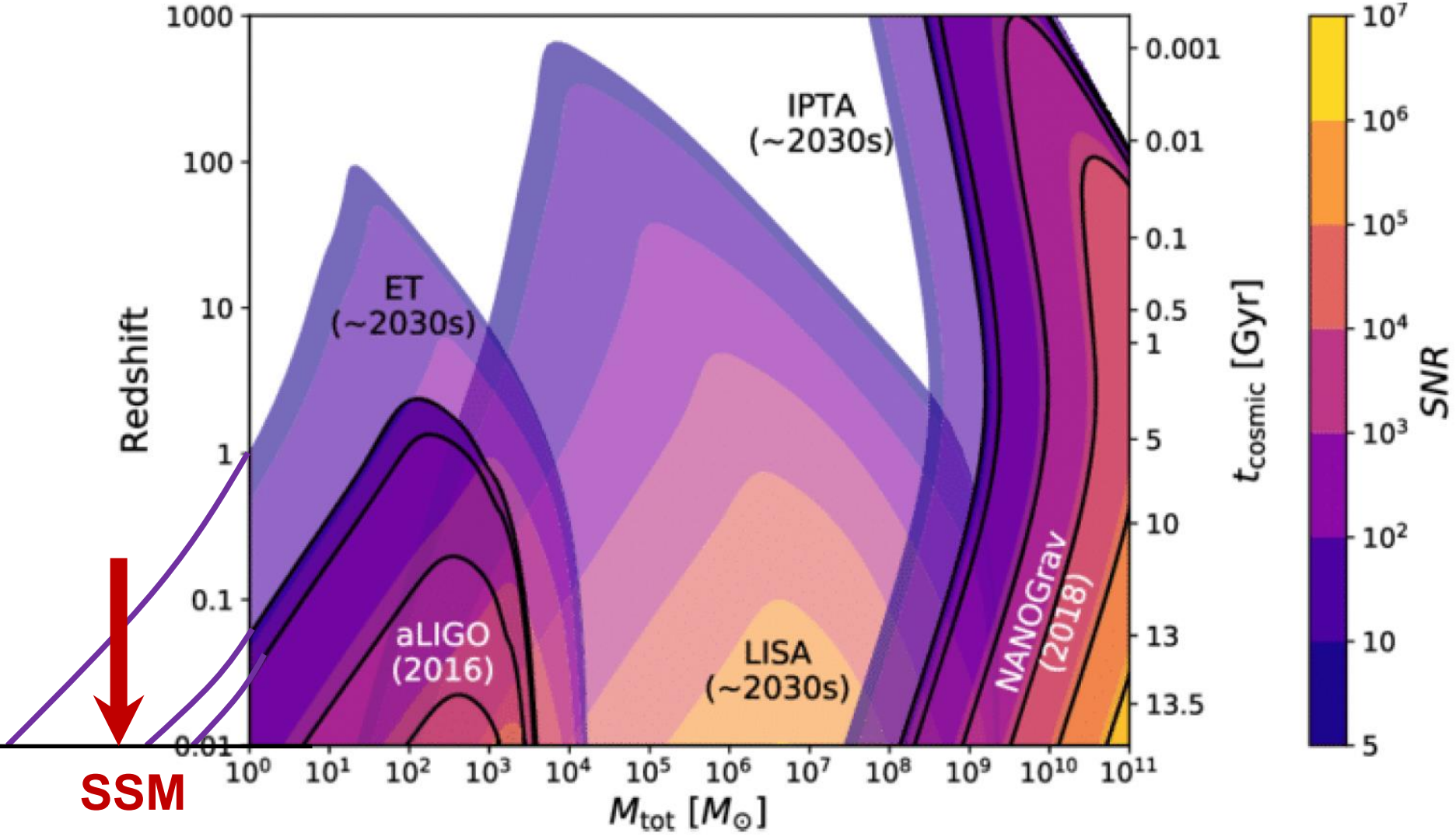


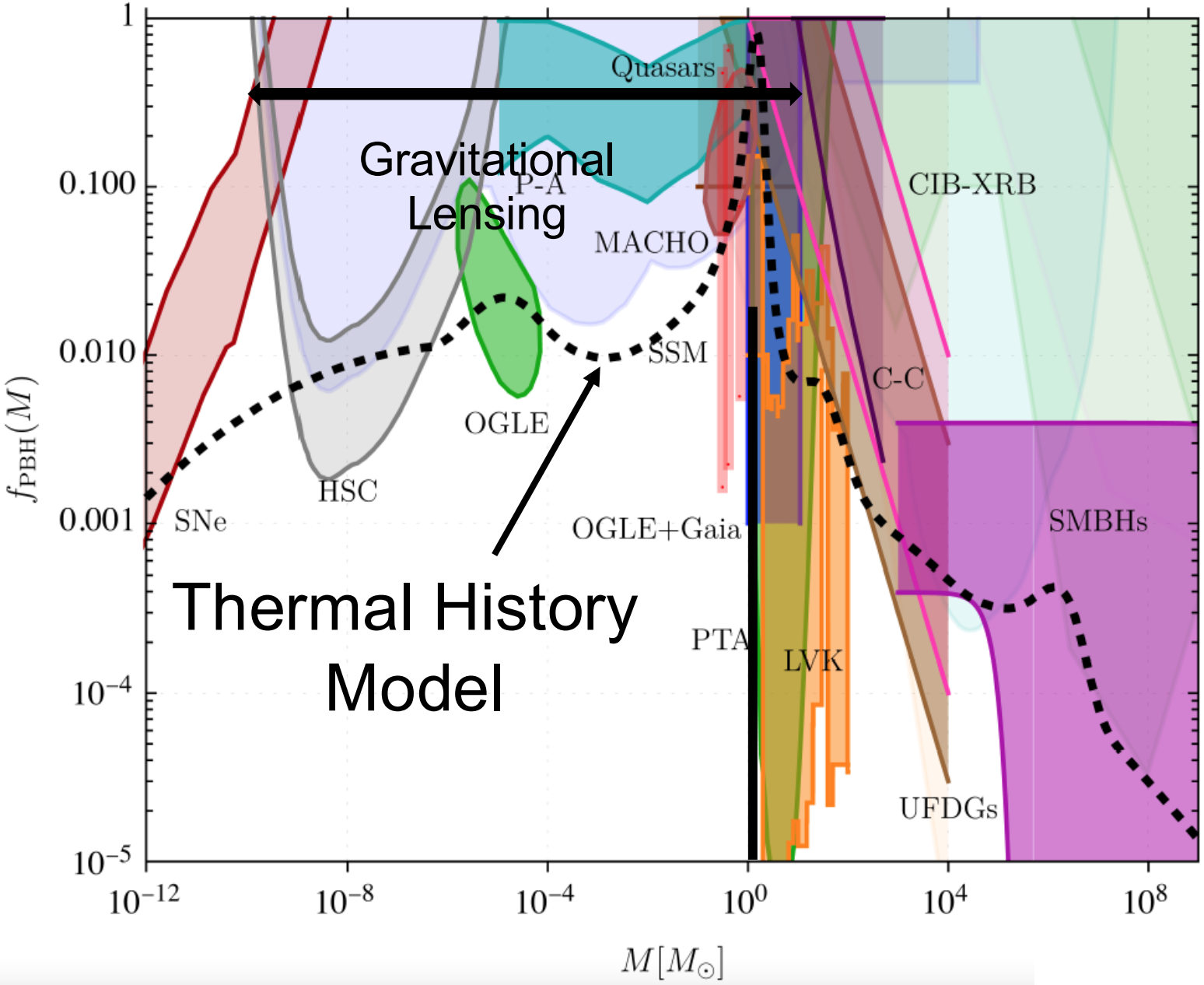
Figure 44. Redshift range of LISA for equal-mass BBH coalescences as a function of the total system mass and comparison with the range of other detectors and pulsar timing arrays. The color scale represents the expected SNR.

Conclusions

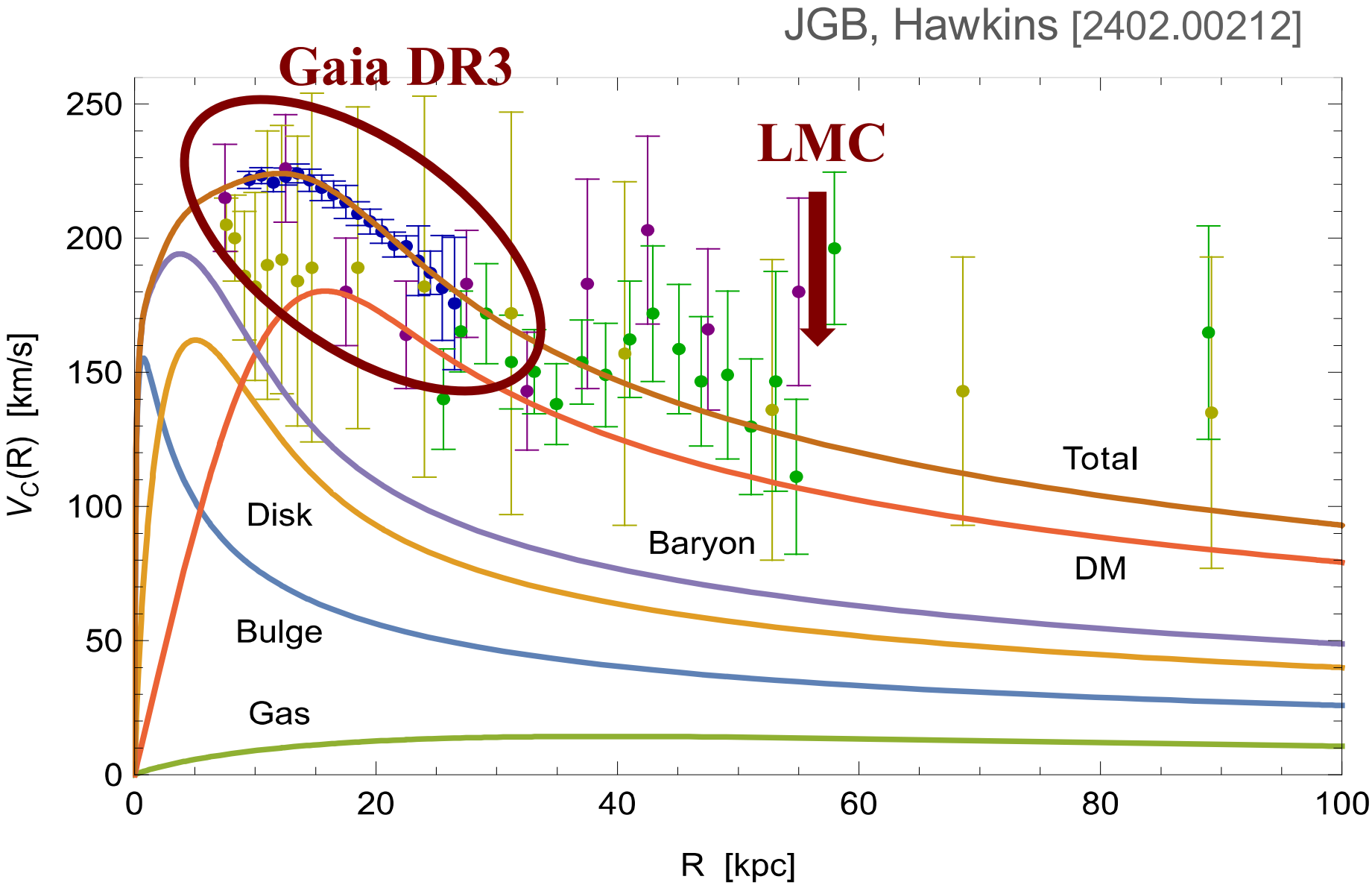
- Thermal history predicts **clustered** PBH with multimodal mass distribution $\sim 10^{-5}, 1, 100, 10^{6}\, M_\odot$
- The predicted PBH spin and mass distribution has been measured by LIGO/Virgo + OGLE/Gaia around 1-100 $M_\odot$ (features: peak & plateau)
- Other peaks could be explored with microlensing of stars towards LMC and Andromeda.
- PBH scenario can explain various cosmic conundra (LSS)
- Paradigm shift in Structure Formation of the Universe
- Very rich phenomenology: multi-scale, multi-epoch, multi-probe => Future 3G detectors (LISA, ET)

Observational evidence for primordial black holes

Carr, Clesse, JGB, Hawkins, Kühnel [2306.03903]

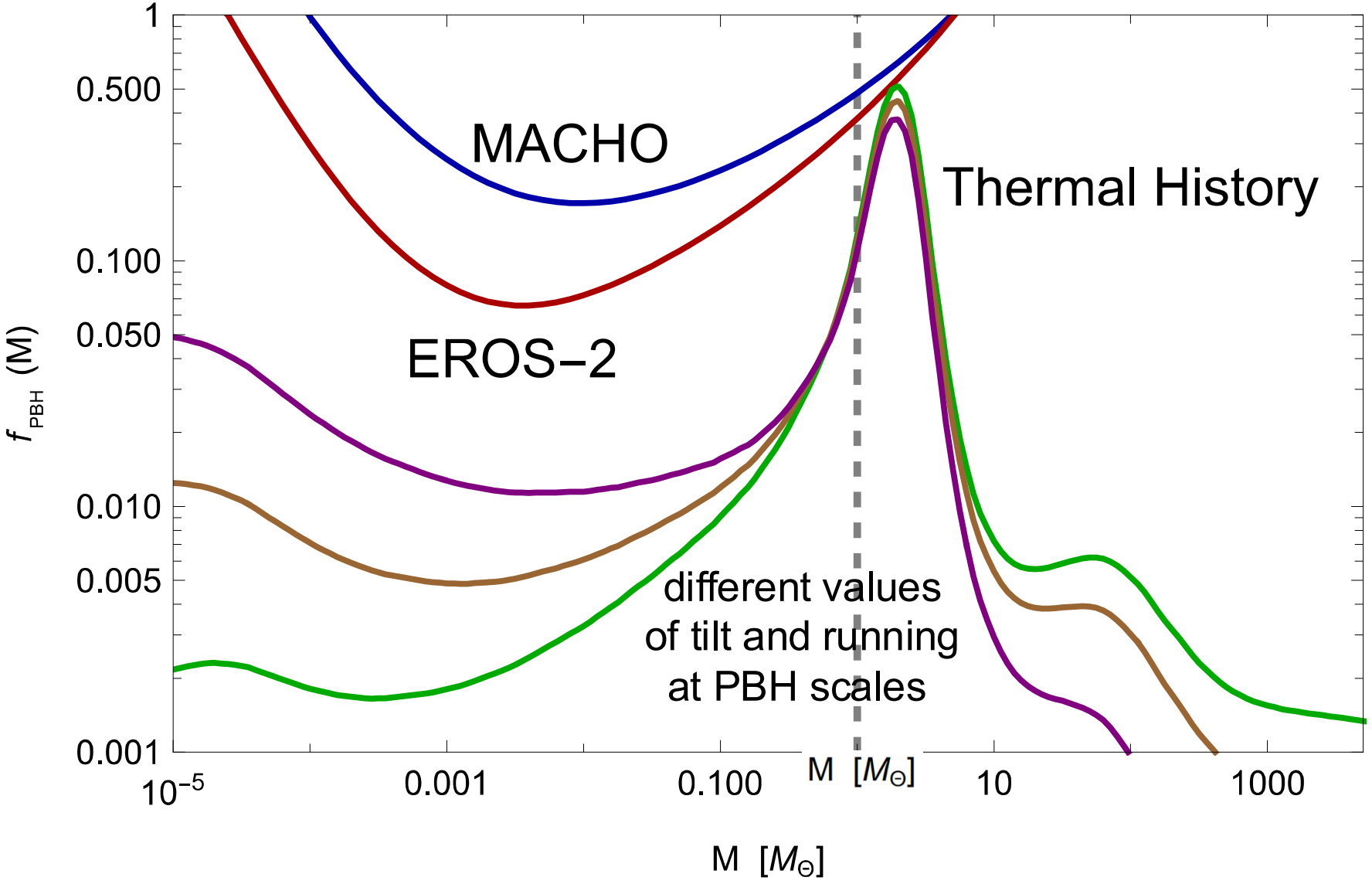


Milky Way rotation curves



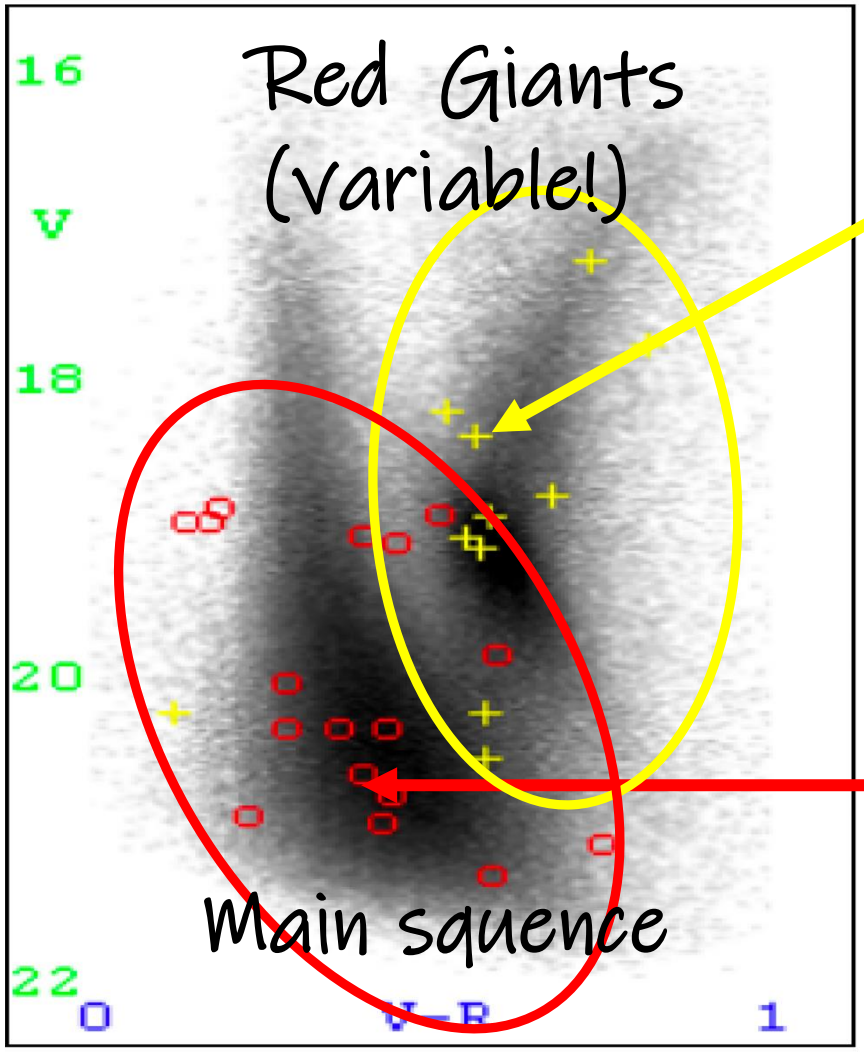
PBH Constraints from microlensing

JGB, Hawkins [2402.00212]

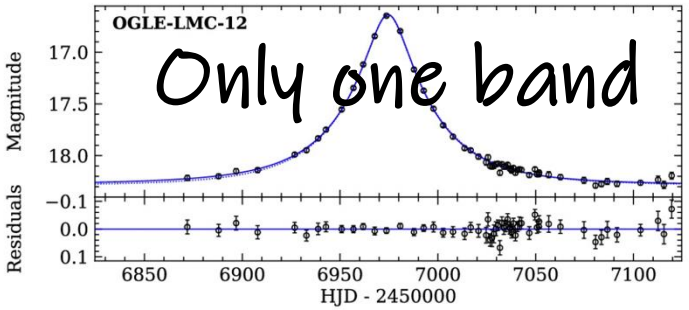


OGLE-IV Selection Criteria

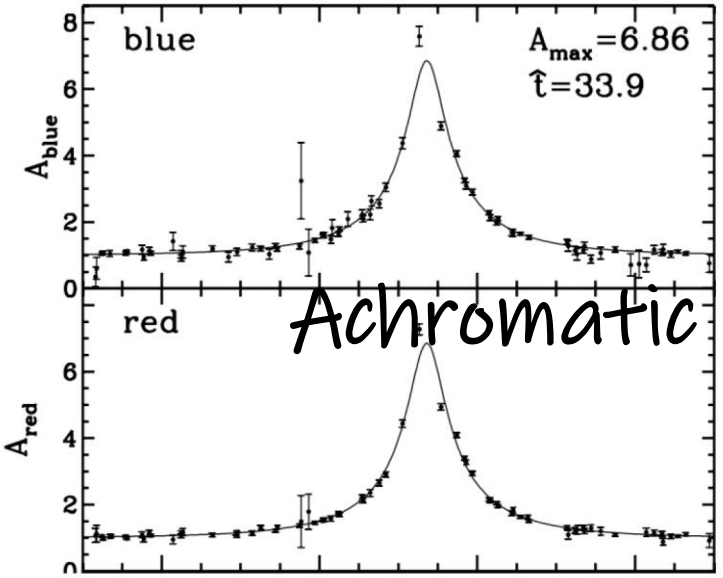
Hawkins, JGB [2509.05400]



OGLE-IV (2025)

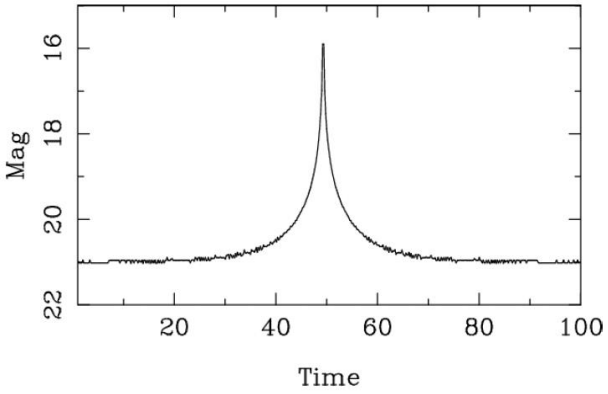


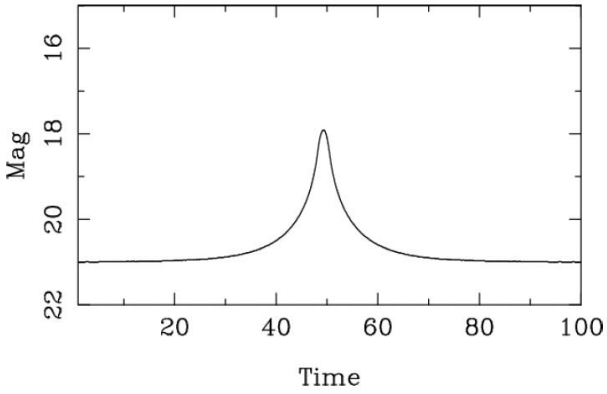
MACHO (1995)

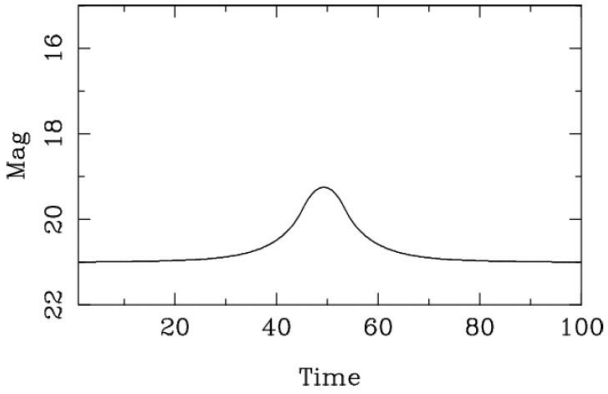


OGLE-IV Selection Criteria

Microlensing event follows a Paczinsky curve

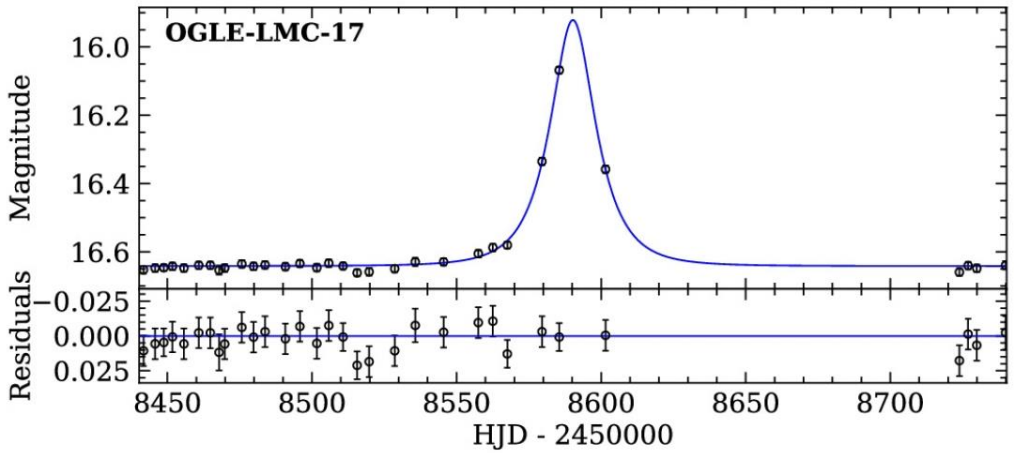






Point Source

Source radius = $R_E/10$ or $R_E/3$

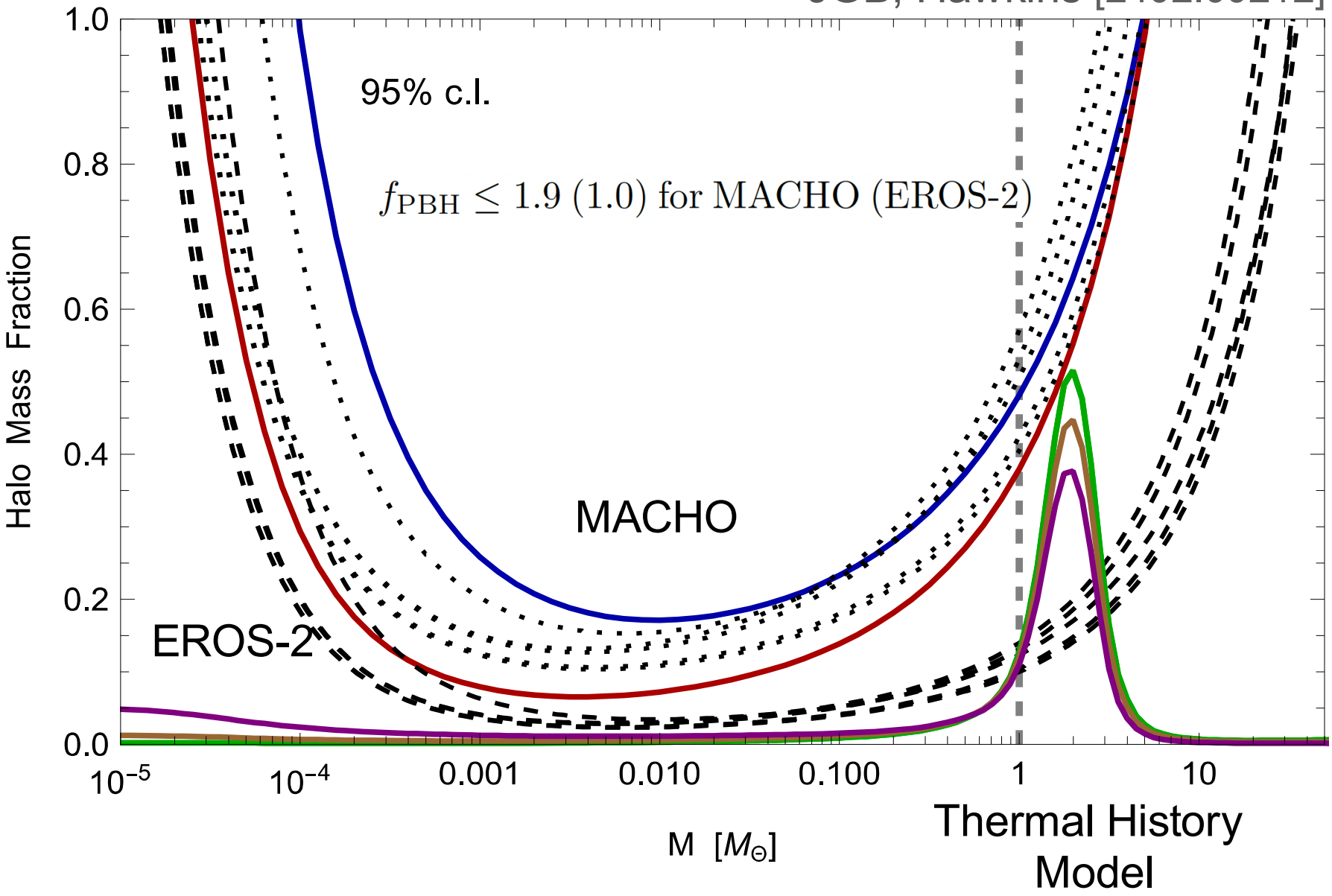


Time gaps larger than event duration

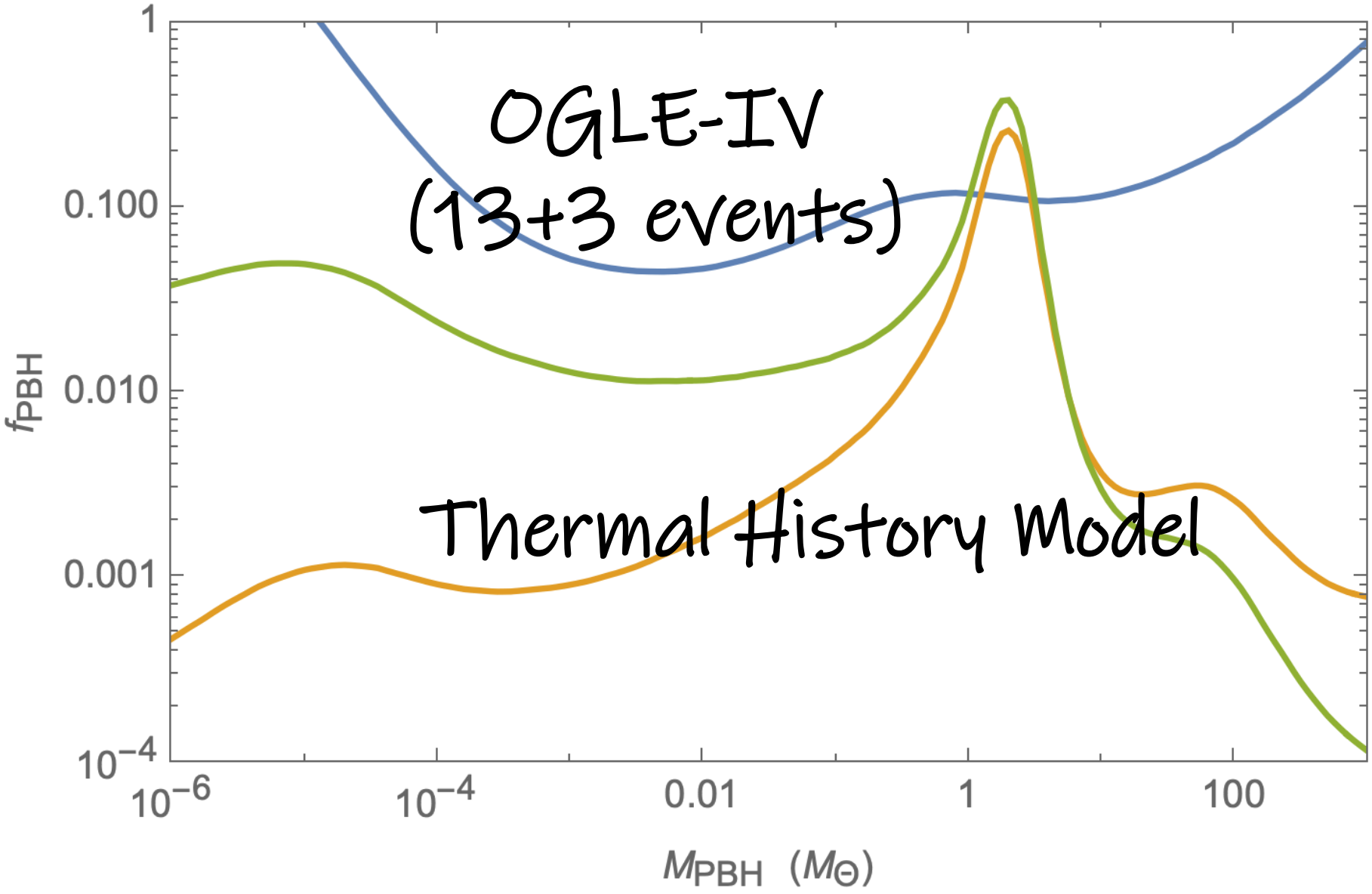
Hawkins, JGB [2509.05400]

Halo Mass Fraction

JGB, Hawkins [2402.00212]



OGLE-IV Constraints



Standard Model Lagrangian

$$S = \int d^4x\sqrt{-g}\left[\frac{M_{\rm P}^2}{2}R + \xi\,\Phi^\dagger\Phi\,R \right.$$
$$- (D_\mu\Phi)^\dagger D^\mu\Phi - V(\Phi)$$
$$\left. + \mathcal{L}_{\rm gauge} + \mathcal{L}_{\rm Yuk} + \mathcal{L}_{\rm vac}\right],$$

$$V = -m^2\,\Phi^\dagger\Phi + \lambda\,(\Phi^\dagger\Phi)^2,$$

$$\mathcal{L}_{\rm Yuk} = -\bar{Q}\,Y_u\tilde{\Phi}\,u_R - \bar{Q}\,Y_d\Phi\,d_R - \bar{L}\,Y_e\Phi\,e_R + \text{h.c.},$$

$$\mathcal{L}_{\rm vac} = -\rho_\Lambda + \alpha_1 R^2 + \alpha_2\,C_{\mu\nu\rho\sigma}C^{\mu\nu\rho\sigma} + \alpha_3\,\mathcal{E},$$

$$\mathcal{E} = R^2_{\mu\nu\rho\sigma} - 4R^2_{\mu\nu} + R^2$$

the one-loop RGE are

$$\beta^{(1)}_{g'} = \frac{41}{6} g'^3, \qquad \beta^{(1)}_{g} = -\frac{19}{6} g^3, \qquad \beta^{(1)}_{g_s} = -7 g_s^3, \tag{12}$$

$$\beta^{(1)}_{Y_u} = Y_u \left[\tfrac{3}{2} \left(Y_u^\dagger Y_u - Y_d^\dagger Y_d \right) + T - 8 g_s^2 - \tfrac{9}{4} g^2 - \tfrac{17}{12} g'^2 \right], \tag{13}$$

$$\beta^{(1)}_{Y_d} = Y_d \left[\tfrac{3}{2} \left(Y_d^\dagger Y_d - Y_u^\dagger Y_u \right) + T - 8 g_s^2 - \tfrac{9}{4} g^2 - \tfrac{5}{12} g'^2 \right], \tag{14}$$

$$\beta^{(1)}_{Y_e} = Y_e \left[\tfrac{3}{2} Y_e^\dagger Y_e + T - \tfrac{9}{4} g^2 - \tfrac{15}{4} g'^2 \right], \tag{15}$$

$$\begin{aligned} \beta^{(1)}_{\lambda} = {} & 24\lambda^2 + 4\lambda T - 3\lambda(3g^2 + g'^2) \\ & + \tfrac{3}{8} \left[2g^4 + (g^2 + g'^2)^2 \right] \\ & - 2 \operatorname{Tr} \left[3 (Y_u^\dagger Y_u)^2 + 3 (Y_d^\dagger Y_d)^2 + (Y_e^\dagger Y_e)^2 \right], \end{aligned} \tag{16}$$

$$\gamma^{(1)}_{m^2} = 12\lambda + 2T - \tfrac{9}{2} g^2 - \tfrac{3}{2} g'^2, \tag{17}$$

$$\beta^{(1)}_{\xi} = \left(\xi + \frac{1}{6} \right) \left[12\lambda + 2T - \tfrac{9}{2} g^2 - \tfrac{3}{2} g'^2 \right]. \tag{18}$$

$$\beta^{(1)}_{y_t} = y_t\left[\tfrac{9}{2}y_t^2 + \tfrac{3}{2}y_b^2 + y_\tau^2 - 8g_s^2 - \tfrac{9}{4}g^2 - \tfrac{17}{12}g'^2\right],$$

$$\beta^{(1)}_{y_b} = y_b\left[\tfrac{3}{2}y_t^2 + \tfrac{9}{2}y_b^2 + y_\tau^2 - 8g_s^2 - \tfrac{9}{4}g^2 - \tfrac{5}{12}g'^2\right],$$

$$\beta^{(1)}_{y_\tau} = y_\tau\left[3y_t^2 + 3y_b^2 + \tfrac{5}{2}y_\tau^2 - \tfrac{9}{4}g^2 - \tfrac{15}{4}g'^2\right].$$

$$\beta^{(1)}_{\rho_\Lambda} = 2m^4, \qquad \beta^{(1)}_{M_{\rm P}^2} = -8m^2\left(\xi + \frac{1}{6}\right),$$

$$\beta^{(1)}_{\alpha_1} = -2\left(\xi + \frac{1}{6}\right)^2,$$

$$\beta^{(1)}_{\alpha_2} = -\frac{N_s + 6N_D + 12N_v}{120} = -\frac{283}{120},$$

$$\beta^{(1)}_{\alpha_3} = \frac{N_s + 11N_D + 62N_v}{360} = \frac{1991}{720}.$$

The three-loop SM beta functions

$$\beta_{g_s}^{(3)} = g_s^3\Big[\tfrac{65}{2}g_s^4 - 40g_s^2y_t^2 + 15y_t^4 + 21g^2g_s^2 + \tfrac{77}{9}g_s^2g'^2 + \tfrac{109}{8}g^4 - \tfrac{1}{8}g^2g'^2 - \tfrac{2615}{216}g'^4 - \tfrac{93}{8}g^2y_t^2 - \tfrac{101}{24}g'^2y_t^2\Big],$$

$$\beta_{g}^{(3)} = g^3\Big[\tfrac{324953}{1728}g^4 + 39g^2g_s^2 + \tfrac{291}{32}g^2g'^2 + \tfrac{3}{2}g^2\lambda - \tfrac{729}{32}g^2y_t^2 + 81g_s^4 - \tfrac{1}{3}g_s^2g'^2 - 7g_s^2y_t^2 - \tfrac{5597}{576}g'^4 + \tfrac{1}{2}g'^2\lambda - \tfrac{593}{96}g'^2y_t^2 - 3\lambda^2 + \tfrac{147}{16}y_t^4\Big],$$

$$\beta_{g'}^{(3)} = g'^3\Big[-\tfrac{388613}{5184}g'^4 + \tfrac{1315}{64}g^4 - g^2g_s^2 + \tfrac{205}{96}g^2g'^2 + \tfrac{3}{2}g^2\lambda - \tfrac{785}{32}g^2y_t^2 + 99g_s^4 - \tfrac{137}{27}g_s^2g'^2 - \tfrac{29}{3}g_s^2y_t^2 + \tfrac{3}{2}g'^2\lambda - \tfrac{2827}{288}g'^2y_t^2 - 3\lambda^2 + \tfrac{315}{16}y_t^4\Big].$$

$$\beta_{y_t}^{(3)} = y_t\Big[\Big(\tfrac{339}{8} + \tfrac{27}{2}\zeta_3\Big)y_t^6 + 198\lambda y_t^4 + \tfrac{15}{4}\lambda^2y_t^2 - 36\lambda^3 - 157g_s^2y_t^4 + 16g_s^2\lambda y_t^2 + \Big(\tfrac{3827}{6} - 228\zeta_3\Big)g_s^4y_t^2 + \Big(-\tfrac{4166}{3} + 640\zeta_3\Big)g_s^6\Big],$$

$$\beta_{\lambda}^{(3)} = (7176 + 4032\zeta_3)\lambda^4 + 1746\lambda^3y_t^2 + (1719 + 1512\zeta_3)\lambda^2y_t^4 + \Big(\tfrac{117}{4} - 396\zeta_3\Big)\lambda y_t^6 - \Big(\tfrac{1599}{4} + 72\zeta_3\Big)y_t^8 + g_s^2\Big[(-2448 + 2304\zeta_3)\lambda^2y_t^2 + (1790 - 2592\zeta_3)\lambda y_t^4 + (-76 + 480\zeta_3)y_t^6\Big] + g_s^4\Big[\Big(\tfrac{2488}{3} - 96\zeta_3\Big)\lambda y_t^2 + \Big(-\tfrac{532}{3} + 64\zeta_3\Big)y_t^4\Big],$$

$$\gamma_{m^2}^{(3)} = 2052\lambda^3 + 297\lambda^2y_t^2 + \Big(\tfrac{351}{2} + 432\zeta_3\Big)\lambda y_t^4 + \Big(\tfrac{1605}{8} + 90\zeta_3\Big)y_t^6 + g_s^2\Big[(-1224 + 1152\zeta_3)\lambda y_t^2 + (447 - 720\zeta_3)y_t^4\Big] + \Big(\tfrac{1244}{3} - 48\zeta_3\Big)g_s^4y_t^2,$$

$$\beta_{\xi}^{(3)} = (\xi + \tfrac{1}{6})\gamma_{m^2}^{(3)}.$$

We use the PDG averages [45] listed in Table I. The $\overline{\rm MS}$ couplings at $\mu = M_t$ are obtained from the NNLO matching of Ref. [17],

$$\lambda(M_t) = 0.12604 + 0.00206\,(M_h - 125.15) - 0.00004\,(M_t - 173.34),$$

$$y_t(M_t) = 0.93690 + 0.00556\,(M_t - 173.34) - 0.00042\,\frac{\alpha_s - 0.1184}{0.0007},$$

$$g_s(M_t) = 1.1666 + 0.00314\,\frac{\alpha_s - 0.1184}{0.0007} - 0.00046\,(M_t - 173.34),$$

$$g(M_t) = 0.64779 + 0.00004\,(M_t - 173.34) + 0.00011\,\frac{M_W - 80.384}{0.014},$$

$$g'(M_t) = 0.35830 + 0.00011\,(M_t - 173.34) - 0.00020\,\frac{M_W - 80.384}{0.014},$$

$$\xi(M_t) = 35,$$

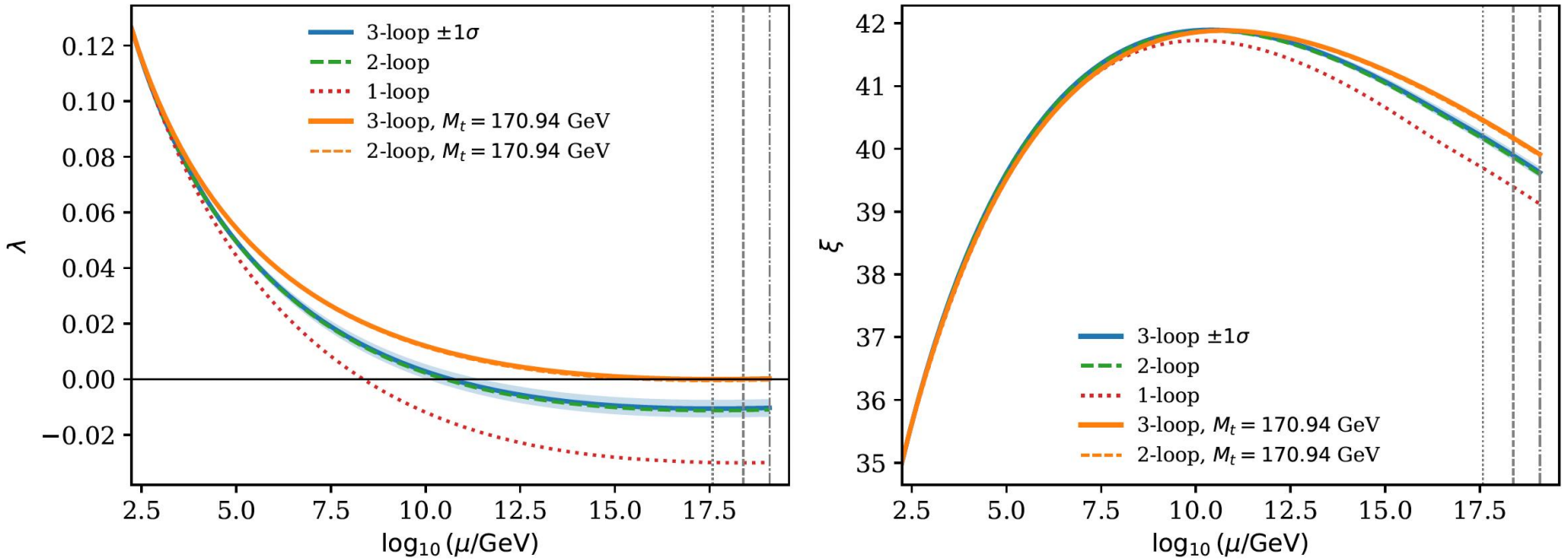


FIG. 1. Running of λ (left) and ξ (right) from M_t to M_P with $\xi(M_t) = 35$, at the measured top mass. Solid: three loops with the 1σ band; dashed: two loops; dotted: one loop. Orange lines: λ (left) and ξ (right) for the critical top mass $M_t = 170.94\,\mathrm{GeV}$ at three loops (solid) and two loops (dashed); λ just touches zero near M_P, and ξ reaches $\xi_* \simeq 40.5$ at the plateau scale $M_P/\sqrt{\xi_*} \simeq 3.8 \times 10^{17}\,\mathrm{GeV}$, within the ACT window of Sec. IX. Vertical lines mark the plateau scale $M_P/\sqrt{\xi_*} \simeq 3.8 \times 10^{17}\,\mathrm{GeV}$ (dotted), the reduced Planck mass $M_P = 2.4 \times 10^{18}\,\mathrm{GeV}$ (dashed) and the Planck mass $1.2 \times 10^{19}\,\mathrm{GeV}$ (dash-dotted).

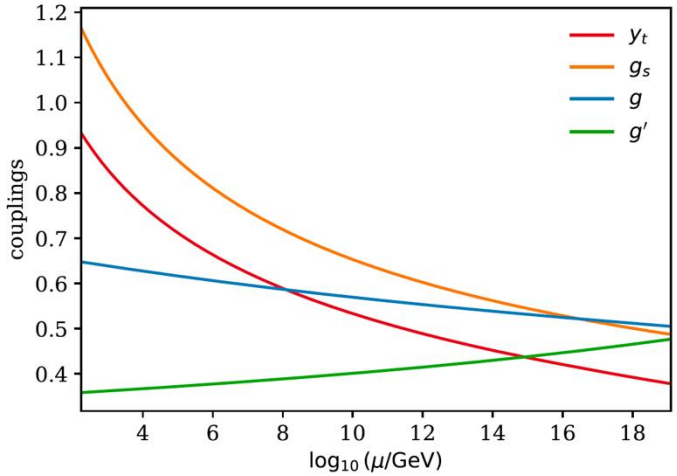


FIG. 2. Three-loop running of y_t, g_s, g and g' with 1σ bands.